

## Supporting Online Information

This document presents groundwater age dating methods (S1),  $\Delta^{18}\text{O}_{\text{late-glacial}}$  calculation details (S2), inter-model simulation details (S3) and tabulated data and sources (S4).

### **S1. Groundwater age dating**

Mean  $^{14}\text{C}$ -based groundwater ages ( $t$ , the time elapsed since recharge) were calculated for each groundwater sample by accounting for the radioactive decay of  $^{14}\text{C}$  and for the dissolution of  $^{14}\text{C}$ -dead aquifer materials (Clark and Fritz, 1997):

$$t = -8033 \times \ln\left(\frac{A}{q \times A_0}\right) \quad \text{Equation S1.}$$

where  $t$  is the time elapsed since the groundwater sample recharged (i.e., groundwater age),  $A$  is the measured  $^{14}\text{C}$  activity in a groundwater sample,  $A_0$  is the initial  $^{14}\text{C}$  activity ( $\sim 100$  pmC) and  $q$  is a correction factor applied to account for the dissolution of aquifer material with zero  $^{14}\text{C}$  (i.e.,  $^{14}\text{C}$ -dead). In cases where  $\delta^{13}\text{C}$  data was available  $q$  was calculated as:

$$q = \frac{\delta^{13}\text{C}_{\text{measured}} - \delta^{13}\text{C}_{\text{aquifer}}}{\delta^{13}\text{C}_{\text{recharge}} - \delta^{13}\text{C}_{\text{aquifer}}} \quad \text{Equation S2.}$$

where  $\delta^{13}\text{C}_{\text{measured}}$ ,  $\delta^{13}\text{C}_{\text{aquifer}}$  and  $\delta^{13}\text{C}_{\text{recharge}}$  represent the carbon isotope composition of a groundwater sample, the aquifer and recharging groundwater.  $\delta^{13}\text{C}_{\text{aquifer}}$  was set to  $1.0 \pm 3.4$  ‰ PDB (average  $\pm 1$  s.d.) as determined by  $\delta^{13}\text{C}$  values of 16359 rock and sediment samples (Veizer et al., 1999).  $\delta^{13}\text{C}_{\text{recharge}}$  was set to  $-12.6 \pm 4.3$  ‰ PDB (average  $\pm 1$  s.d.) as determined by 120 groundwater samples having a  $^{14}\text{C}$  activity of greater than 90 p.m.C. compiled in this study (i.e., recently recharged water bearing near-atmospheric radioactive activities; Burchuladze et al., 1989).  $q$  was set to  $0.76 \pm 0.41$  in cases where  $\delta^{13}\text{C}_{\text{measured}}$  data were unavailable, as determined by the most common  $\delta^{13}\text{C}$ -based  $q$  values ( $q = 0.76 \pm 0.41$  represents the average and

22 one standard deviation of all  $\delta^{13}\text{C}$ -based  $q$  values calculated in this compilation). Uncertainties in  
23 groundwater ages were calculated by Gaussian error propagation (calculated values of  $q$   
24 exceeding 1 were set to a value of 1). The  $\delta^{13}\text{C}_{recharge}$  and  $\delta^{13}\text{C}_{aquifer}$  ranges do not encompass all  
25 possible geochemical scenarios, and likely introduce additional errors into our groundwater age  
26 dates.

27 Equivalent calendar year ages were estimated from  $^{14}\text{C}$ -ages by applying a polynomial fit  
28 of compiled  $^{14}\text{C}$ -to-calender age corrections (Reimer et al., 2013). Samples were then divided  
29 into two age categories: (i) the late-Holocene ( $^{14}\text{C}$ -based age of less than 5,000 calendar years  
30 before present, or having a  $^3\text{H}$  activity of greater than 4 T.U., indicating modern recharge), or (ii)  
31 the late-glacial ( $^{14}\text{C}$ -based age of 20,000 to less than ~50,000 calendar years before present and  
32 samples with  $^{14}\text{C}$  activities below analytical detection). An upper late-glacial limit of less than  
33 ~50,000 years before present was set because of limitations with  $^{14}\text{C}$  age calculations, even  
34 though the most recent ice age extends to ~110,000 years before present (Lisiecki and Raymo,  
35 2005). However,  $^{14}\text{C}$ -based ages cannot distinguish ~50,000 year old water from much older  
36 groundwaters on the order of  $10^5$  years before present, meaning that some of the last glacial  
37 period groundwater samples may represent older glacial climates (e.g.,  $^{36}\text{Cl}$ -based versus  $^{14}\text{C}$ -  
38 based ages presented by Kulongoski et al., 2004).

## 39 **S2. $\Delta^{18}\text{O}_{\text{late-glacial}}$ calculation**

40  $\Delta^{18}\text{O}_{\text{late-glacial}}$  values (defined as  $\Delta^{18}\text{O}_{\text{late-glacial}} = \delta^{18}\text{O}_{\text{late-glacial}} - \delta^{18}\text{O}_{\text{late-Holocene}}$ ) were  
41 analyzed on an aquifer-by-aquifer basis. Comparisons of isotopic data for the late-glacial and the  
42 late-Holocene were made by subtracting median  $\delta^{18}\text{O}$  and  $\delta^2\text{H}$  values from each age group, with  
43 uncertainties representing error propagation of one standard deviation of  $\delta^{18}\text{O}$  and  $\delta^2\text{H}$  values for  
44 the two data groups (i.e., late-Holocene and last glacial period age groups). Samples were

45 omitted from our analysis if they exhibited an evaporative signature ( $\delta^2\text{H} - 8 \times \delta^{18}\text{O}$  of less than  
46 0), contained a mixture of modern and late-glacial groundwater ( $^3\text{H}$  activity of greater than 1  
47 tritium unit and a  $^{14}\text{C}$ -age of more than 20,000 calendar years before present), were suspected to  
48 have mixed with intruding seawater (e.g., Geyh and Söfner, 1989; Bouchaou et al., 2008) or  
49 were presumed to have been recharged by subglacial meltwaters beneath the Fennoscandinavian  
50 (e.g., Karro et al., 2004) or the Laurentide (e.g., Grasby and Chen, 2005; Ferguson et al., 2007;  
51 Stotler et al., 2010) ice sheets (review by McIntosh et al., 2012).

52 Ice core and speleothem  $\Delta^{18}\text{O}_{\text{late-glacial}}$  values were calculated by comparing  $\delta^{18}\text{O}$  values  
53 from the late-Holocene (<5,000 years before present) and the latter half of the late-glacial  
54 (20,000 to ~50,000 years before present). A threshold of less than ~50,000 years before present  
55 was selected as an upper limit for the latter half of the last ice age  $\delta^{18}\text{O}$  value for consistency  
56 with the groundwater records. Speleothem as  $\Delta^{18}\text{O}_{\text{late-glacial}}$  values were corrected to account for  
57 different temperatures during the late-glacial relative to the late-Holocene that impact the water-  
58 calcite isotopic fractionation factor. Temperature-based  $\text{H}_2\text{O}$ - $\text{CaCO}_3$  fractionation factors were  
59 obtained from O'Neil et al. (1969) with temperatures calculated under the assumption that  
60 atmospheric temperatures are indicative of temperatures in the shallow subsurface. Temperatures  
61 for the late-Holocene were assumed to be equivalent to modern mean annual near surface  
62 temperatures (New et al., 2002), potentially introducing  $<1^\circ\text{C}$  of error because of temperature  
63 change throughout the last 5,000 years (Marcott et al., 2013). Adding  $1^\circ\text{C}$  of added uncertainty  
64 into late-Holocene temperature equates to an added  $\pm 0.4 \text{‰}$  ( $\delta^{18}\text{O}$ ) of uncertainty in the  
65 temperature-corrected difference between the late-glacial and the late-Holocene  $\delta^{18}\text{O}$  values  
66 (O'Neil et al., 1969). Last glacial period temperatures were calculated by applying the  
67 temperature offset of the last glacial maximum (Figure 1; Annan and Hargreaves, 2013) to  
68 gridded values of modern mean annual air temperatures (New et al., 2002).

69           **S3. Simulated precipitation  $\delta^{18}\text{O}$**

70           Simulated precipitation  $\Delta^{18}\text{O}_{\text{late-glacial}}$  values compiled from five general circulation  
71 models are reported in this study. Table S1 describes model-specific parameterizations, input  
72 data and boundary conditions.

73           **S4. Groundwater, speleothem and ice core isotope records**

74           Tabulated paleowater isotope records of groundwater (Tables S2 to S3), speleothem  
75 (Table S4), glacier ice (Table S5) and ground ice (Table S6) records presented in the following  
76 supplemental tables.

77           **S5. Groundwater  $\delta^{18}\text{O}$  change over time**

78           Figures S1 – S57 present groundwater  $\delta^{18}\text{O}$  variations from the last ice age to present day  
79 for 57 globally-distributed aquifer systems (two ground ice records not included in this series of  
80 plots). Figures S1 to S57 are sorted by alphabetically by country title. Exact ages for Germany's  
81 Benker-sandstein aquifer are not available, however, the stable isotope data two data clusters are  
82 interpreted to be representative of late-Holocene and Pleistocene climate states (Figure S20, van  
83 Geldern et al., 2014). The most recent age end member for the late-glacial time period—usually  
84 set to 20,000 years before present—was set to 22,000 years before present for the Pannonian  
85 Basin to avoid samples with  $^{14}\text{C}$ -ages between 20,000 and 22,000 years before present showing  
86 evidence of groundwater mixing (Figure S22; Varsanyi et al., 2011). Aleppo Basin (Syria) and  
87 Mahomet Aquifer (USA) groundwaters having a  $\delta^{13}\text{C}$ -based  $q$  values of less than 0.3 were not  
88 included in our analysis on the basis of highly uncertain groundwater ages at low values of  $q$   
89 (Figures S44 and S55; Hackley et al., 2010; Al-Charideh, 2012; Stadler et al., 2012). Late-glacial  
90 to late-Holocene  $\delta^{18}\text{O}$  and  $\delta^2\text{H}$  shifts are shown in Figure S58 for 44 aquifers.

92 **Table S1.** Information for isotope enabled general circulation models compiled in this study

<b>Model name:</b>	<b>CAM3iso</b>	<b>ECHAM5- wiso</b>	<b>GISSE2-R, NINT</b>	<b>IsoGSM</b>	<b>LMDZ4</b>
<b>Reference for model:</b>	Collins et al., 2006	Roeckner et al., 2006	Schmidt et al., 2014	Kanamitsu et al., 2002	Hourdin et al., 2006
<b>Reference for isotopic version:</b>	Noone and Sturm, 2009; Sturm et al., 2010	Werner et al., 2011	LeGrande and Schmidt, 2009 *	Yoshimura et al., 2008	Risi et al., 2010
<b>Forced or coupled simulation:</b>	Forced	Forced	Coupled	Forced	Forced
<b>Sea surface temperature forcing (if forced):</b>	Monthly-mean anomalies from a LGM simulation by the CCSM3 coupled model (Otto-Bliesner et al., 2006)	Monthly-mean anomalies from GLAMAP reconstruction (footnote: LGM anomalies were calculated with respect to a pre-industrial simulation, and added to present-day observed SSTs from AMIP)	N/A	Monthly-mean anomalies from a LGM simulation by the IPSL coupled model (footnote: LGM anomalies were calculated with respect to a pre-industrial simulation, and added to present-day observed SSTs from AMIP)	Monthly-mean anomalies from a LGM simulation by the IPSL coupled model (footnote: LGM anomalies were calculated with respect to a pre-industrial simulation, and added to present-day observed SSTs from AMIP)
<b>Sea ice forcing (if forced):</b>	Same as SSTs	Same as SSTs	N/A	Same as SSTs	Same as SSTs
<b>Climatological or inter-annual forcing:</b>	Climatological (average over 100 years)	Climatological	N/A	Climatological (average over 30 years)	Climatological (average over 30 years)
<b>Topography/land ice:</b>	Ice 5G (Peltier, 1994)	As advised by PMIP3 (Braconnot et al., 2012)	Ice 5.2G, with LIS of Licciardi et al. (1998)	Ice 5G (Peltier, 1994)	Ice 5G (Peltier, 1994)

<b>Model name:</b>	<b>CAM3iso</b>	<b>ECHAM5-wiso</b>	<b>GISSE2-R, NINT</b>	<b>IsoGSM</b>	<b>LMDZ4</b>
<b>Aerosol:</b>	Pre-industrial	None	NINT physics (Koch et al., 2011; Shindell et al., 2006) and includes a tuned aerosol indirect effect (AIE) following (Hansen et al., 2005)	None	None
<b>Solar/orbital forcing:</b>	PMIP2 protocol	PMIP3 protocol	PMIP3 protocol	PMIP2 protocol	PMIP2 protocol
<b>Number of years:</b>	15	12 years and last 10 years average	1500	30 years and last 20 years average	3
<b>Horizontal resolution:</b>	2.8° x 2.8°	1.1° x 1.1° (T106 spectral resolution)	Atmosphere: 2.0° x 2.5°; Ocean: 1.0° x 1.25°	1.8° x 1.8° (T62 spectral resolution)	2.5° latitude x 3.75° longitude
<b>Vertical resolution:</b>	26 levels	31 levels	Ocean: 26 levels; atmosphere: 40 levels, top at 0.1 mb	28 levels	19 levels
<b>Seawater <math>\delta^{18}\text{O}</math> (modern):</b>	0 ‰, globally constant	LeGrande and Schmidt, 2006	0 ‰ mean, but coupled	0 ‰, globally constant	0.5 ‰, globally constant
<b>Seawater <math>\delta^{18}\text{O}</math> (LGM):</b>	+1.1‰ with respect to present	+1‰ with respect to present	+1‰ with respect to present, but coupled	0 permil, globally constant; +1 per mille added after to account for seawater change	+1.2 ‰ with respect to present

93 \* Last Glacial Maximum simulation described in Ullman et al. (2014)

94

95 **Table S2.** Groundwater datasets compiled in this study

Country	Aquifer	Citation(s)
Algeria	Great Oriental Erg: CI	Edmunds et al., 2003
Botswana	Kalahari: Ntane	Kulongoski et al., 2004
Botswana	Lokalane-Nakojane	Rahube, 2003
Burkina Faso	Taoudeni basin	Huneau et al., 2011
Chad	Chad aquifer	Edmunds, 2009
Egypt	Nubian aquifer	Shehata and Al-Ruwaih, 1999; Patterson et al., 2005; Edmunds, 2009
Mali	Mali aquifer	Edmunds, 2009
Morocco	Souss Plain	Bouchaou et al., 2008
Namibia	Omatako basin	Külls, 2000
Niger	Djardo-Bilma	Dodo and Zuppi, 1997; 1999
Niger	Irhazer: CI	Andrews et al., 1994; Edmunds et al., 2004
Niger	Iullemeden: CT	Le Gal La Salle et al., 2001; Beyerle et al., 2003
Nigeria	Chad basin	Maduabuchi et al., 2006
Senegal	Senegalese CT	Castany et al., 1974; Edmunds, 2009
South Africa	Uitenhage aquifer	Heaton et al., 1986
Tunisia	Kairouan Plain	Derwich et al., 2012
Zimbabwe	Zimbabwe aquifer	Larsen et al., 2002
Australia	Canning basin	Harrington et al., 2011
Bangladesh	Bengal basin	Aggarwal et al., 2000; Sikdar and Sahu, 2009; Majumder et al., 2011; Hoque and Burgess, 2012
China	Songnen Plain	Chen et al., 2011
China	North China Plain	Zongyu et al., 2003; Kreuzer et al., 2009
China	Yuncheng basin	Currell et al., 2010
India	Cuddalore sandstone	Sukhija et al., 1998
India	Tiruvadanai aquifer	Kumar et al., 2009
Indonesia	Jakarta basin	Geyh and Söfner, 1989
Israel	Israel coastal aquifer	Yeichieli et al., 2009
Israel	Dead Sea rift valley	Gat and Galai, 1982; Mazor et al., 1995
Kuwait	Al-Raudhatain and Damman aquifers	Al-Ruwaih and Shehata, 2004; Fadlilmawla et al., 2008
Oman	Batinah coastal plain	Weyhenmeyer et al., 2000; 2002
Oman	Najd aquifer	Clark et al., 1987; Al-Mashaikhi et al., 2012
Syria	Aleppo basin	Al-Charideh, 2012; Stadler et al., 2012
Belgium	Ledo-Paniselian	Walraevens, 1990; Walraevens et al., 2001
Czech Rep.	Sokolov aquifer	Noseck et al., 2009
Denmark	Ribe Formation	Hinsby et al., 2001
France	Bathonian coast	Barbecot et al., 2000
France	Lorraine sandstone	Celle-Jeanton et al., 2009
France	Aquitaine basin	Le Gal La Salle et al., 1996
Germany	Benker-Sandstein	van Geldern et al., 2014

Country	Aquifer	Citation(s)
Hungary	Great Hungarian Plain	Stute and Deak, 1989
Hungary	Pannonian basin	Varsanyi et al., 2011
Italy	Emilia-Romagna Plain	Martinelli et al., 2011
Poland	S. Poland carbonates	Samborska et al., 2013
Poland	Malm limestone	Zuber et al., 2004
Portugal	Sado basin	Galego Fernandes and Carreira, 2008
Turkey	Kazan Trona Ore Field	Arslan et al., 2014
United Kingdom	Lincolnshire limestone	Darling et al., 1997
United Kingdom	Chalk aquifer	Darling and Bath, 1988; Dennis et al., 1997; Elliot et al., 1999
U.S.A.	Columbia Flood Bslts.*	Douglas et al., 2007; Brown et al., 2010
U.S.A.	Idaho Batholith	Schlegel et al., 2009
U.S.A.	Mahomet aquifer	Hackley et al., 2010
U.S.A.	Aquia aquifer	Aeschbach-Hertig et al., 2002
U.S.A.	High Plains: Central	Dutton, 1995; Clark et al. 1998
U.S.A.	High Plains: South	Dutton, 1995; Mehta et al., 2000
U.S.A.	San Juan Basin	Phillips et al., 1986
U.S.A.	Floridan aquifer	Clark et al., 1997
Brazil	Potiguar basin: Acu	Salati et al., 1974
Brazil	Botacatu: central	Gouvea da Silva, 1983
Russia	Bykovsky Peninsula**	Meyer et al., 2002
Canada	Near Dawson City***	Kotler and Burn, 2000

96 \* Columbia Flood Basalt late-glacial groundwater may be glacial Lake Missoula floodwaters  
97 rather than regional precipitation (Brown et al., 2010).

98 \*\* Ground ice record – comparison of ice wedge  $\delta^{18}\text{O}$  values <1m from edge (Holocene) and  
99 inner-most (2.5m – 5m; Pleistocene) samples (horizontal ice wedge sample transect MKh-3).

100 \*\*\* Ground ice record – comparison of ground ice  $\delta^{18}\text{O}$  values from the Dago Hill (Holocene)  
101 and Quartz Creek (Pleistocene) formations.

**Table S3.** Groundwater  $\delta^{18}\text{O}_{\text{late-Holocene}}$  and  $\delta^{18}\text{O}_{\text{late-glacial}}$  values

Country	Aquifer	Lon.	Lat.	$\delta^{18}\text{O}_{\text{late-Holo.}}$	$\delta^{18}\text{O}_{\text{glacial}}$	$\Delta^{18}\text{O}_{\text{glacial}}$
Australia	Canning basin	125	-17	-7.0±1.7	-7.4±0.5	-0.5±1.8
Indonesia	Jakarta basin	107	-6	-6.1±0.1	-6.0±0.5	0.1±0.5
Bangladesh	*Bengal basin	90	24	-4.9±1.1	-3.4±0.6	1.5±1.3
China	Songnen plain	125	46	-10.4±1.4	-10.2±0.4	0.3±1.5
China	*North China Plain	115	38	-8.5±0.5	-10.8±0.4	-2.3±0.6
China	Yuncheng basin	111	35	-8.7±1.3	-9.9±1.0	-1.1±1.7
India	*Cuddalore sandstone	80	11	-5.6±0.3	-4.9±0.6	0.7±0.7
India	*Tiruvadanai aquifer	79	10	-3.9±0.5	-5.6±0.3	-1.7±0.6
Algeria	*Great Oriental Erg: CI	6	32	-7.1±1.0	-8.4±0.3	-1.3±1.1
Botswana	*Kalahari: Ntane	25	-24	-4.8±0.0	-5.6±0.1	-0.8±0.1
Botswana	*Lokalane-Nakojane	22	-22	-6.0±0.0	-7.2±0.1	-1.2±0.1
Burkina Faso	*Taoudeni basin	-5	13	-5.1±0.6	-6.0±0.3	-0.9±0.7
Chad	*Chad aquifer	18	11	-3.9±1.2	-5.6±0.6	-1.7±1.3
Egypt	Nubian aquifer	29	26	-8.6±2.0	-10.4±0.3	-1.9±2.1
Mali	Mali aquifer	-7	15	-5.2±0.7	-6.5±0.5	-1.4±0.9
Morocco	Souss Plain	-7	33	-6.2±0.9	-6.3±0.6	-0.1±1.1
Namibia	Omatako basin	18	-20	-8.6±0.7	-9.0±0.1	-0.4±0.7
Niger	Djardo-Bilma	13	19	-7.8±4.0	-8.1±0.3	-0.2±4.0
Niger	*Irhazer: CI	7	17	-5.1±1.8	-7.3±0.8	-2.3±2.0
Niger	*Iullemeden: CT	3	14	-4.5±0.9	-7.3±0.3	-2.9±0.9
Nigeria	*Chad basin	13	12	-4.0±0.8	-6.2±0.5	-2.2±1.0
Senegal	Senegalese CT	-16	15	-6.1±0.7	-6.0±0.5	0.1±0.8
S. Africa	*Uitenhage aquifer	25	-34	-4.7±0.2	-5.4±0.1	-0.8±0.2
Tunisia	Kairouan Plain	10	35	-5.5±0.3	-5.7±0.5	-0.2±0.6
Zimbabwe	*Zimbabwe aquifer	28	-20	-5.9±0.4	-6.9±0.3	-1.0±0.5
Kuwait	Al-Raudhatain and Damman aquifers	48	30	-2.7±0.4	-4.5±0.4	-1.8±0.6
Oman	Batinah coastal plain	58	24	-2.4±1.2	-1.6±0.6	0.9±1.3
Oman	*Najd aquifer	54	18	-1.5±2.4	-4.7±0.7	-3.2±2.5
Syria	*Aleppo basin	37	36	-4.5±0.2	-7.2±0.8	-2.7±0.8
Belgium	Ledo-Paniselian	4	51	-6.5±1.6	-7.0±0.2	-0.5±1.6
Czech Rep.	Sokolov aquifer	13	50	-9.1±0.1	-9.5±0.4	-0.4±0.4
Denmark	Ribe Formation	9	56	-7.9±0.1	-8.8±0.5	-0.8±0.5
France	*Bathonian coast	0	49	-6.6±0.1	-7.1±0.1	-0.5±0.2
France	*Lorraine sandstone	7	49	-8.9±0.0	-10.0±0.4	-1.0±0.4
France	Aquitaine basin	0	46	-5.7±0.2	-6.7±0.5	-1.0±0.6
Germany	*Benkerstein	11	49	-9.3±0.2	-10.5±0.1	-1.3±0.2
Hungary	*Great Hungarian Plain	21	48	-9.6±0.0	-11.3±0.5	-1.7±0.5
Hungary	*Pannonian basin	20	46	-9.3±0.4	-13.0±0.3	-3.7±0.5
Italy	*Emilia Romagna plain	11	45	-8.3±0.5	-10.3±0.6	-1.9±0.8
Israel <sup>x</sup>	Israel coastal aquifer	35	32	-4.8±0.4	-4.6±0.1	0.3±0.4
Israel	*Dead Sea rift valley	35	31	-4.7±0.1	-6.6±0.5	-1.8±0.6

Country	Aquifer	Lon.	Lat.	$\delta^{18}\text{O}_{\text{late-Holo.}}$	$\delta^{18}\text{O}_{\text{glacial}}$	$\Delta^{18}\text{O}_{\text{glacial}}$
Poland	*S. Poland carbonates	19	51	-10.2±0.4	-11.4±0.8	-1.3±0.9
Poland	*Malm limestone	20	50	-10.2±0.4	-11.2±0.8	-1.0±0.9
Portugal	Sado basin	-9	38	-4.7±0.3	-4.7±0.1	0.0±0.3
Turkey	*Kazan Trona Ore Field	40	33	-9.3±0.8	-12.1±0.6	-2.8±1.0
U.K.	*Lincolnshire limestone	0	53	-7.8±0.1	-8.1±0.3	-0.3±0.3
U.K.	Chalk aquifer	-1	51	-7.4±0.0	-7.6±0.2	-0.2±0.2
Brazil	Potiguar basin: Acu	-37	-6	-1.8±1.2	-4.5±0.3	-2.7±1.3
Brazil	Botacatu: central	-49	-22	-8.9±1.4	-8.3±1.0	0.6±1.7
U.S.A.	*Columbia Flood Bslts	-119	47	-15.3±0.9	-18.0±0.6	-2.8±1.1
U.S.A.	*Idaho Batholith	-116	44	-16.5±0.7	-17.5±0.5	-1.0±0.8
U.S.A.	*San Juan Basin	-108	36	-12.0±0.6	-14.5±0.8	-2.5±1.0
U.S.A.	Mahomet aquifer	-89	40	-6.8±0.2	-7.2±0.5	-0.3±0.6
U.S.A.	*High Plains: Central	-101	38	-9.3±1.6	-12.0±0.9	-2.7±1.8
U.S.A.	*High Plains: South	-102	35	-6.3±0.7	-8.7±1.2	-2.4±1.3
U.S.A.	Aquia aquifer	-77	39	-7.0±0.2	-7.1±0.3	-0.1±0.4
U.S.A.	*Floridan aquifer	-82	32	-4.7±0.2	-3.7±0.4	1.0±0.4
Russia	Bykovsky Peninsula	129	72	-25.4	-30.8±1.3	-5.4±1.3
Canada	*Near Dawson City	-139	64	-26.1±0.8	-31.5±0.4	-5.5±0.9

103 \* aquifers where  $\delta^{18}\text{O}_{\text{late-Holocene}}$  values are statistically distinct ( $p < 0.05$ ) from  $\delta^{18}\text{O}_{\text{late-glacial}}$  values  
104 (two tailed heteroscedastic t-test comparing  $\delta^{18}\text{O}_{\text{late-Holo.}}$  values with  $\delta^{18}\text{O}_{\text{late-glacial}}$  values). 34 of  
105 57 (60%) groundwater records show a significant change in  $\delta^{18}\text{O}$  from the late-Holocene (<5,000  
106 calendar years before present) to the latter half of the last glacial period (>20,000 calendar years  
107 before present). Of the 34 aquifers having significant ( $p < 0.05$ ) shifts between the late-Holocene  
108 and the last glacial period, 31 aquifers have a  $\Delta^{18}\text{O}_{\text{late-glacial}}$  values of less than zero (exceptions  
109 Bengal Basin (Bangladesh), Floridan Aquifer (USA) and the Cuddalore Sandstone (India)).

110 <sup>x</sup> Some samples show evidence of seawater intrusion and were excluded on the basis of total  
111 dissolved solids, where samples exceeding 2,000 mg/L were excluded.

112

113 **Table S4.** Speleothem  $\delta^{18}\text{O}$  change from the late-glacial to the late-Holocene

Cave	Cntry.	Reference	Lon.	Lat.	$\Delta^{18}\text{O}_{\text{late-glacial}}$	Corr. <sup>x</sup>
Gunung Buda	Borneo	Partin et al., 2007	114.8	4.0	+2.0±0.3	-0.9±0.2
Botuverá Cave	Brazil	Cruz et al., 2005; Wang et al., 2007	-49.2	-27.2	-0.7±0.4	-0.9±0.2
Dongge <sup>t</sup>	China	Dykoski et al., 2005; Yuan et al., 2004	108.1	25.3	+2.6±0.5	-0.9±0.2
Hulu <sup>*</sup>	China	Wang et al., 2001	119.2	32.5	+1.6±0.3	-1.0±0.2
Jiuxian <sup>t</sup>	China	Cai et al., 2010	109.1	33.6	+1.3±1.9	-1.0±0.2
Yaman <sup>t</sup>	China	Yang et al., 2010	107.9	24.5	+2.7±0.5	-0.9±0.2
Soreq	Israel	Bar-Matthews et al., 2003	35.0	31.5	+2.3±0.2	-1.0±0.1
Peqin <sup>*</sup>	Israel	Bar-Matthews et al., 2003	35.2	32.6	+2.0±0.5	-0.9±0.2
Jerusalem W	Israel	Frumkin et al., 1999	35.2	31.7	+1.8±0.6	-1.0±0.2
NW South Island	New Zealand	Williams et al., 2010	172.0	-42.0	+0.4±0.2	-1.0±0.3
Cold Air Cave	South Africa	Holmgren et al., 2003	29.1	-24.0	+1.2±0.5	-1.0±0.1
Sofular	Turkey	Fleitmann et al., 2009	31.9	41.4	-4.7±0.2	-1.0±0.2
Fort Stanton <sup>*</sup>	U.S.A.	Asmerom et al., 2010	-105.3	33.3	-2.0±1.0	-1.0±0.2
Cave of the bells <sup>*</sup>	U.S.A.	Wagner et al., 2010	-110.8	31.8	-2.4±0.2	-1.0±0.2
Moomi <sup>*</sup>	Yemen	Shakun et al., 2007	54.0	12.5	+2.2±0.6	-0.9±0.2

114 <sup>\*</sup> early Holocene value used (i.e., shift likely larger than shown)

115 <sup>t</sup> values from 15.0 ka used

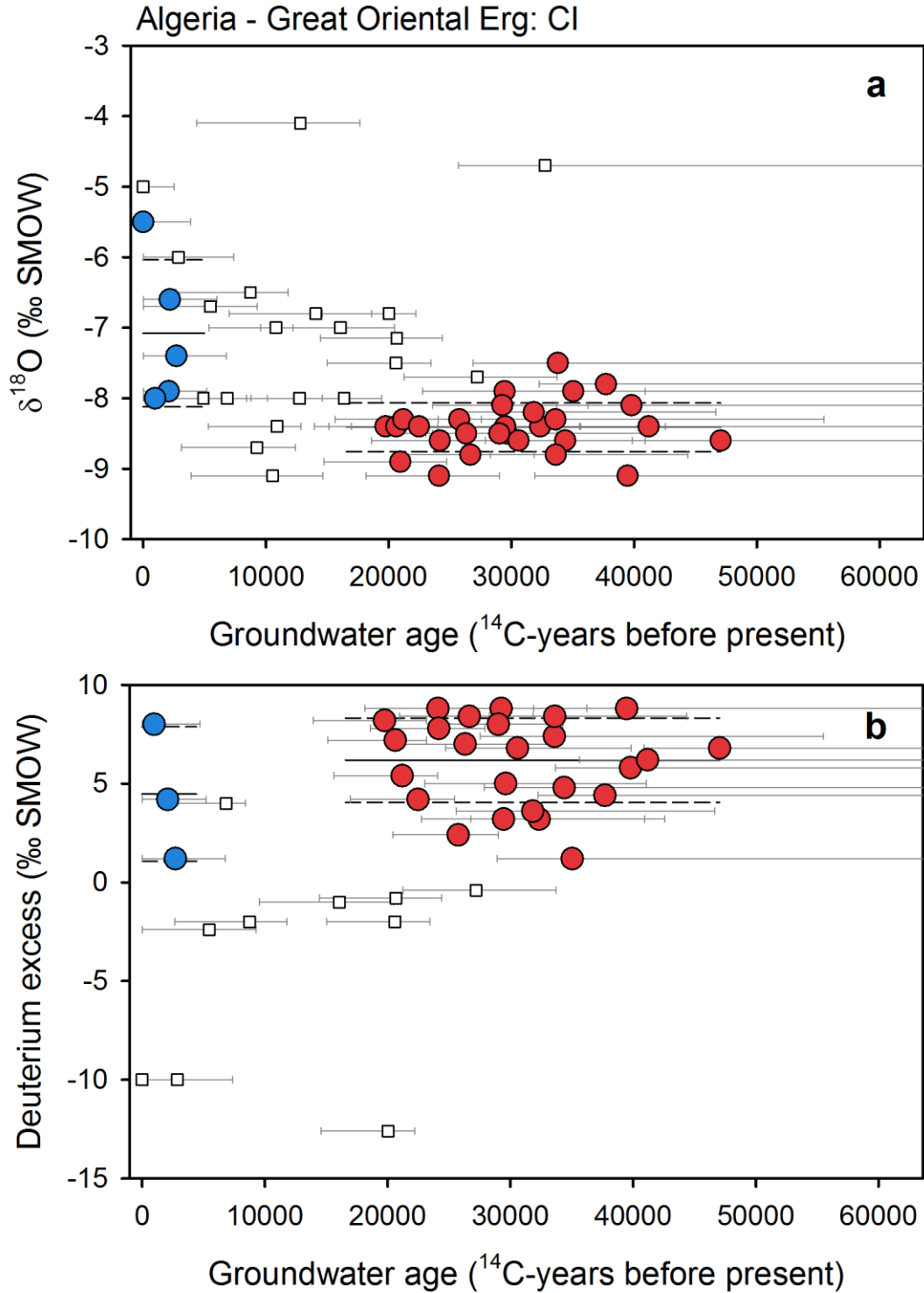
116 <sup>x</sup> Calcite-water fractionation correction subtracted from raw observed  $\Delta^{18}\text{O}_{\text{late-glacial}}$  to correct for  
 117 the 4.0±0.8 °C colder climate (Annan and Hargreaves, 2013) at the last glacial stage (from  
 118 O'Neil et al., 1969; modern temperatures from New et al., 2002;  $\Delta^{18}\text{O}_{\text{late-glacial}}$  values in  
 119 preceding column are shown in raw (i.e, uncorrected) form.

120

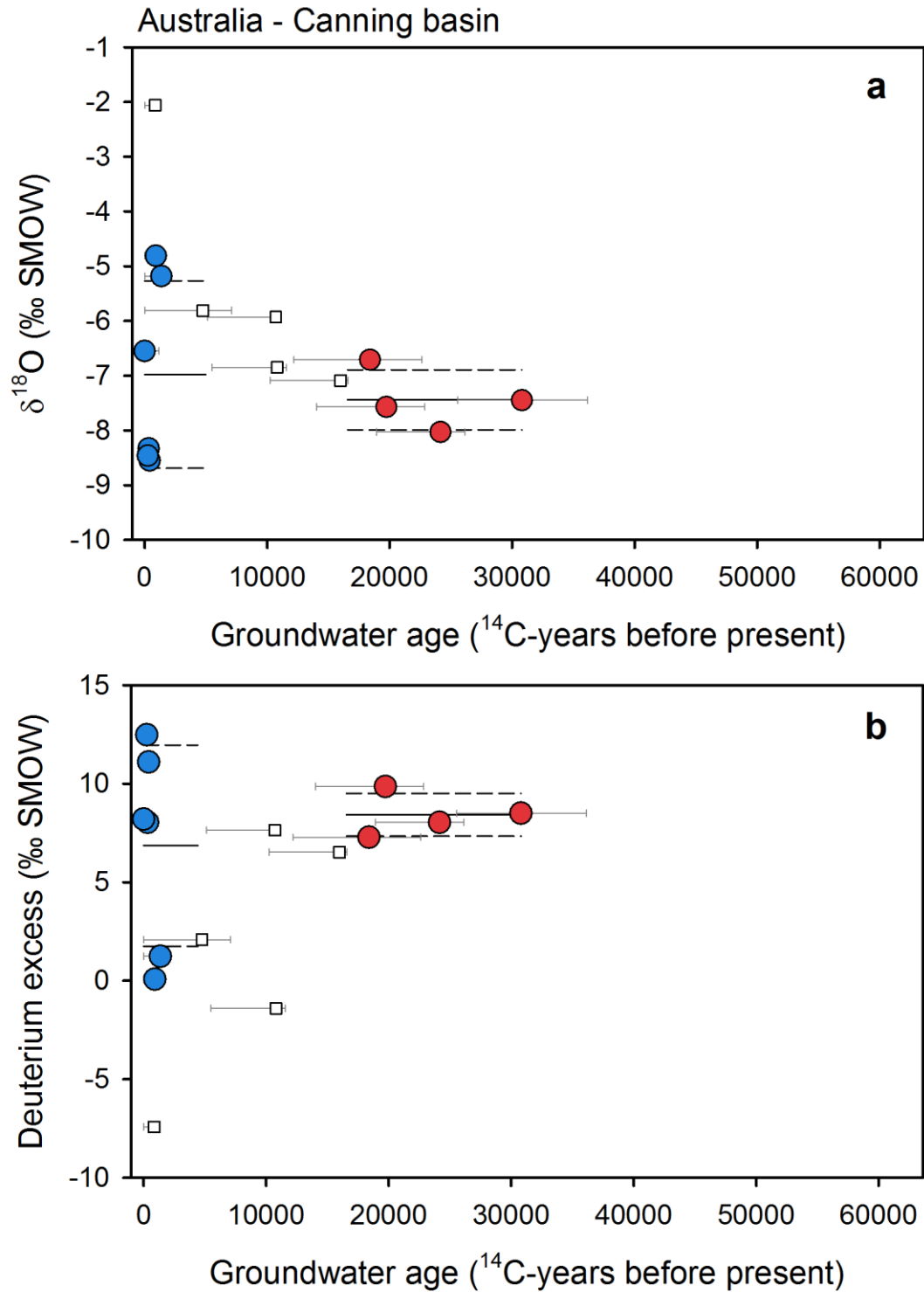
121 **Table S5.** Ice core  $\delta^{18}\text{O}$  change from the late-glacial to the late-Holocene

Ice core	Country	Reference	Lon.	Lat.	$\Delta^{18}\text{O}_{\text{late-glacial}}$
Sajama	Bolivia	Thompson et al., 1998	-68.8	-18.1	-4.6±1.0
Huascarán	Peru	Thompson et al., 1995	-77.6	-9.1	-6.3±1.3
Qinghai-Tibetan	Tibet	Thompson et al., 1997	81.5	35.3	-0.6±2.8
Devon Island	Canada	Patterson et al., 1977	-82.3	75.3	-4.7±2.4
TALD Ice	Antarctica	Buiron et al., 2011	159.2	-72.8	-4.0±0.7
Byrd Glacier	Antarctica	Blunier and Brook, 2001	-119.5	-80.0	-5.9±0.9
Dome Fuji	Antarctica	Kawamura et al. 2007	39.7	-77.3	-3.6±0.9
Dronning Maud	Antarctica	EPICA Community, 2006	2.0	-75.0	-5.2±1.0
Law Dome	Antarctica	Pedro et al. 2011	112.8	-66.8	-6.7±0.7
Siple Dome	Antarctica	Pedro et al. 2011	-148.8	-81.7	-7.1±1.0
Renland ice core	Greenland	Vinther et al., 2008	-27.0	71.0	-3.9±1.0
NGRIP1	Greenland	Vinther et al., 2006	-42.3	75.1	-7.0±1.9

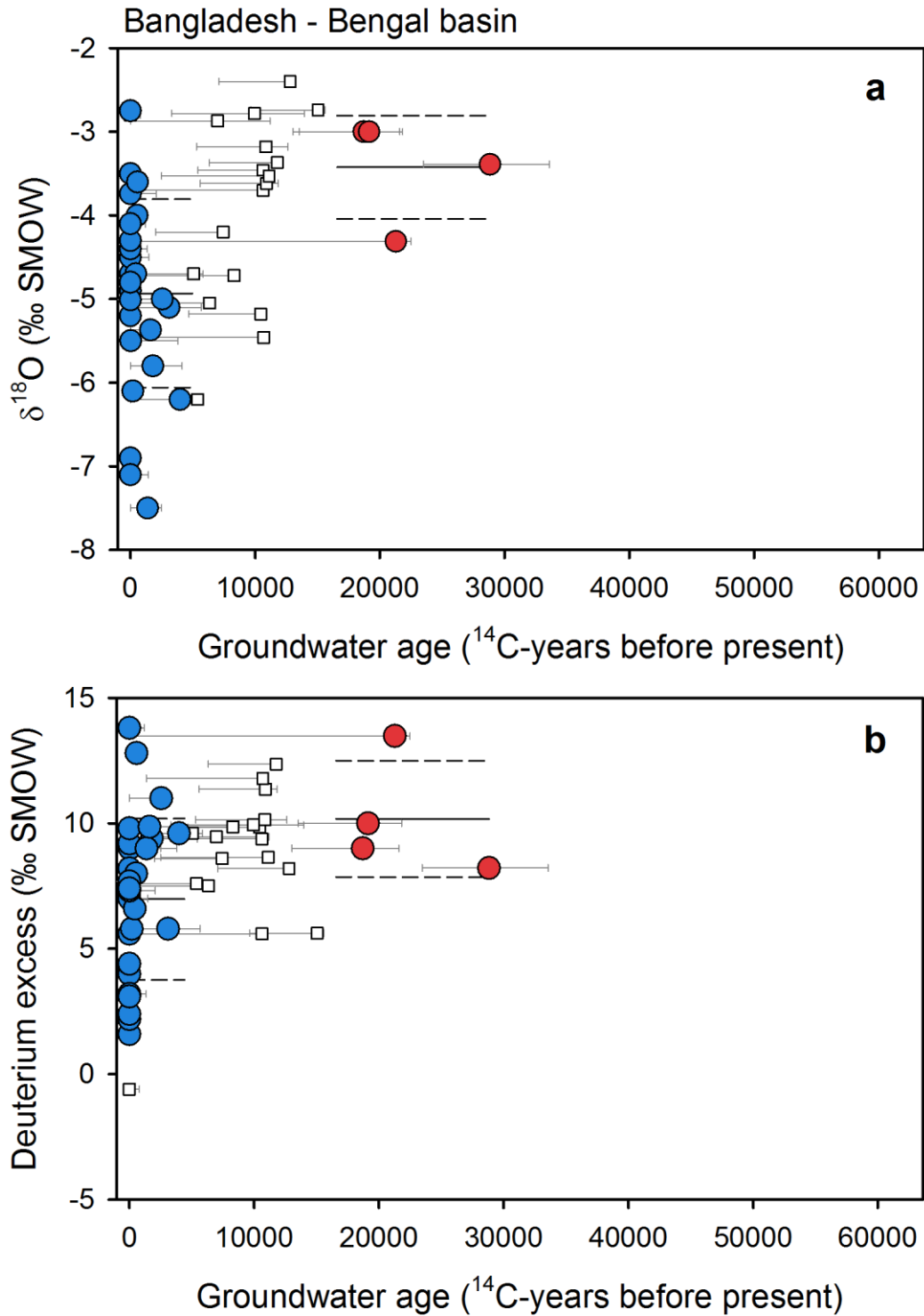
122



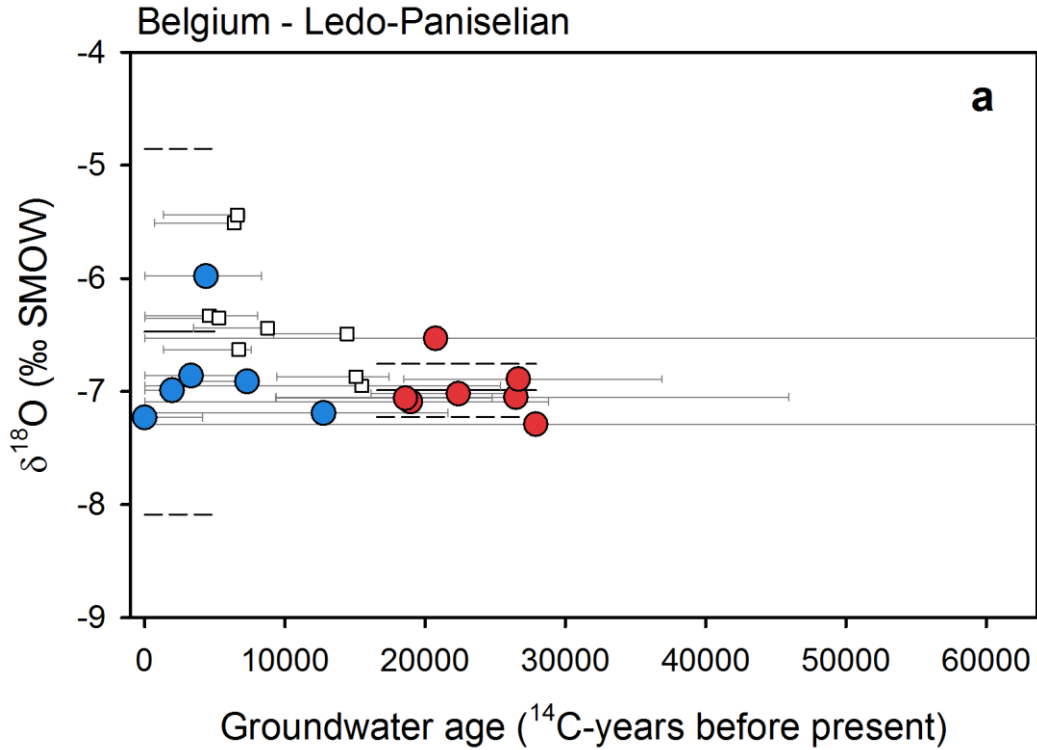
123  
 124 **Figure S1.** Groundwater isotope composition of the Great Oriental Erg (Continental Intercalaire)  
 125 aquifer. Groundwater  $\delta^{18}\text{O}$  (a) and deuterium excess (b) plotted against corrected  $^{14}\text{C}$  ages for  
 126 late-Holocene (blue circles) and late-glacial (red circles) groundwaters. Lines mark the average  
 127 (solid line) and one standard deviation (dashed lines) for each age group (Edmunds et al., 2004).



128  
 129 **Figure S2.** Groundwater isotope composition of the Canning basin. Groundwater δ<sup>18</sup>O (a) and  
 130 deuterium excess (b) plotted against corrected <sup>14</sup>C ages for late-Holocene (blue circles) and late-  
 131 glacial (red circles) groundwaters. Lines mark the average (solid line) and one standard deviation  
 132 (dashed lines) for each age group (Harrington et al., 2011).

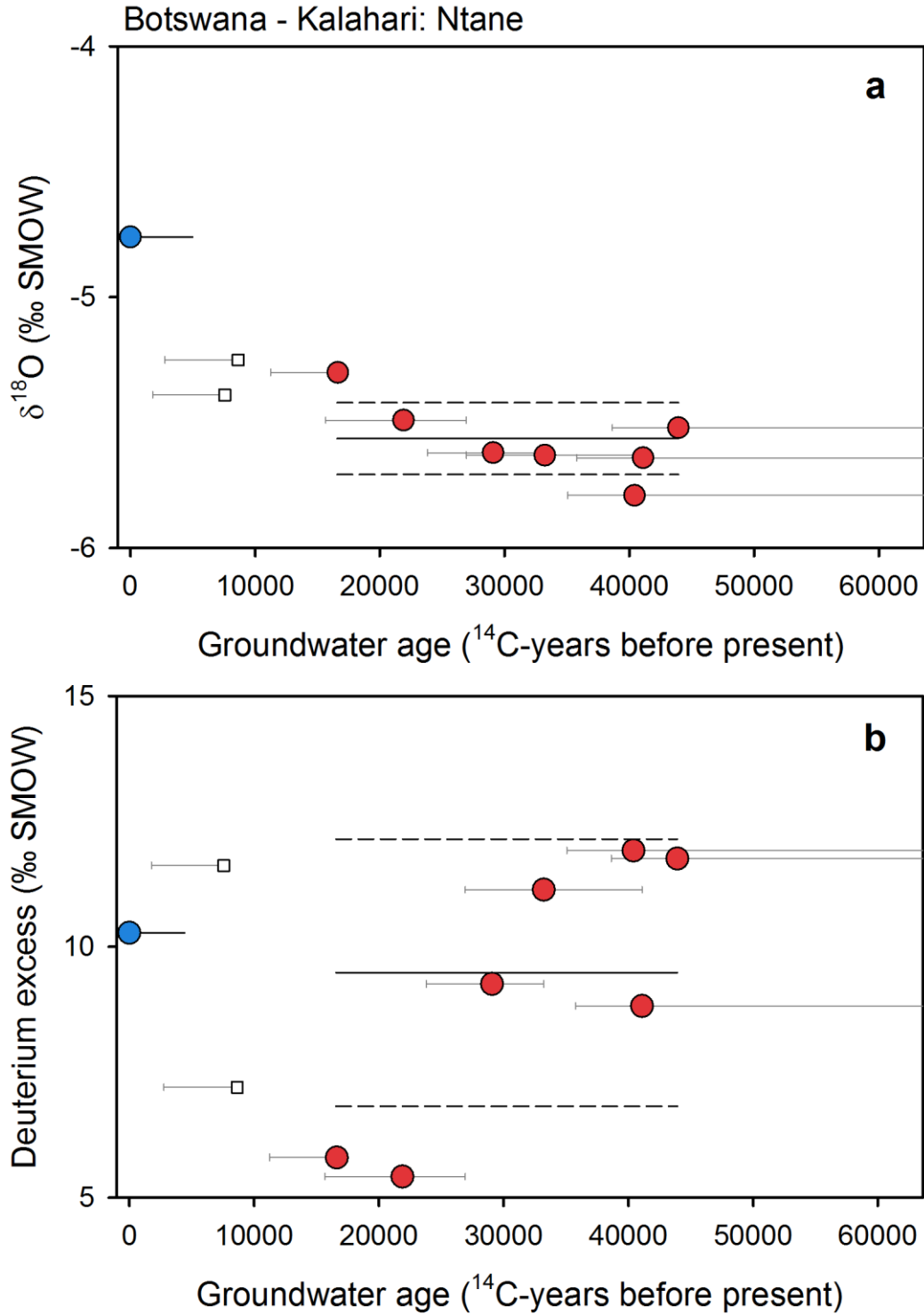


133  
 134 **Figure S3.** Groundwater isotope composition of the Bengal basin. Groundwater  $\delta^{18}\text{O}$  (a) and  
 135 deuterium excess (b) against corrected  $^{14}\text{C}$  ages for late-Holocene (blue circles) and late-glacial  
 136 (red circles) groundwaters. Lines mark average (solid line) and 1 s.d. (dashed lines) for each  
 137 group (Aggarwal et al., 2000; Sikdar and Sahu, 2009; Majumder et al., 2011; Hoque and  
 138 Burgess, 2012).

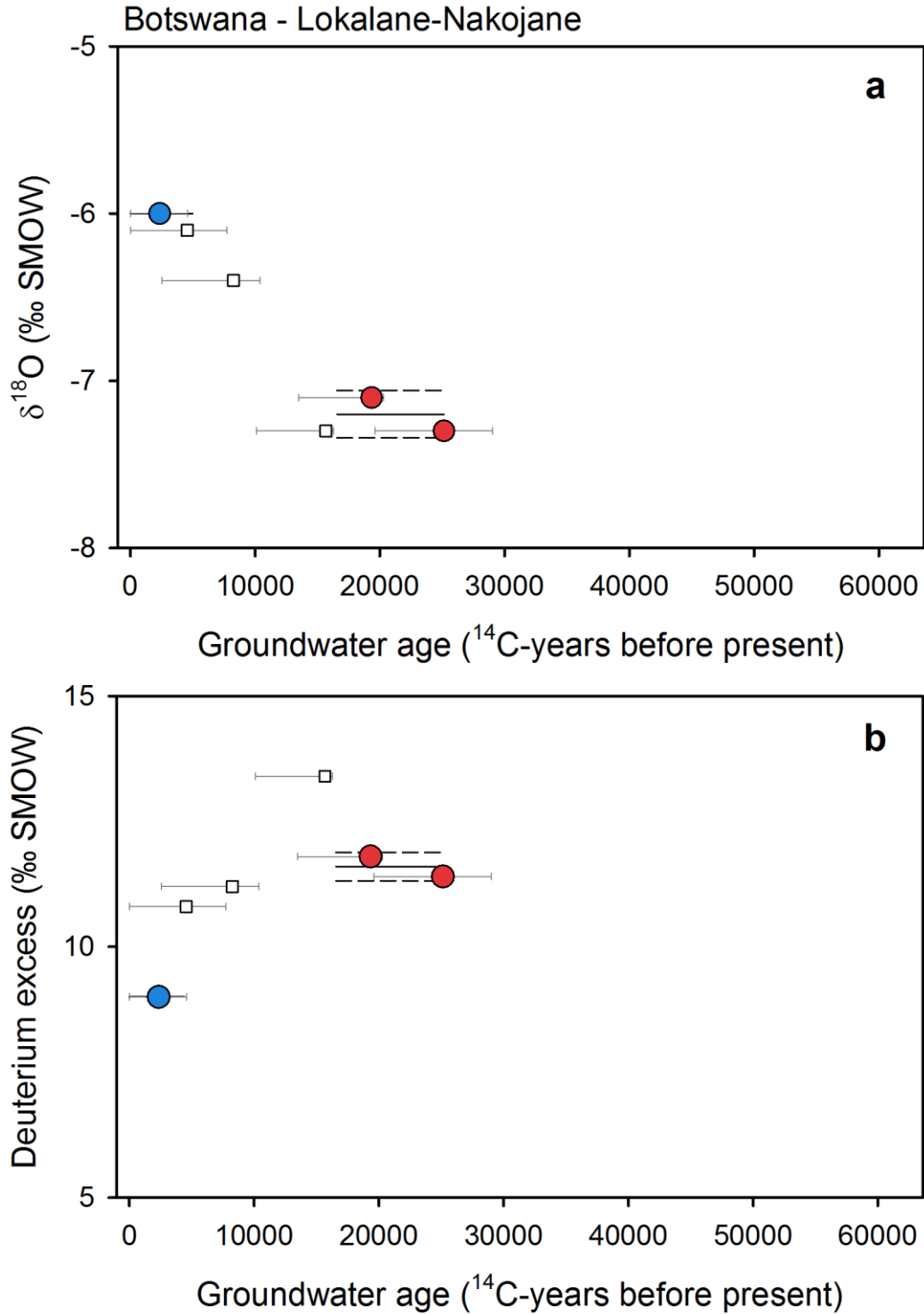


139

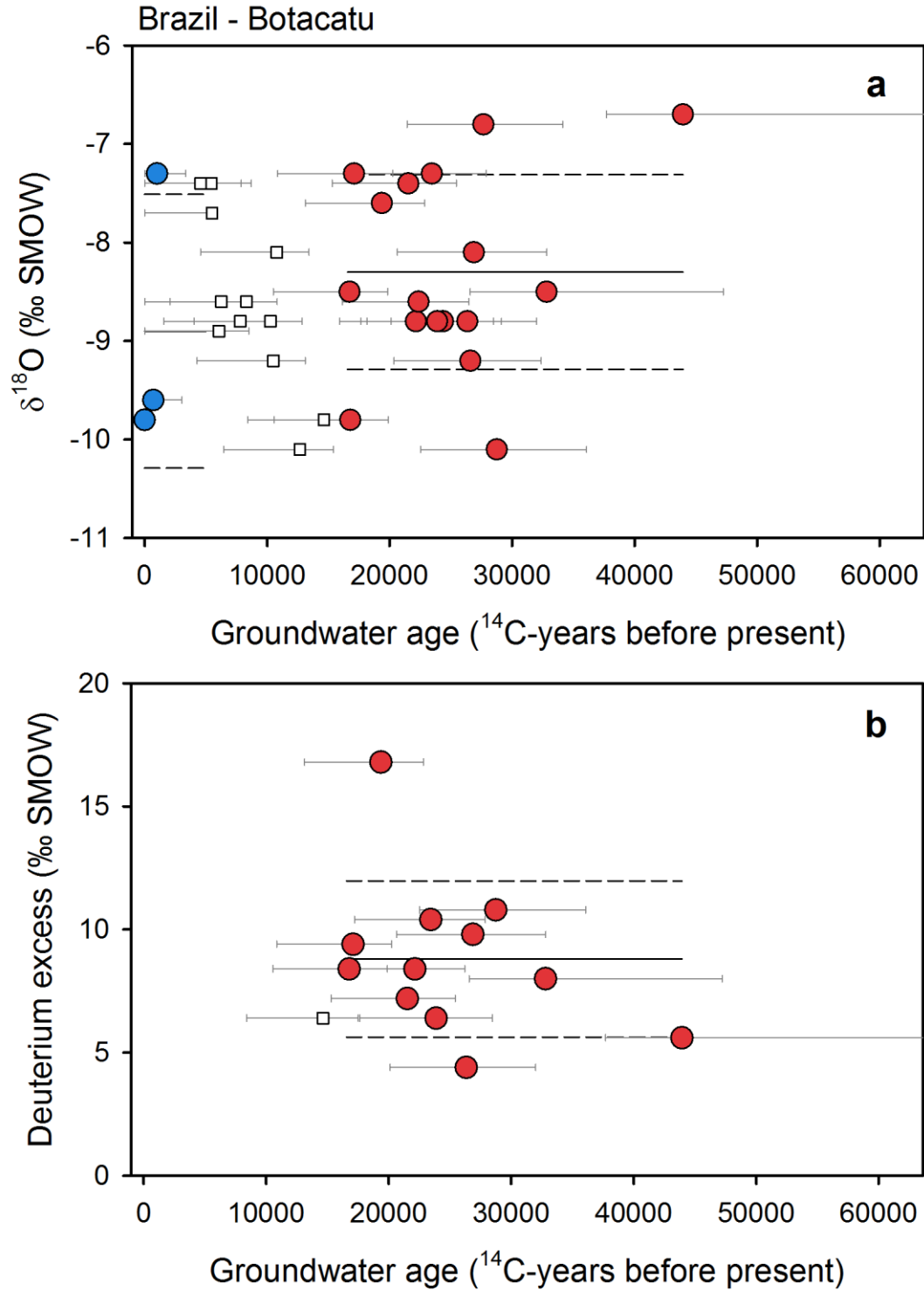
140 **Figure S4.** Groundwater isotope composition of the Ledo-Paniselian aquifer. Groundwater  $\delta^{18}\text{O}$   
 141 plotted against corrected  $^{14}\text{C}$  ages for late-Holocene (blue circles) and late-glacial (red circles)  
 142 groundwaters. Lines mark the average (solid line) and one standard deviation (dashed lines) for  
 143 each age group (Walraevens, 1990; Walraevens et al., 2001).



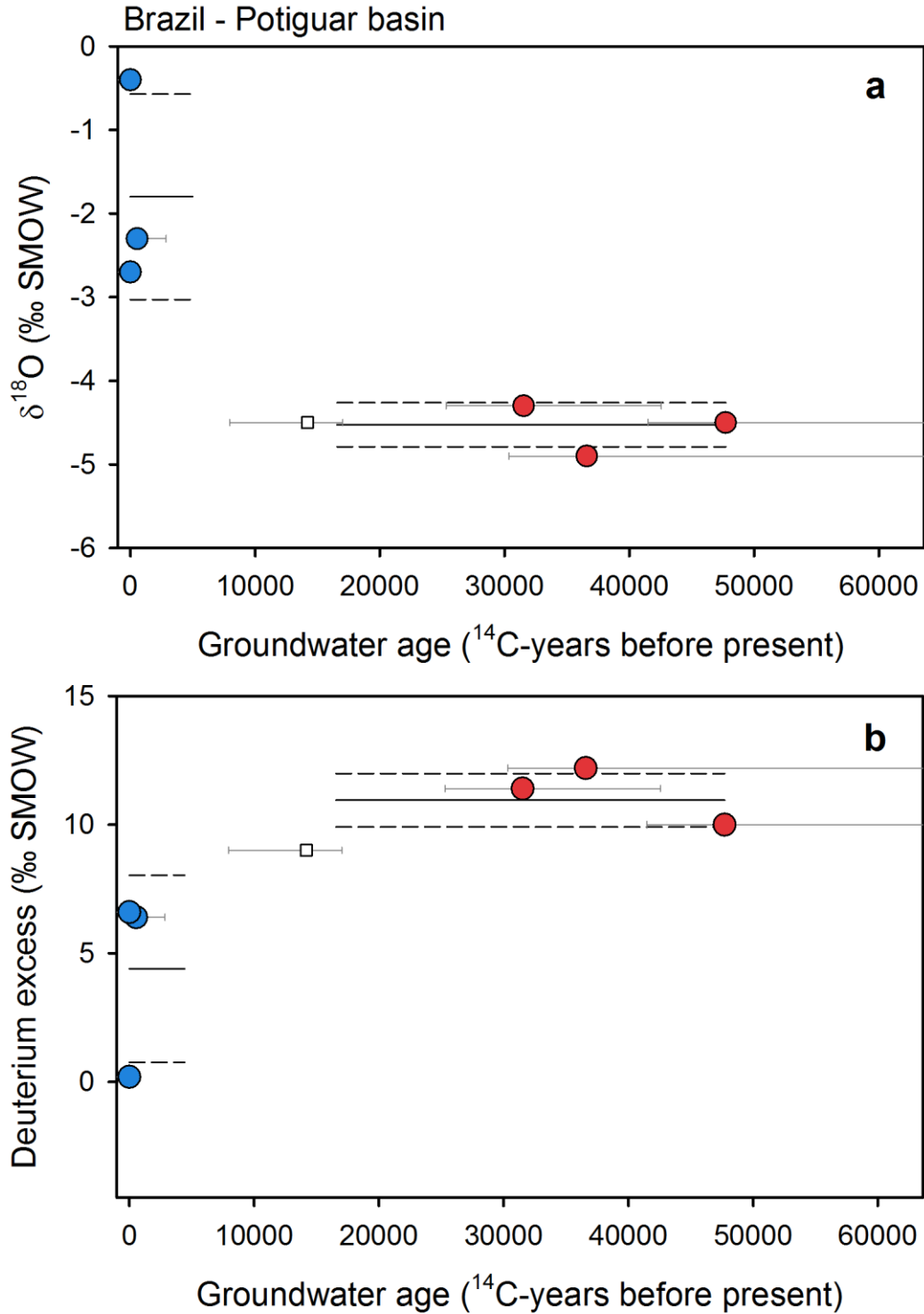
144  
 145 **Figure S5.** Groundwater isotope composition of the Ntane Sandstone aquifer. Groundwater  $\delta^{18}\text{O}$   
 146 (a) and deuterium excess (b) plotted against corrected  $^{14}\text{C}$  ages for late-Holocene (blue circles)  
 147 and late-glacial (red circles) groundwaters. Lines mark the average (solid line) and one standard  
 148 deviation (dashed lines) for each age group (Kulongoski et al., 2004).



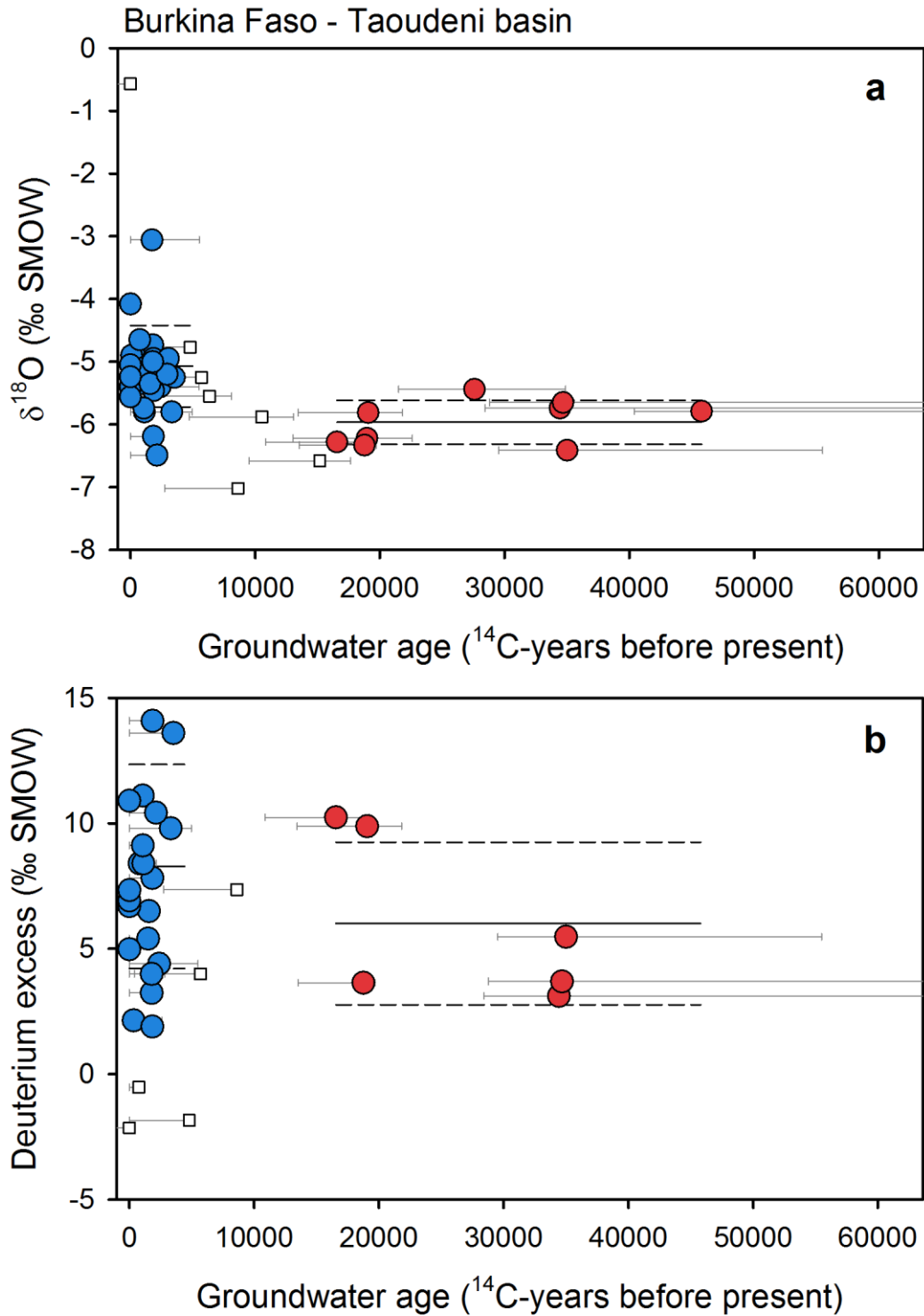
149  
 150 **Figure S6.** Groundwater isotope composition of the Lokelane-Nakojane aquifer. Groundwater  
 151  $\delta^{18}\text{O}$  (a) and deuterium excess (b) plotted against corrected  $^{14}\text{C}$  ages for late-Holocene (blue  
 152 circles) and late-glacial (red circles) groundwaters. Lines mark the average (solid line) and one  
 153 standard deviation (dashed lines) for each age group (Rahube, 2003).



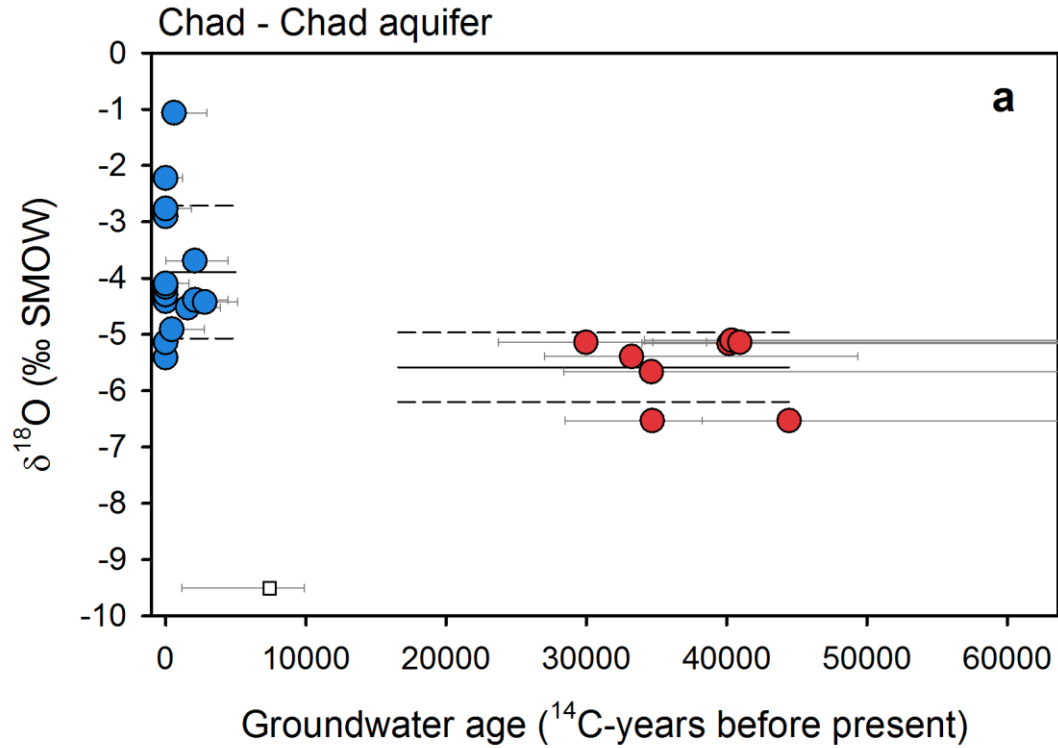
154  
 155 **Figure S7.** Groundwater isotope composition of the Botacatu aquifer system. Groundwater  $\delta^{18}\text{O}$   
 156 (a) and deuterium excess (b) plotted against corrected  $^{14}\text{C}$  ages for late-Holocene (blue circles)  
 157 and late-glacial (red circles) groundwaters. Lines mark the average (solid line) and one standard  
 158 deviation (dashed lines) for each age group (Gouvea da Silva, 1983).



159  
 160 **Figure S8.** Groundwater isotope composition of the Potiguar basin. Groundwater  $\delta^{18}\text{O}$  (a) and  
 161 deuterium excess (b) plotted against corrected  $^{14}\text{C}$  ages for late-Holocene (blue circles) and late-  
 162 glacial (red circles) groundwaters. Lines mark the average (solid line) and one standard deviation  
 163 (dashed lines) for each age group (Salati et al., 1974).

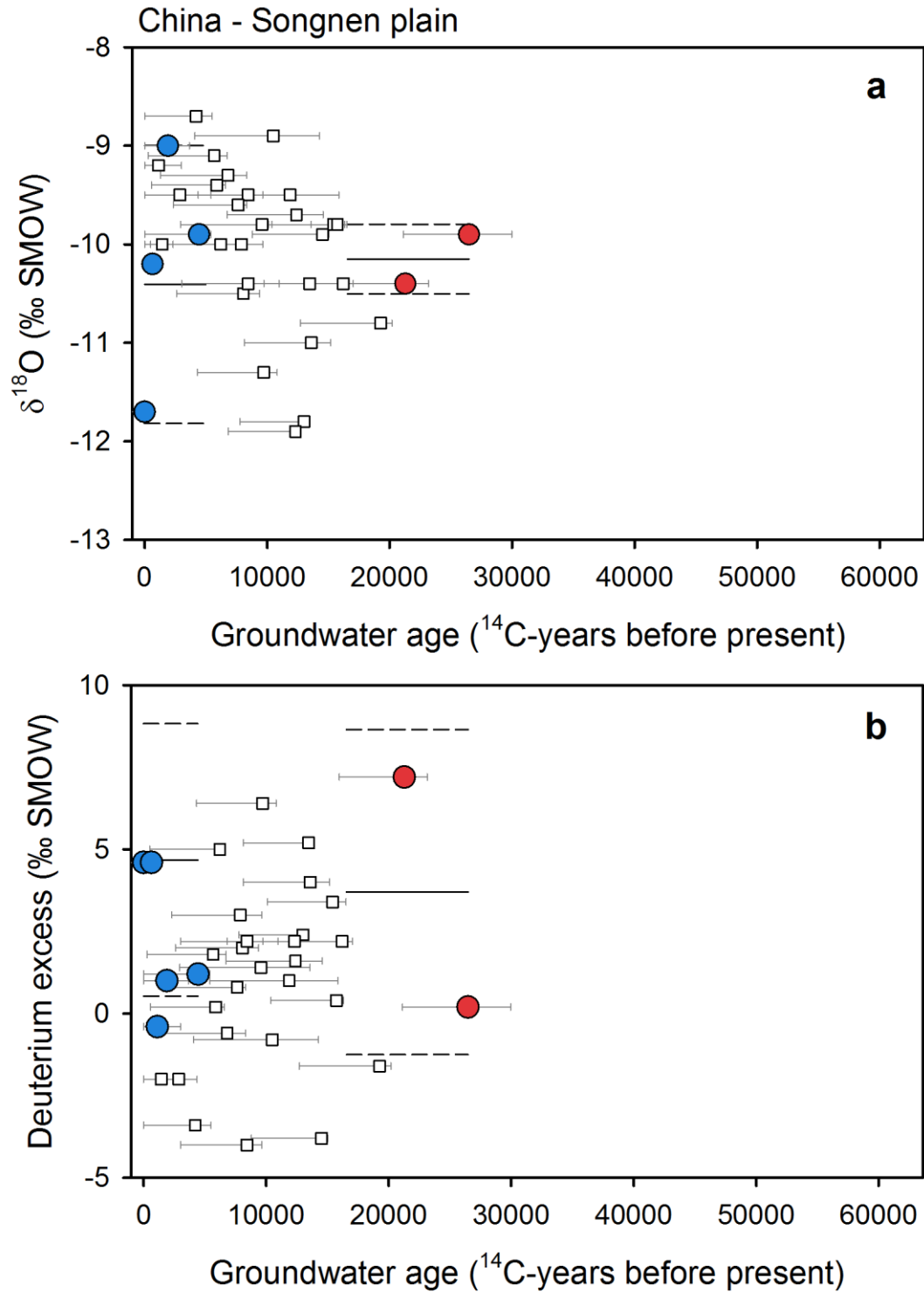


164  
 165 **Figure S9.** Groundwater isotope composition of the Taoudeni basin. Groundwater  $\delta^{18}\text{O}$  (a) and  
 166 deuterium excess (b) plotted against corrected  $^{14}\text{C}$  ages for late-Holocene (blue circles) and late-  
 167 glacial (red circles) groundwaters. Lines mark the average (solid line) and one standard deviation  
 168 (dashed lines) for each age group (Huneau et al., 2011).

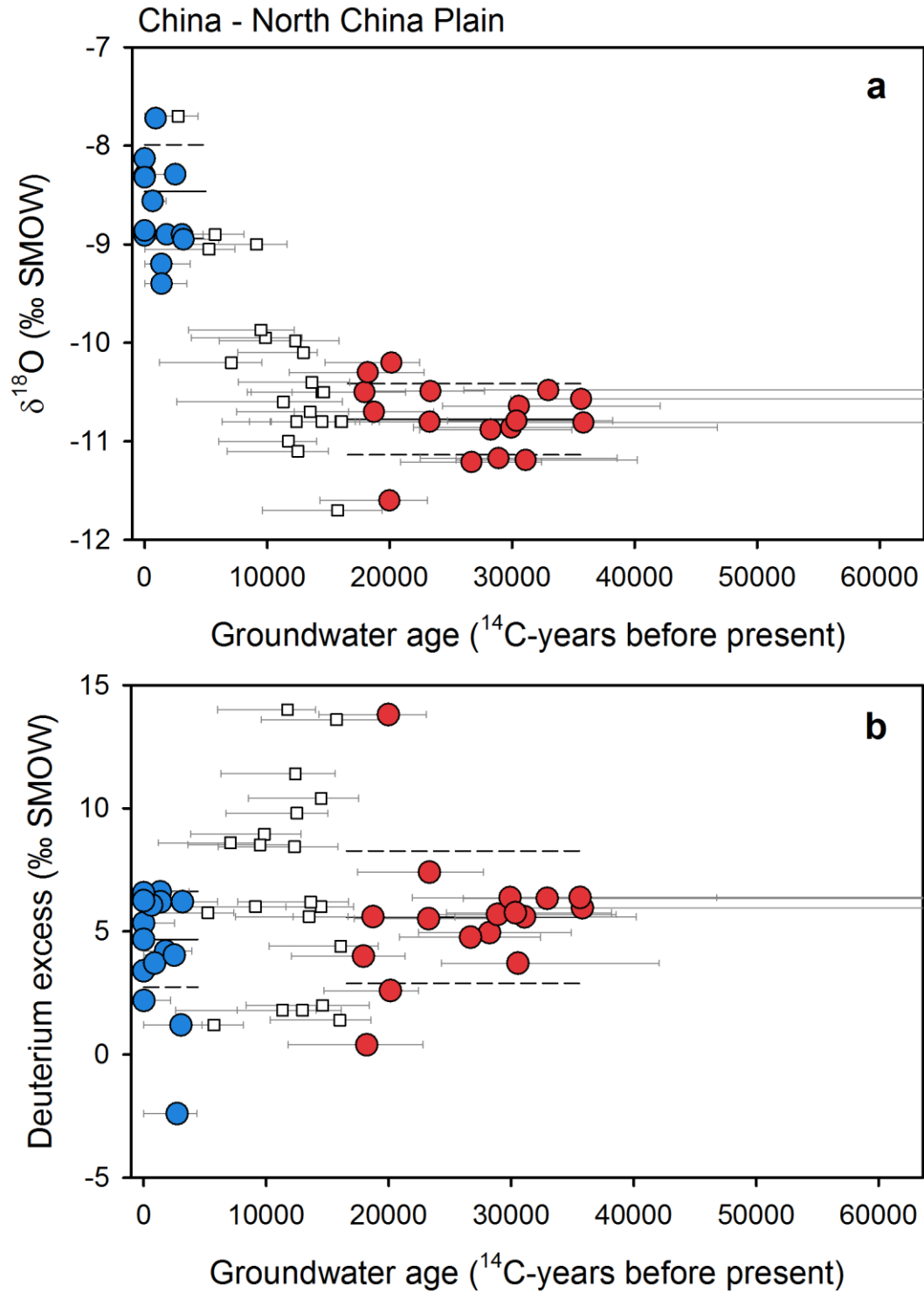


169

170 **Figure S10.** Groundwater isotope composition of the Chad aquifer (in Chad). Groundwater  $\delta^{18}\text{O}$   
 171 plotted against corrected  $^{14}\text{C}$  ages for late-Holocene (blue circles) and late-glacial (red circles)  
 172 groundwaters. Lines mark the average (solid line) and one standard deviation (dashed lines) for  
 173 each age group (Edmunds, 2009).

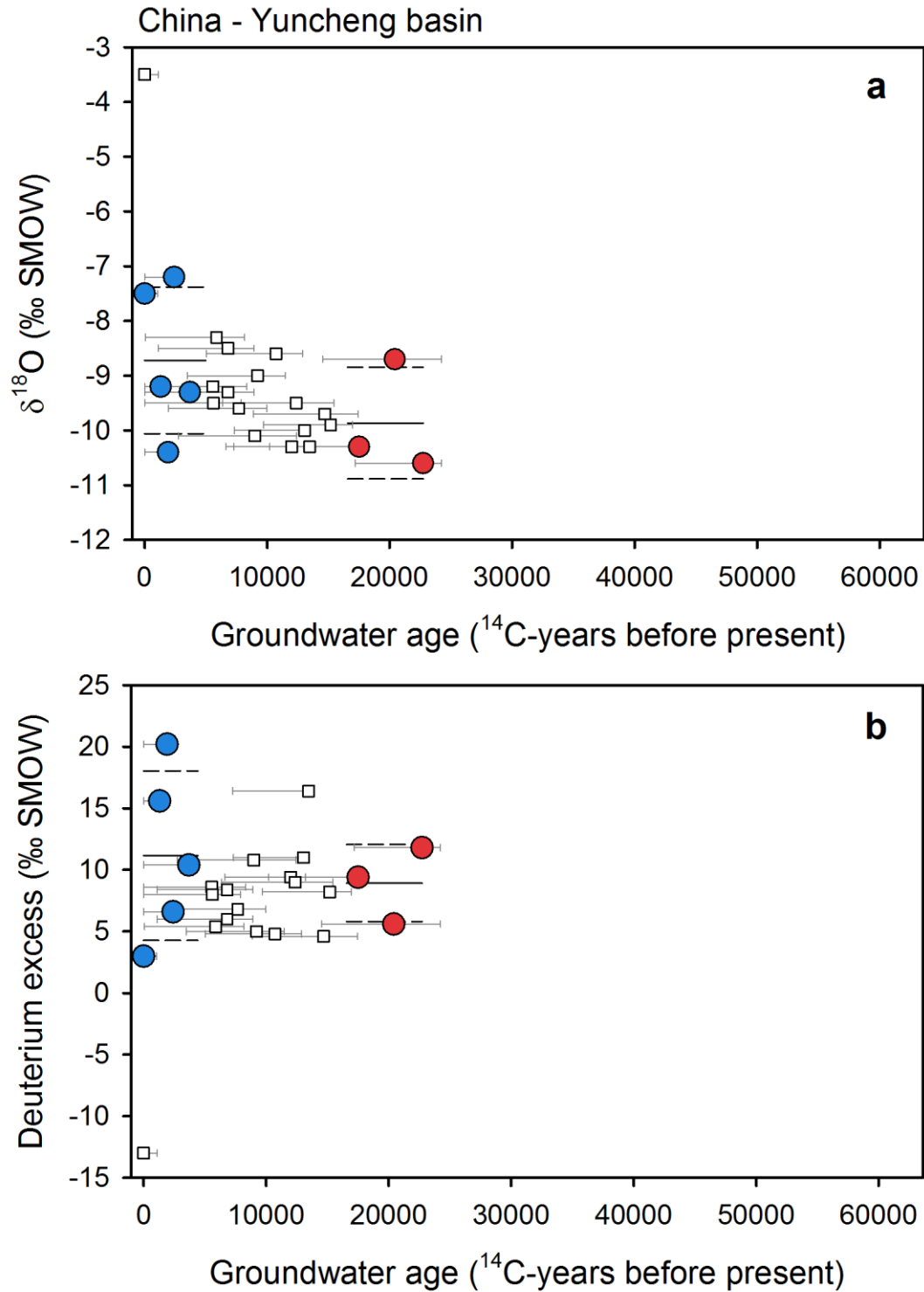


174  
 175 **Figure S11.** Groundwater isotope composition of the Songnen Plain. Groundwater  $\delta^{18}\text{O}$  (a) and  
 176 deuterium excess (b) plotted against corrected  $^{14}\text{C}$  ages for late-Holocene (blue circles) and late-  
 177 glacial (red circles) groundwaters. Lines mark the average (solid line) and one standard deviation  
 178 (dashed lines) for each age group (Chen et al., 2011).

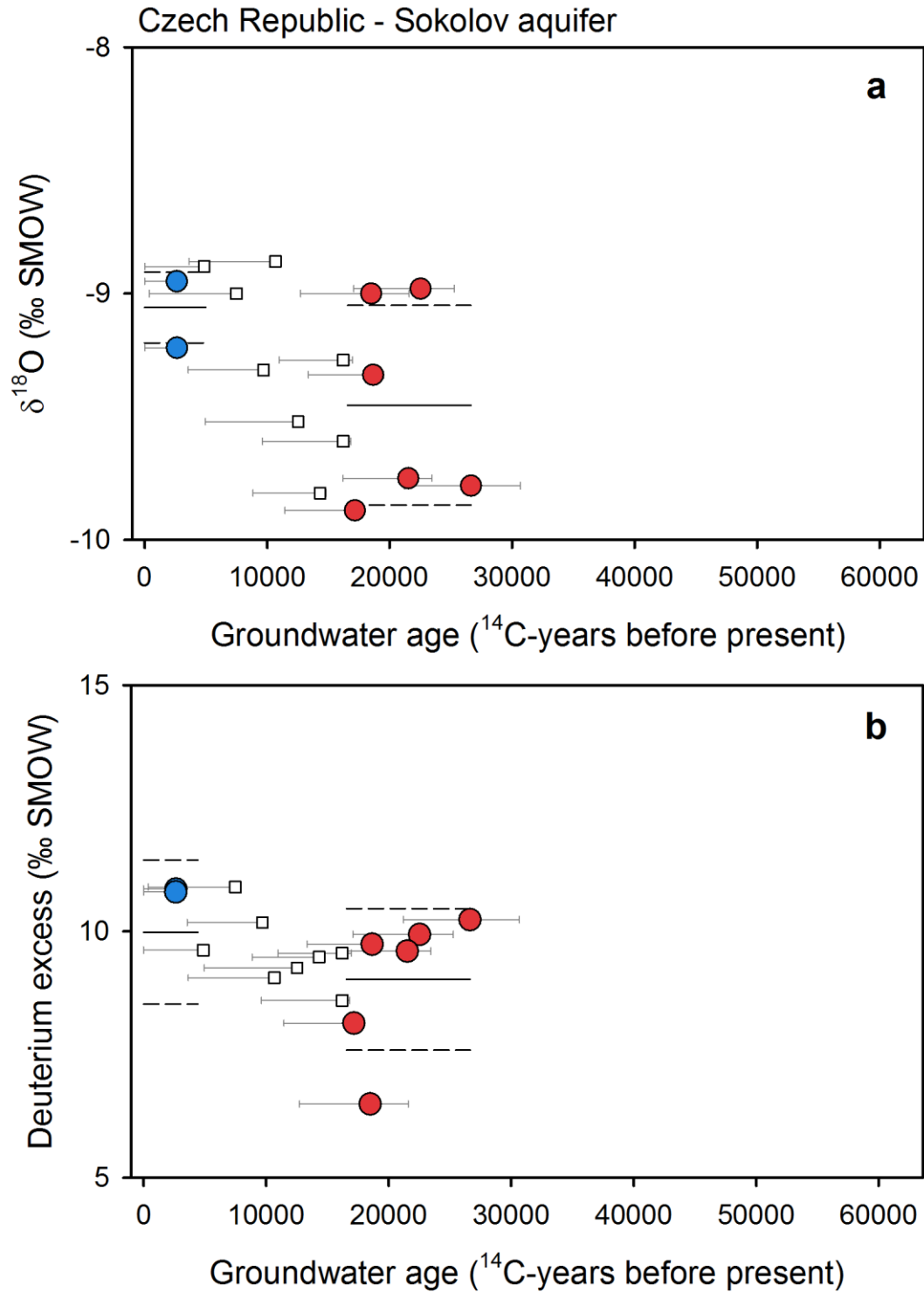


179

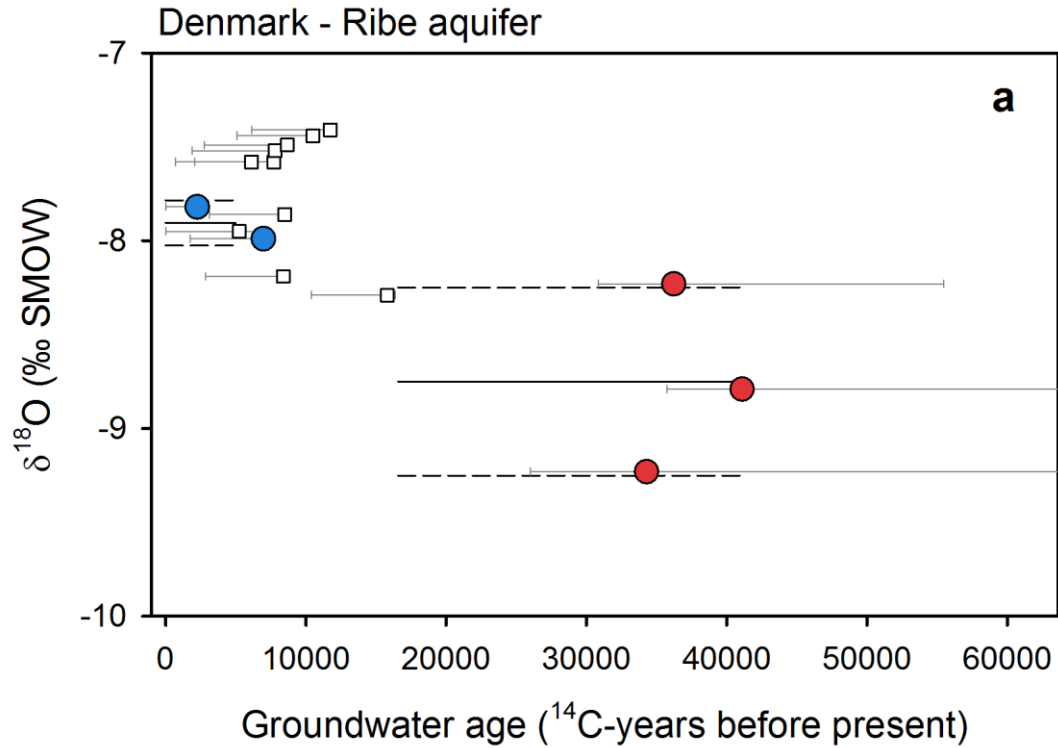
180 **Figure S12.** Groundwater isotope composition of the North China Plain. Groundwater  $\delta^{18}\text{O}$  (a)  
 181 and deuterium excess (b) plotted against corrected  $^{14}\text{C}$  ages for late-Holocene (blue circles) and  
 182 late-glacial (red circles) groundwaters. Lines mark the average (solid line) and one standard  
 183 deviation (dashed lines) for each age group (Zongyu et al., 2003; Kreuzer et al., 2009).



184  
 185 **Figure S13.** Groundwater isotope composition of the Yuncheng basin. Groundwater  $\delta^{18}\text{O}$  (a) and  
 186 deuterium excess (b) plotted against corrected  $^{14}\text{C}$  ages for late-Holocene (blue circles) and late-  
 187 glacial (red circles) groundwaters. Lines mark the average (solid line) and one standard deviation  
 188 (dashed lines) for each age group (Currell et al., 2010).

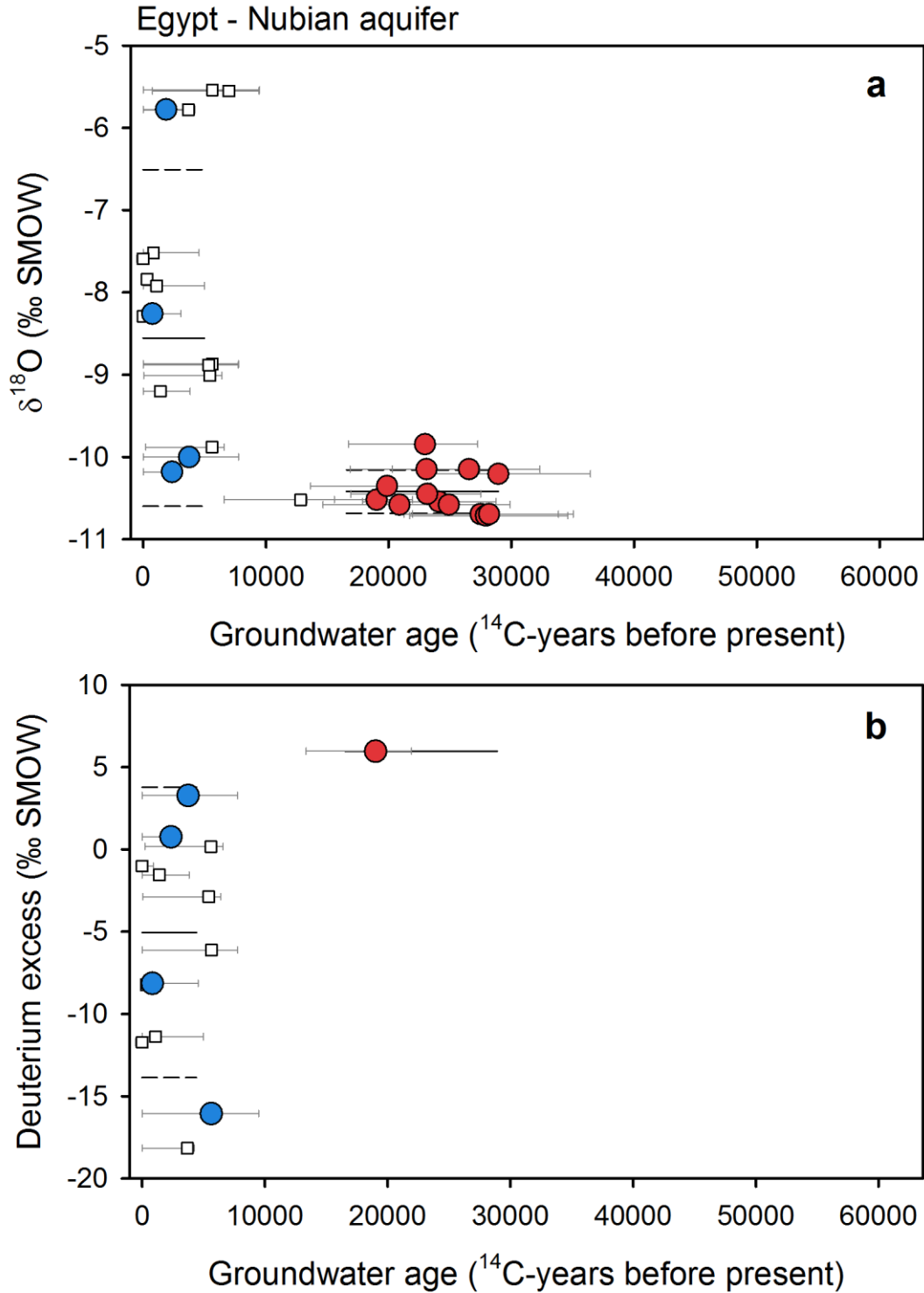


189  
 190 **Figure S14.** Groundwater isotope composition of the Sokolov aquifer. Groundwater  $\delta^{18}\text{O}$  (a) and  
 191 deuterium excess (b) plotted against corrected  $^{14}\text{C}$  ages for late-Holocene (blue circles) and late-  
 192 glacial (red circles) groundwaters. Lines mark the average (solid line) and one standard deviation  
 193 (dashed lines) for each age group (Noseck et al., 2009).

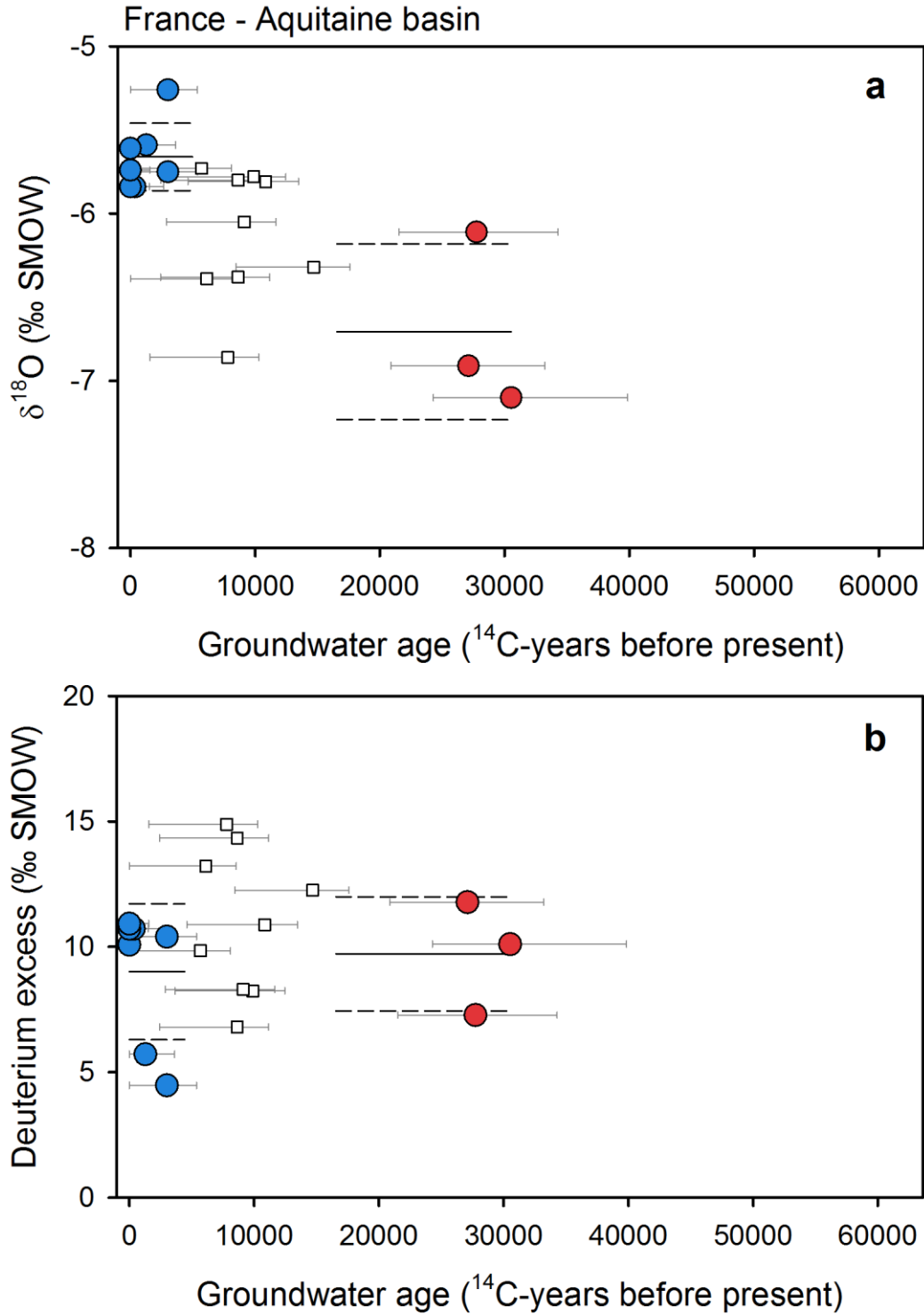


194

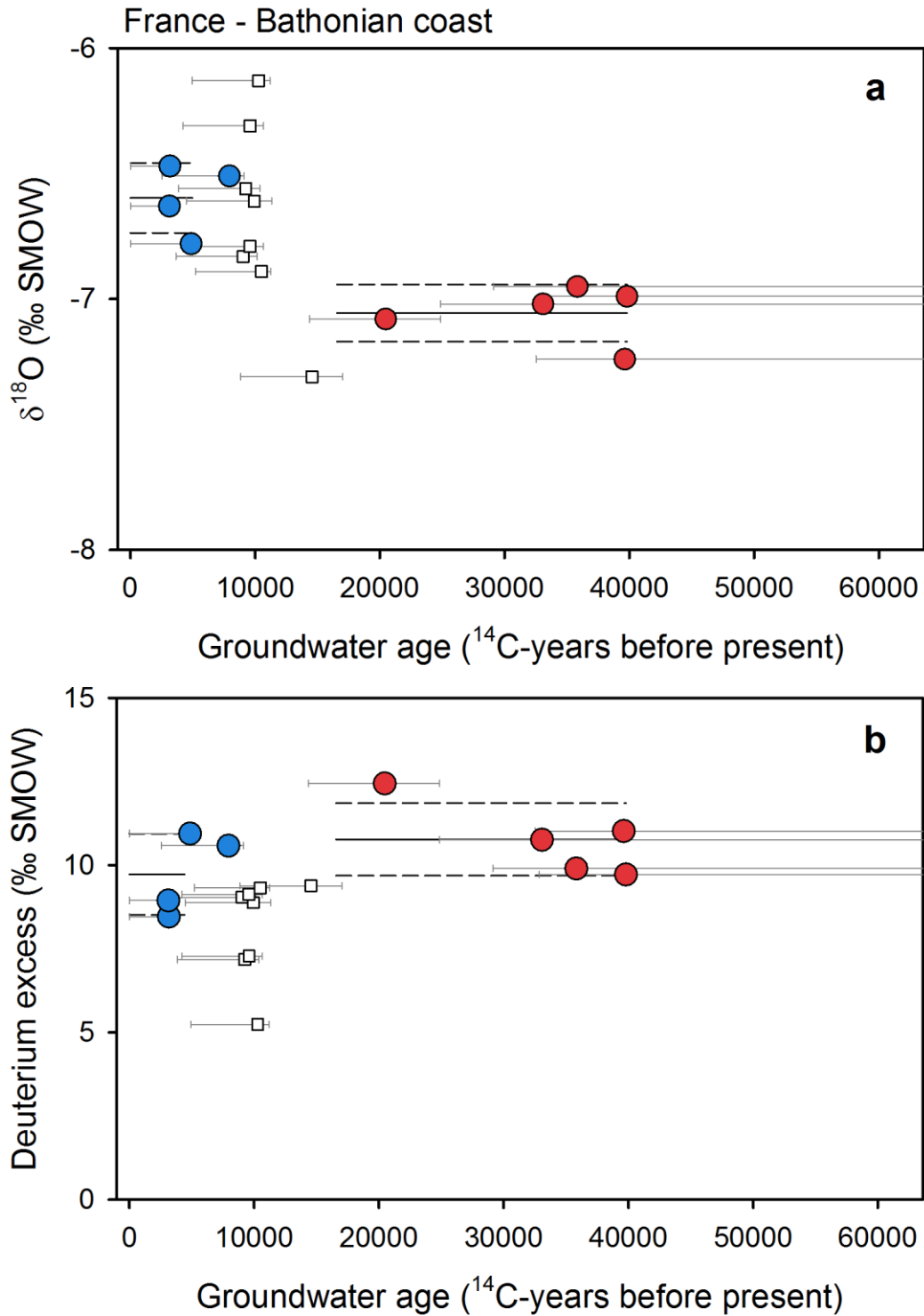
195 **Figure S15.** Groundwater isotope composition of the Ribe aquifer. Groundwater δ<sup>18</sup>O plotted  
 196 against corrected <sup>14</sup>C ages for late-Holocene (blue circles) and late-glacial (red circles)  
 197 groundwaters. Lines mark the average (solid line) and one standard deviation (dashed lines) for  
 198 each age group (Hinsby et al., 2001).



199  
 200 **Figure S16.** Groundwater isotope composition of the Nubian aquifer. Groundwater  $\delta^{18}\text{O}$  (a) and  
 201 deuterium excess (b) plotted against corrected  $^{14}\text{C}$  ages for late-Holocene (blue circles) and late-  
 202 glacial (red circles) groundwaters. Lines mark the average (solid line) and one standard deviation  
 203 (dashed lines) for each age group (Shehata and Al-Ruwaih, 1999; Patterson et al., 2005;  
 204 Edmunds, 2009).

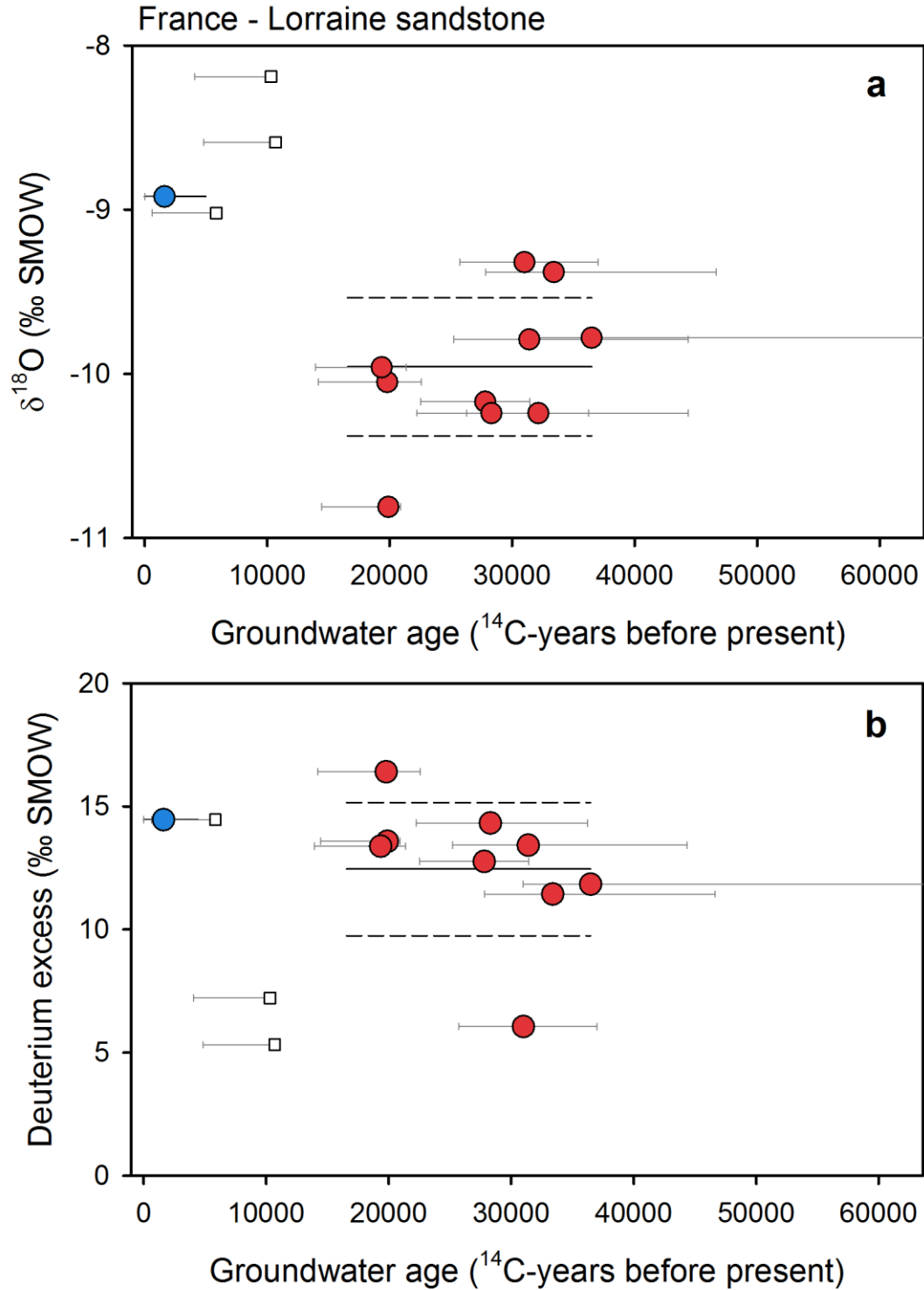


205  
 206 **Figure S17.** Groundwater isotope composition of the Aquitaine basin. Groundwater  $\delta^{18}\text{O}$  (a) and  
 207 deuterium excess (b) plotted against corrected  $^{14}\text{C}$  ages for late-Holocene (blue circles) and late-  
 208 glacial (red circles) groundwaters. Lines mark the average (solid line) and one standard deviation  
 209 (dashed lines) for each age group (Le Gal La Salle et al., 1996).



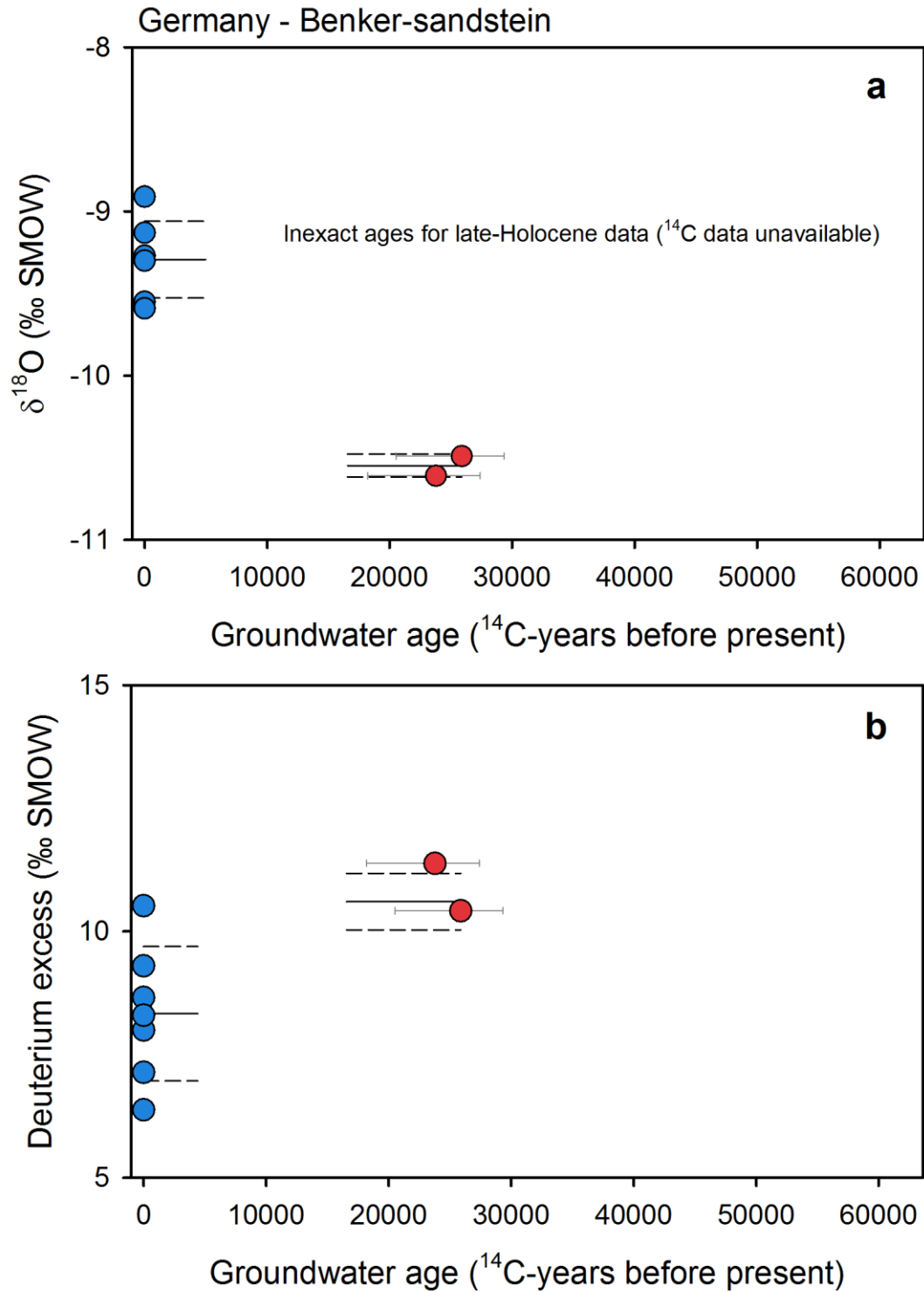
210

211 **Figure S18.** Groundwater isotope composition of the Bathonian coastal aquifer. Groundwater  
 212  $\delta^{18}\text{O}$  (a) and deuterium excess (b) plotted against corrected  $^{14}\text{C}$  ages for late-Holocene (blue  
 213 circles) and late-glacial (red circles) groundwaters. Lines mark the average (solid line) and one  
 214 standard deviation (dashed lines) for each age group (Barbecot et al., 2000).

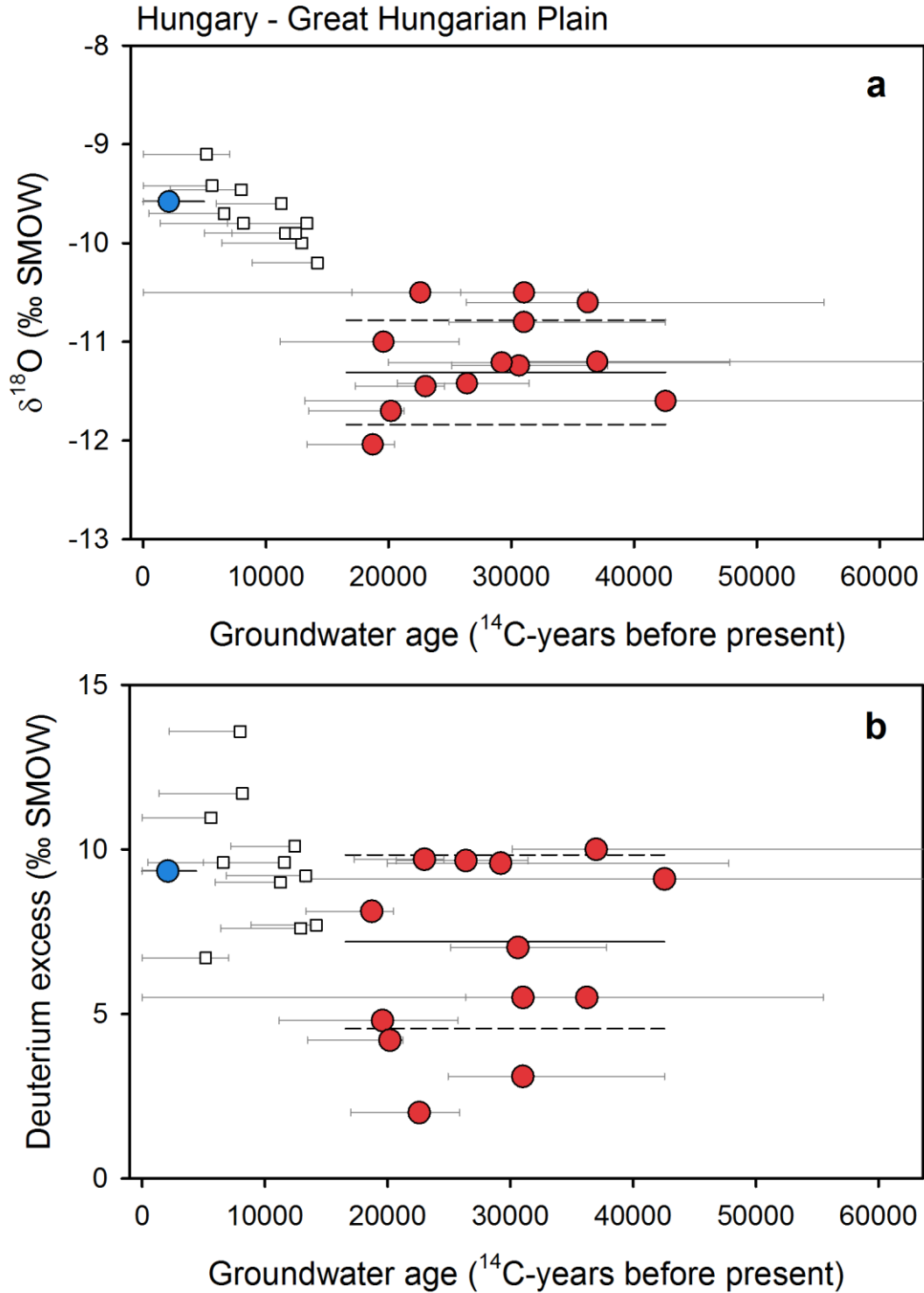


215

216 **Figure S19.** Groundwater isotope composition of the Lorraine sandstone aquifer. Groundwater  
 217  $\delta^{18}\text{O}$  (a) and deuterium excess (b) plotted against corrected  $^{14}\text{C}$  ages for late-Holocene (blue  
 218 circles) and late-glacial (red circles) groundwaters. Lines mark the average (solid line) and one  
 219 standard deviation (dashed lines) for each age group (Celle-Jeanton et al., 2009).

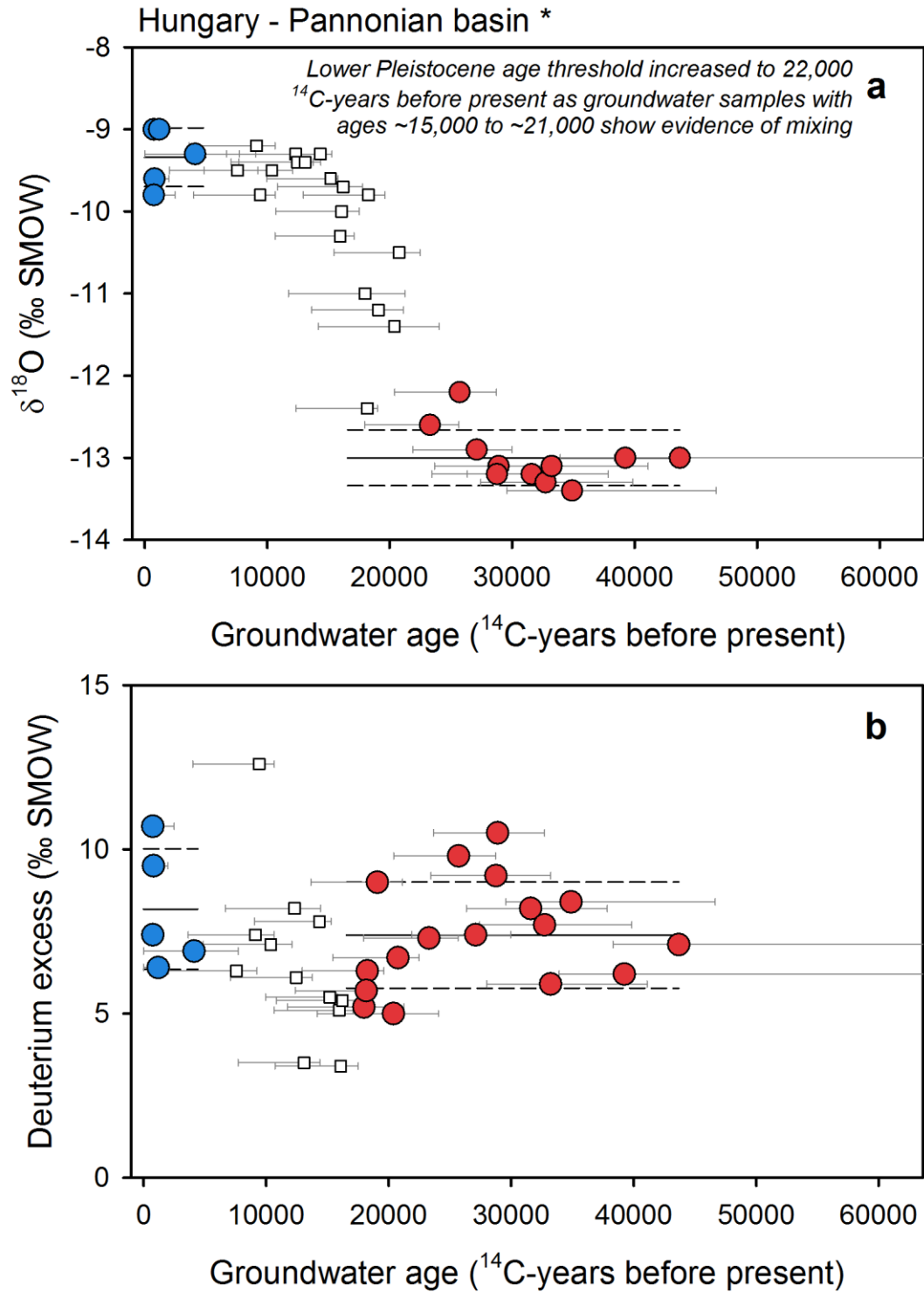


220  
 221 **Figure S20.** Groundwater isotope composition of the Benker-sandstein aquifer. Groundwater  
 222  $\delta^{18}\text{O}$  (a) and deuterium excess (b) plotted against corrected  $^{14}\text{C}$  ages for late-Holocene (blue  
 223 circles) and late-glacial (red circles) groundwaters. Lines mark the average (solid line) and one  
 224 standard deviation (dashed lines) for each age group (van Geldern et al., 2014).



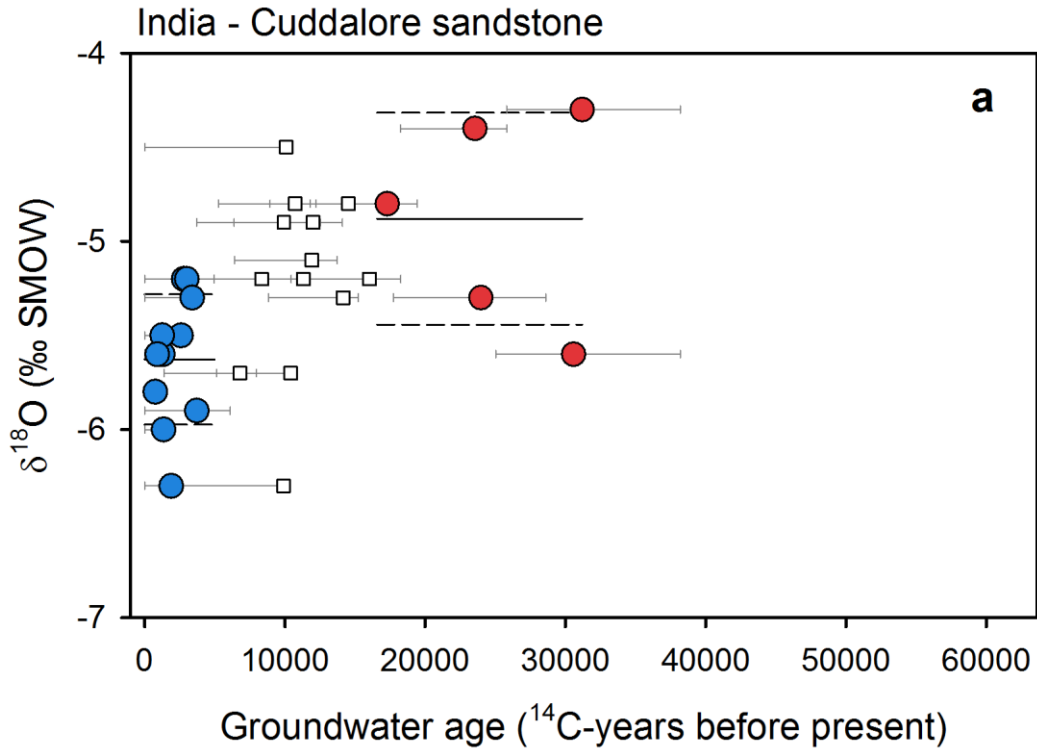
225

226 **Figure S21.** Groundwater isotope composition of the Great Hungarian Plain. Groundwater  $\delta^{18}\text{O}$   
 227 (a) and deuterium excess (b) plotted against corrected  $^{14}\text{C}$  ages for late-Holocene (blue circles)  
 228 and late-glacial (red circles) groundwaters. Lines mark the average (solid line) and one standard  
 229 deviation (dashed lines) for each age group (Stute and Deak, 1989).

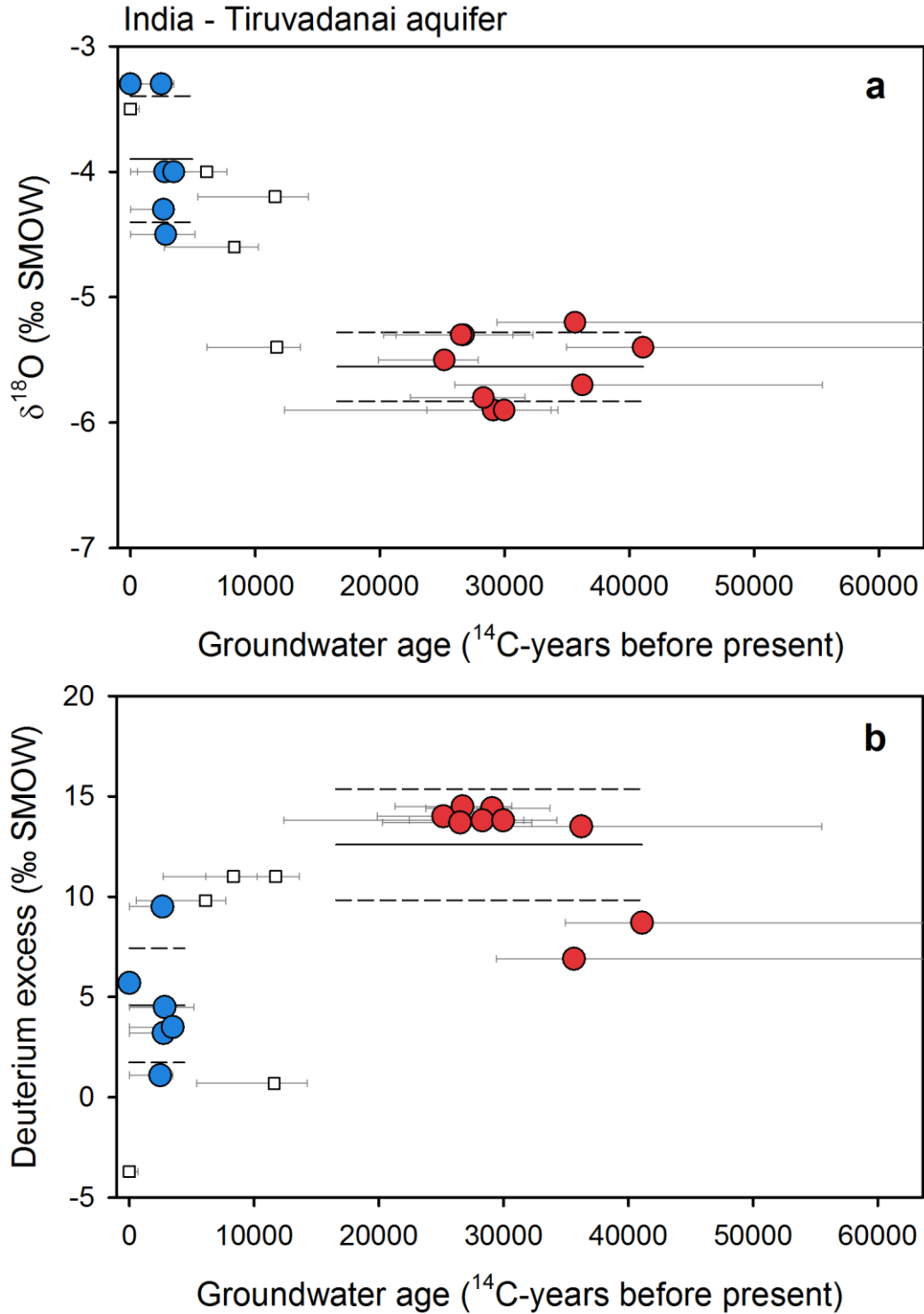


230

231 **Figure S22.** Groundwater isotope composition of the Pannonian basin. Groundwater  $\delta^{18}\text{O}$  (a)  
 232 and deuterium excess (b) plotted against corrected  $^{14}\text{C}$  ages for late-Holocene (blue circles) and  
 233 late-glacial (red circles) groundwaters. Lines mark the average (solid line) and one standard  
 234 deviation (dashed lines) for each age group (Varsanyi et al., 2011).

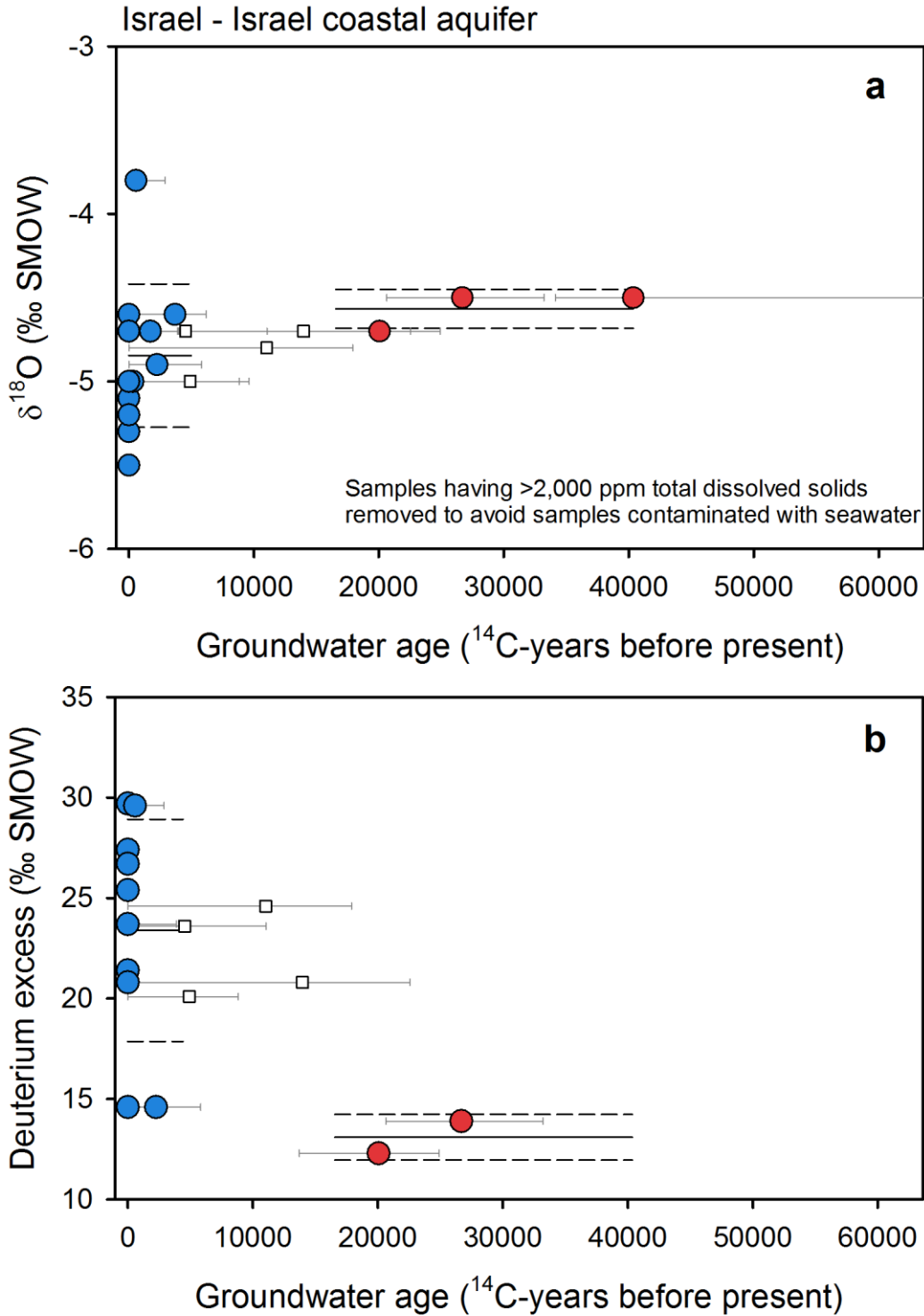


235  
 236 **Figure S23.** Groundwater isotope composition of the Cuddalore sandstone aquifer. Groundwater  
 237  $\delta^{18}\text{O}$  plotted against corrected  $^{14}\text{C}$  ages for late-Holocene (blue circles) and late-glacial (red  
 238 circles) groundwaters. Lines mark the average (solid line) and one standard deviation (dashed  
 239 lines) for each age group (Sukhija et al., 1998).

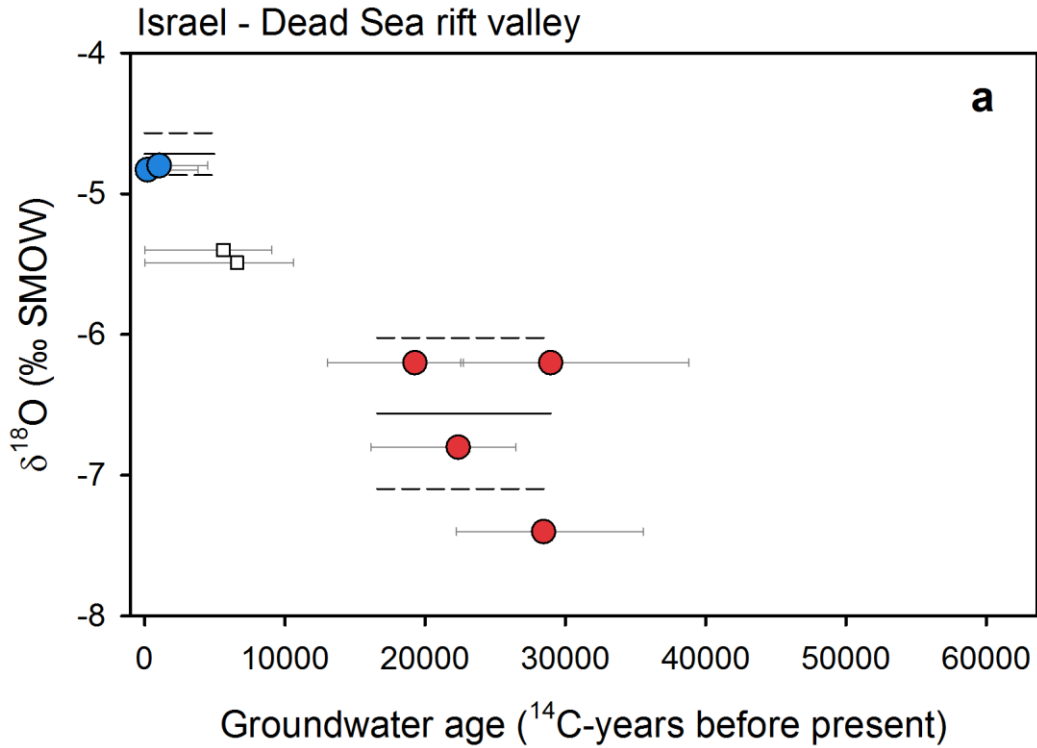


240  
 241 **Figure S24.** Groundwater isotope composition of the Tiruvadanaai aquifer. Groundwater  $\delta^{18}\text{O}$  (a)  
 242 and deuterium excess (b) plotted against corrected  $^{14}\text{C}$  ages for late-Holocene (blue circles) and  
 243 late-glacial (red circles) groundwaters. Lines mark the average (solid line) and one standard  
 244 deviation (dashed lines) for each age group (Kumar et al., 2009).





250  
 251 **Figure S26.** Groundwater isotope composition of the Israel coastal aquifer. Groundwater  $\delta^{18}\text{O}$   
 252 (a) and deuterium excess (b) plotted against corrected  $^{14}\text{C}$  ages for late-Holocene (blue circles)  
 253 and late-glacial (red circles) groundwaters. Lines mark the average (solid line) and one standard  
 254 deviation (dashed lines) for each age group (Yeichieli et al., 2009).



255

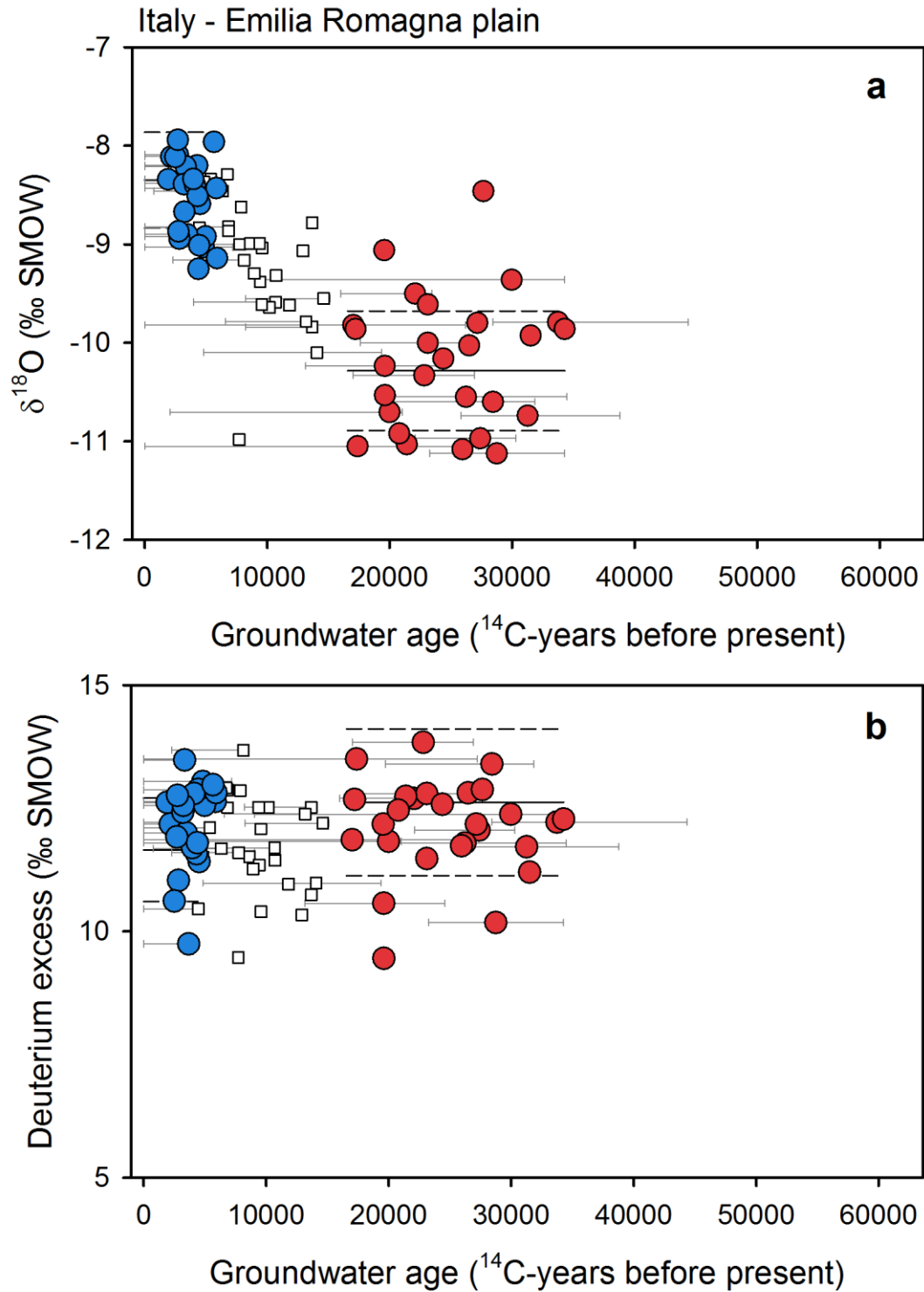
256

257

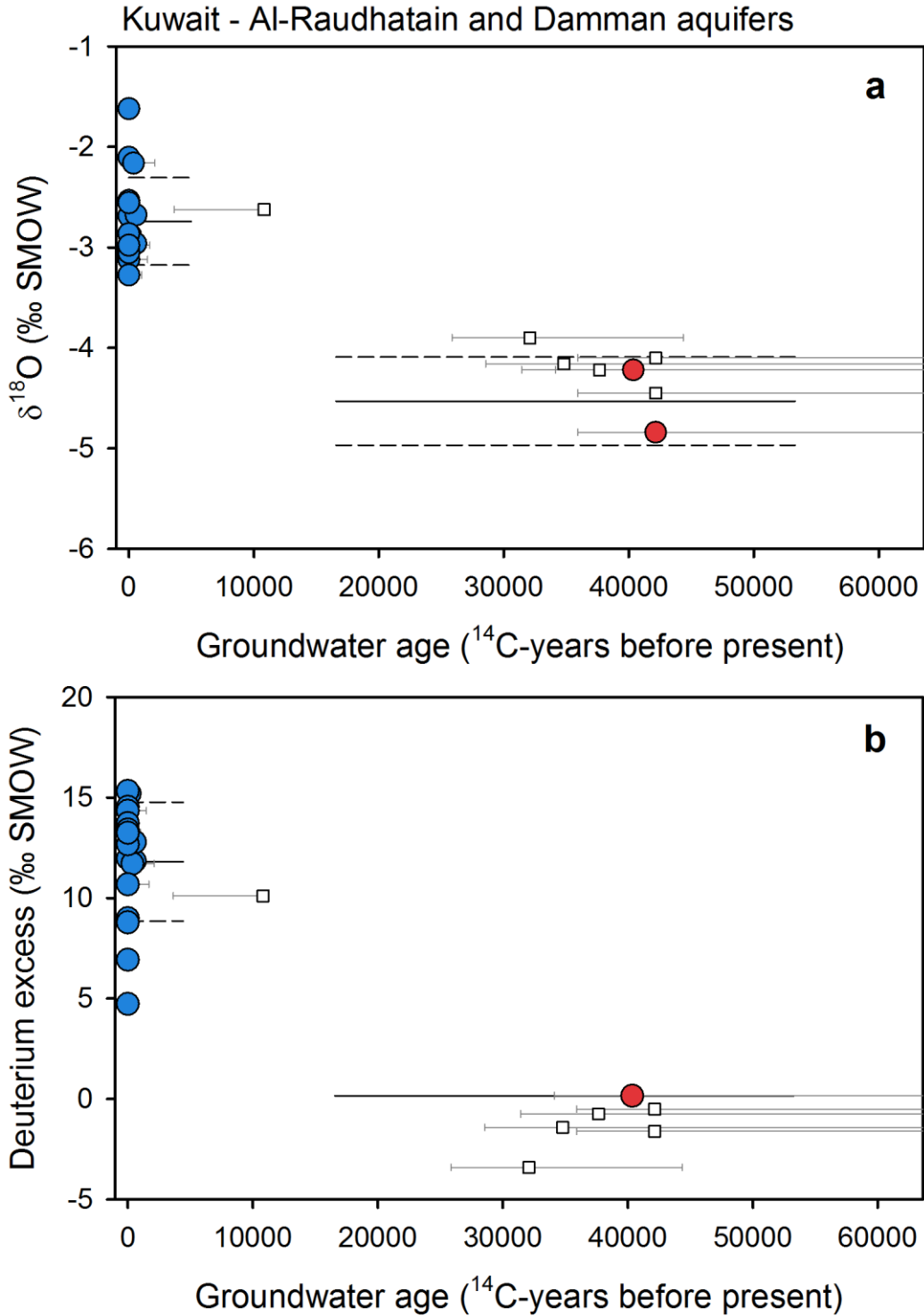
258

259

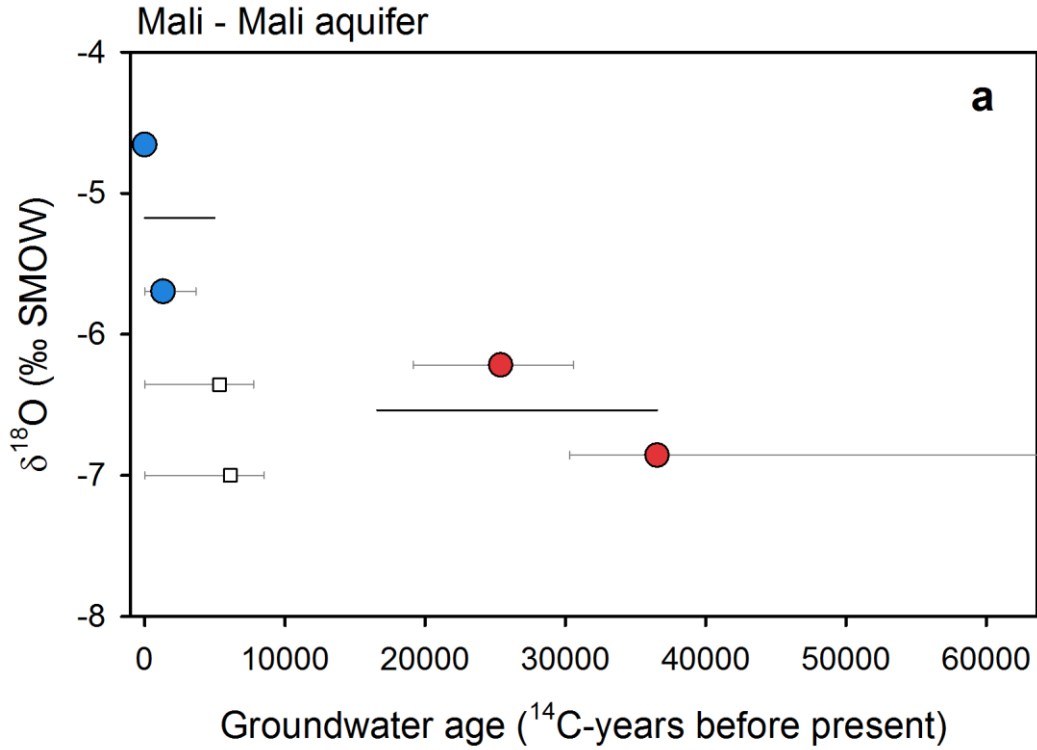
**Figure S27.** Groundwater isotope composition of the Dead Sea Rift aquifer. Groundwater  $\delta^{18}\text{O}$  plotted against corrected  $^{14}\text{C}$  ages for late-Holocene (blue circles) and late-glacial (red circles) groundwaters. Lines mark the average (solid line) and one standard deviation (dashed lines) for each age group (Gat and Galai, 1982; Mazor et al., 1995).



260  
 261 **Figure S28.** Groundwater isotope composition of the Emilia Romagna Plain. Groundwater  $\delta^{18}\text{O}$   
 262 (a) and deuterium excess (b) plotted against corrected  $^{14}\text{C}$  ages for late-Holocene (blue circles)  
 263 and late-glacial (red circles) groundwaters. Lines mark the average (solid line) and one standard  
 264 deviation (dashed lines) for each age group (Martinelli et al., 2011).



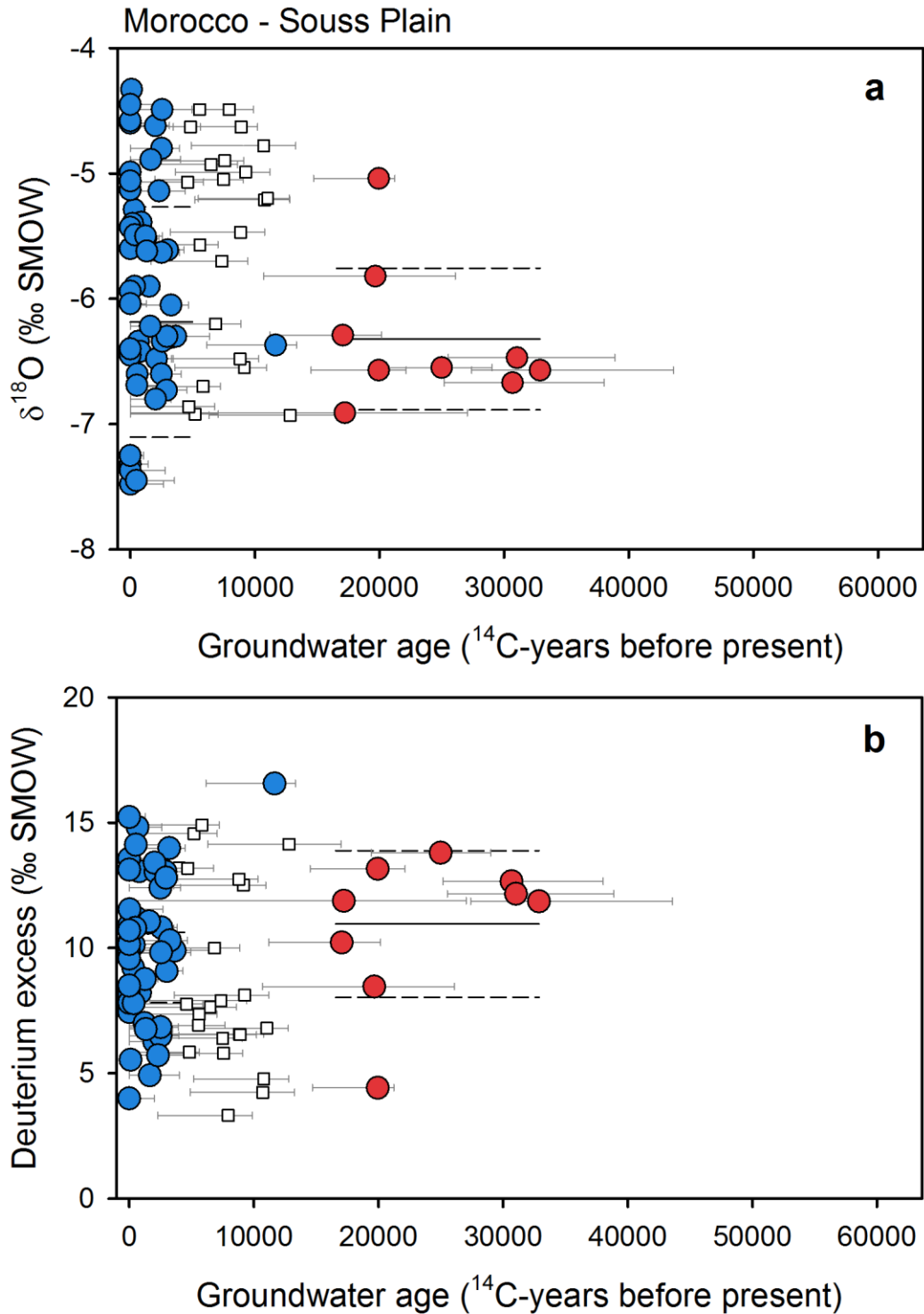
265  
 266 **Figure S29.** Groundwater isotope composition of the Al-Raudhatain and Damman aquifer.  
 267 Groundwater  $\delta^{18}\text{O}$  (a) and deuterium excess (b) plotted against corrected  $^{14}\text{C}$  ages for late-  
 268 Holocene (blue circles) and late-glacial (red circles) groundwaters. The average (solid line) and 1  
 269 s.d. (dashed lines) are shown for each group (Al-Ruwaih and Shehata, 2004; Fadlelmawla et al.,  
 270 2008).



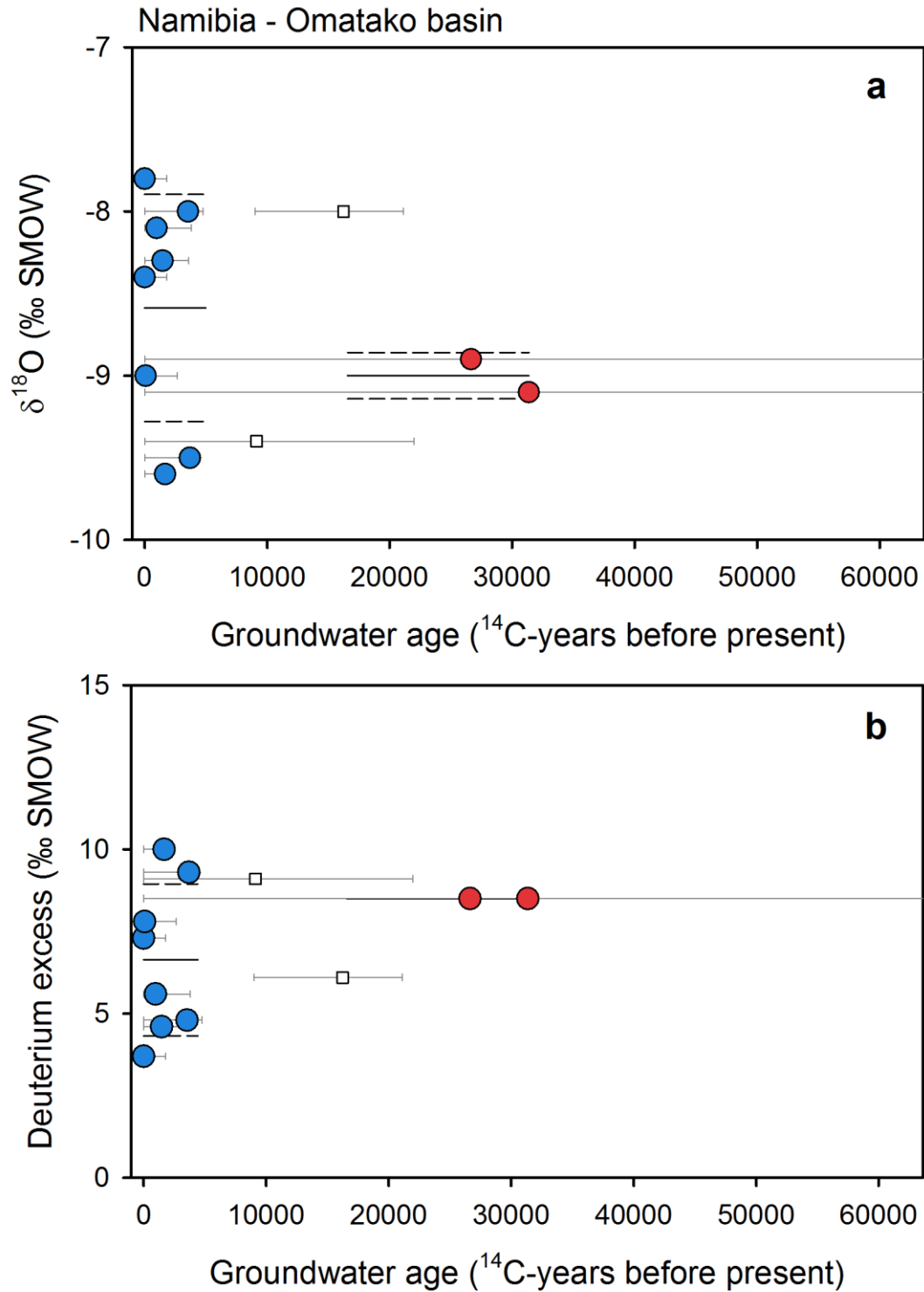
271

272 **Figure S30.** Groundwater isotope composition of the Mali aquifer. Groundwater δ<sup>18</sup>O plotted  
 273 against corrected <sup>14</sup>C ages for late-Holocene (blue circles) and late-glacial (red circles)  
 274 groundwaters. Lines mark the average (solid line) and one standard deviation (dashed lines) for  
 275 each age group (Edmunds, 2009).

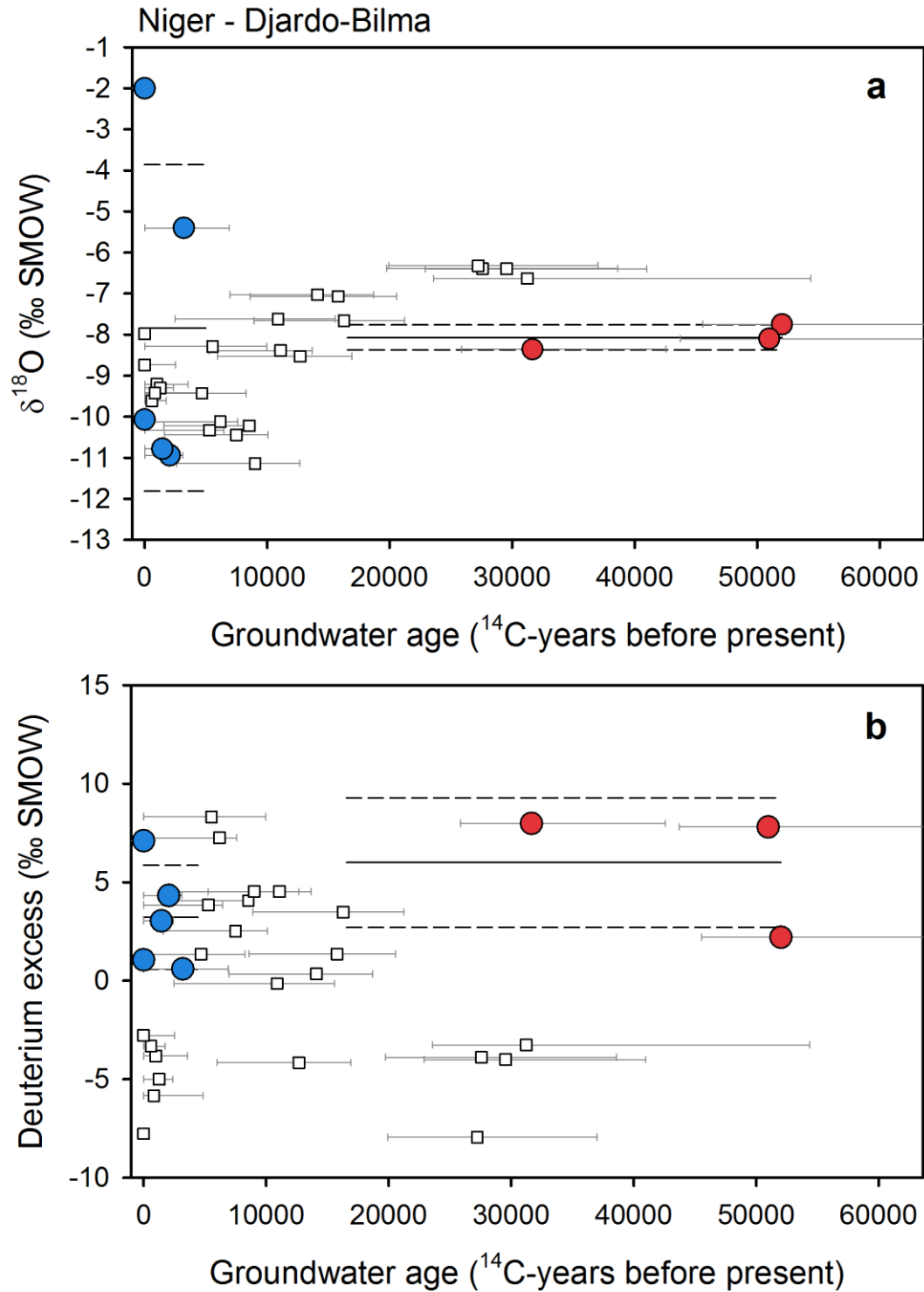
276



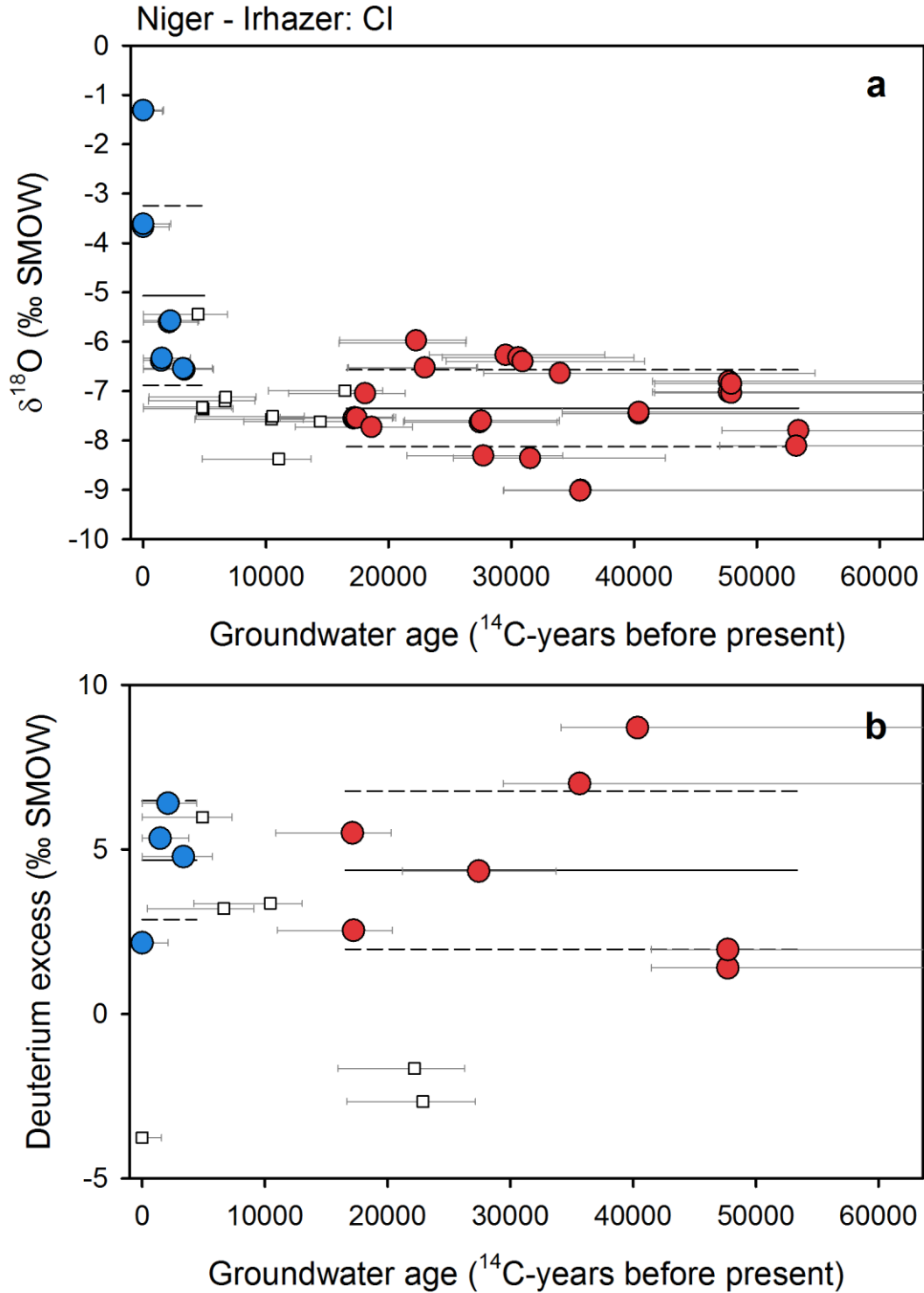
277  
 278 **Figure S31.** Groundwater isotope composition of the Tadla basin. Groundwater  $\delta^{18}\text{O}$  (a) and  
 279 deuterium excess (b) plotted against corrected  $^{14}\text{C}$  ages for late-Holocene (blue circles) and late-  
 280 glacial (red circles) groundwaters. Lines mark the average (solid line) and one standard deviation  
 281 (dashed lines) for each age group (Castany et al., 1974).



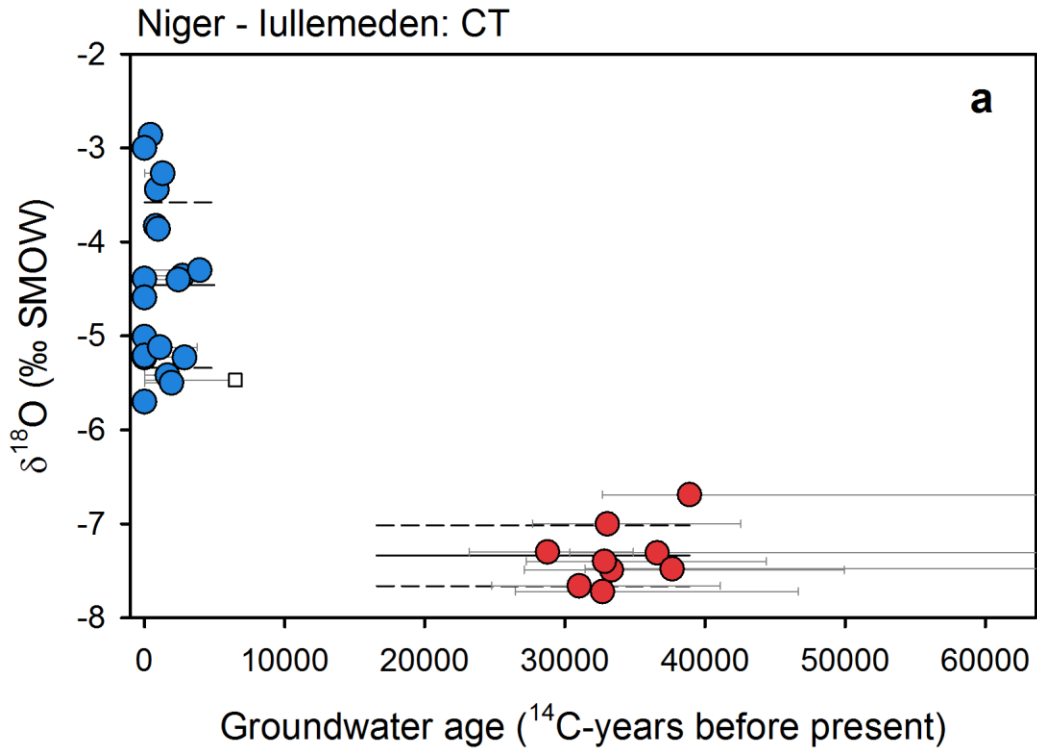
282  
 283 **Figure S32.** Groundwater isotope composition of the Omatako basin. Groundwater  $\delta^{18}\text{O}$  (a) and  
 284 deuterium excess (b) plotted against corrected  $^{14}\text{C}$  ages for late-Holocene (blue circles) and late-  
 285 glacial (red circles) groundwaters. Lines mark the average (solid line) and one standard deviation  
 286 (dashed lines) for each age group (Külls, 2000).



287  
 288 **Figure S33.** Groundwater isotope composition of the Djardo-Bilma basin. Groundwater  $\delta^{18}\text{O}$  (a)  
 289 and deuterium excess (b) plotted against corrected  $^{14}\text{C}$  ages for late-Holocene (blue circles) and  
 290 late-glacial (red circles) groundwaters. Lines mark the average (solid line) and one standard  
 291 deviation (dashed lines) for each age group (Dodo and Zuppi, 1997; 1999).



292  
 293 **Figure S34.** Groundwater isotope composition of the Irhazer aquifer (Continental Intercalaire).  
 294 Groundwater  $\delta^{18}\text{O}$  (a) and deuterium excess (b) plotted against corrected  $^{14}\text{C}$  ages for late-  
 295 Holocene (blue circles) and late-glacial (red circles) groundwaters. Lines mark the average (solid  
 296 line) and one standard deviation (dashed lines) for each age group (Andrews et al., 1994;  
 297 Edmunds, 2004).



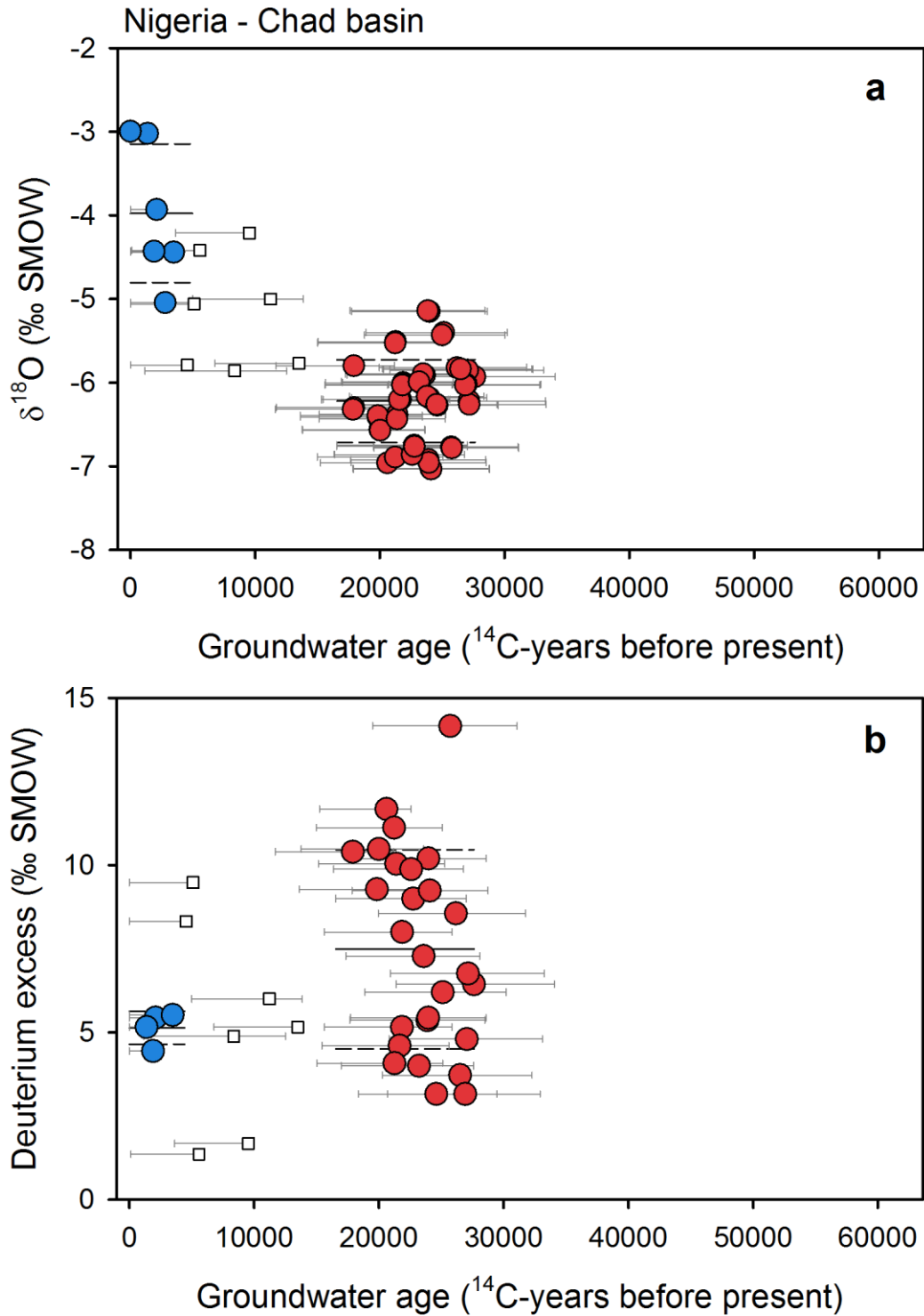
298

299 **Figure S35.** Groundwater isotope composition of the Iullemeden aquifer (Continental Terminal).

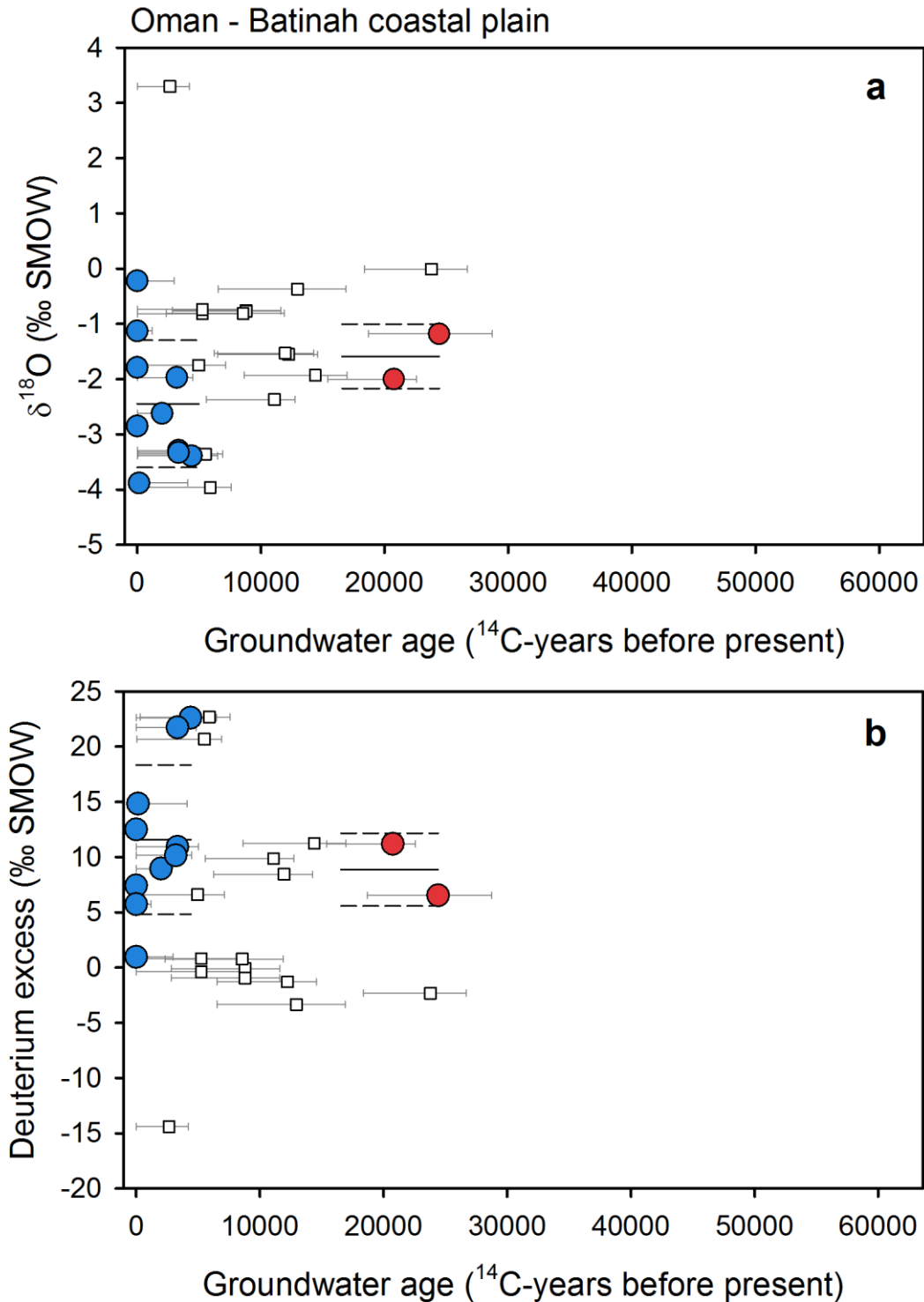
300 Groundwater δ<sup>18</sup>O plotted against corrected <sup>14</sup>C ages for late-Holocene (blue circles) and late-

301 glacial (red circles) groundwaters. Lines mark the average (solid line) and one standard deviation

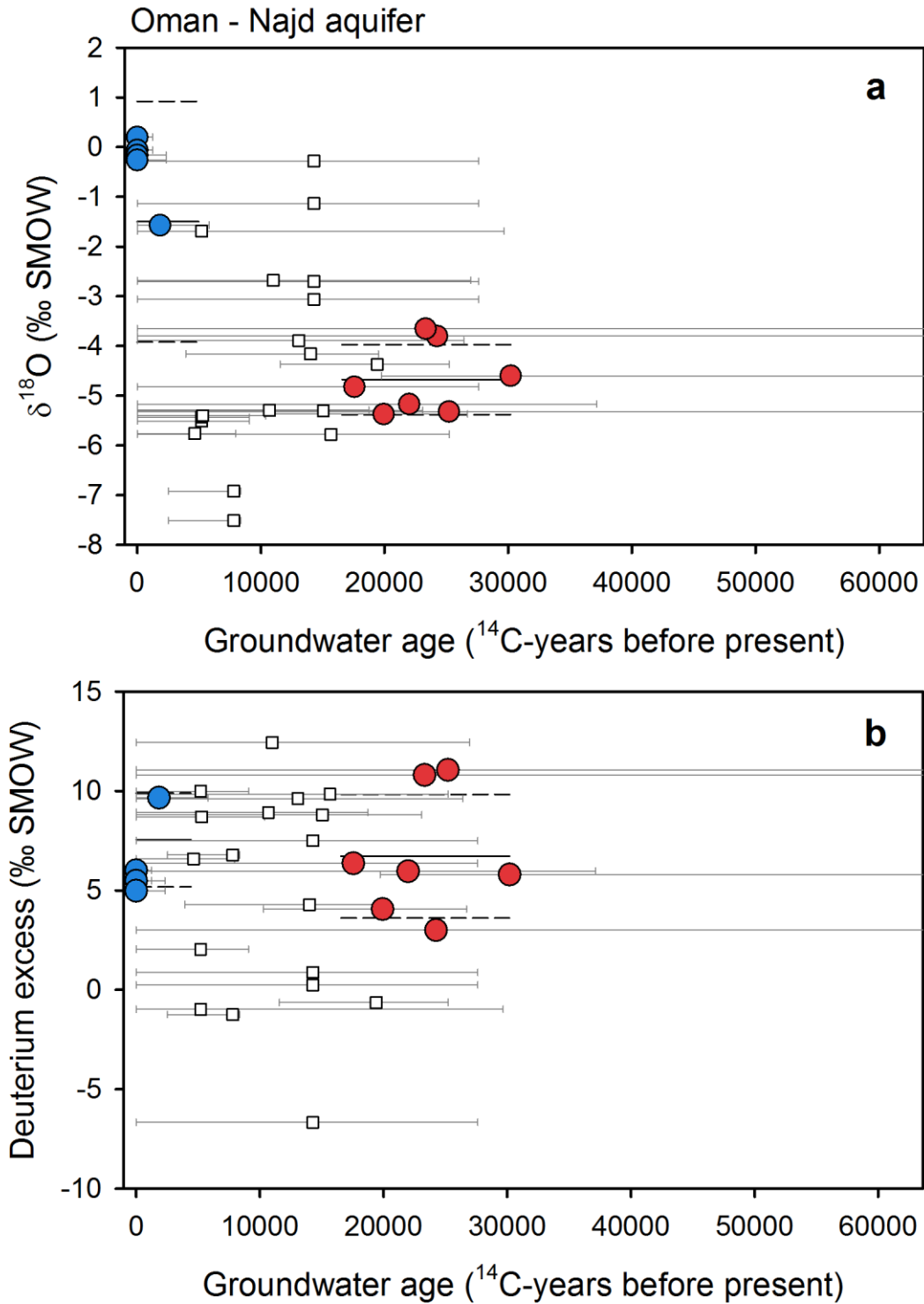
302 (dashed lines) for each age group (Le Gal La Salle et al., 2001; Beyerle et al., 2003).



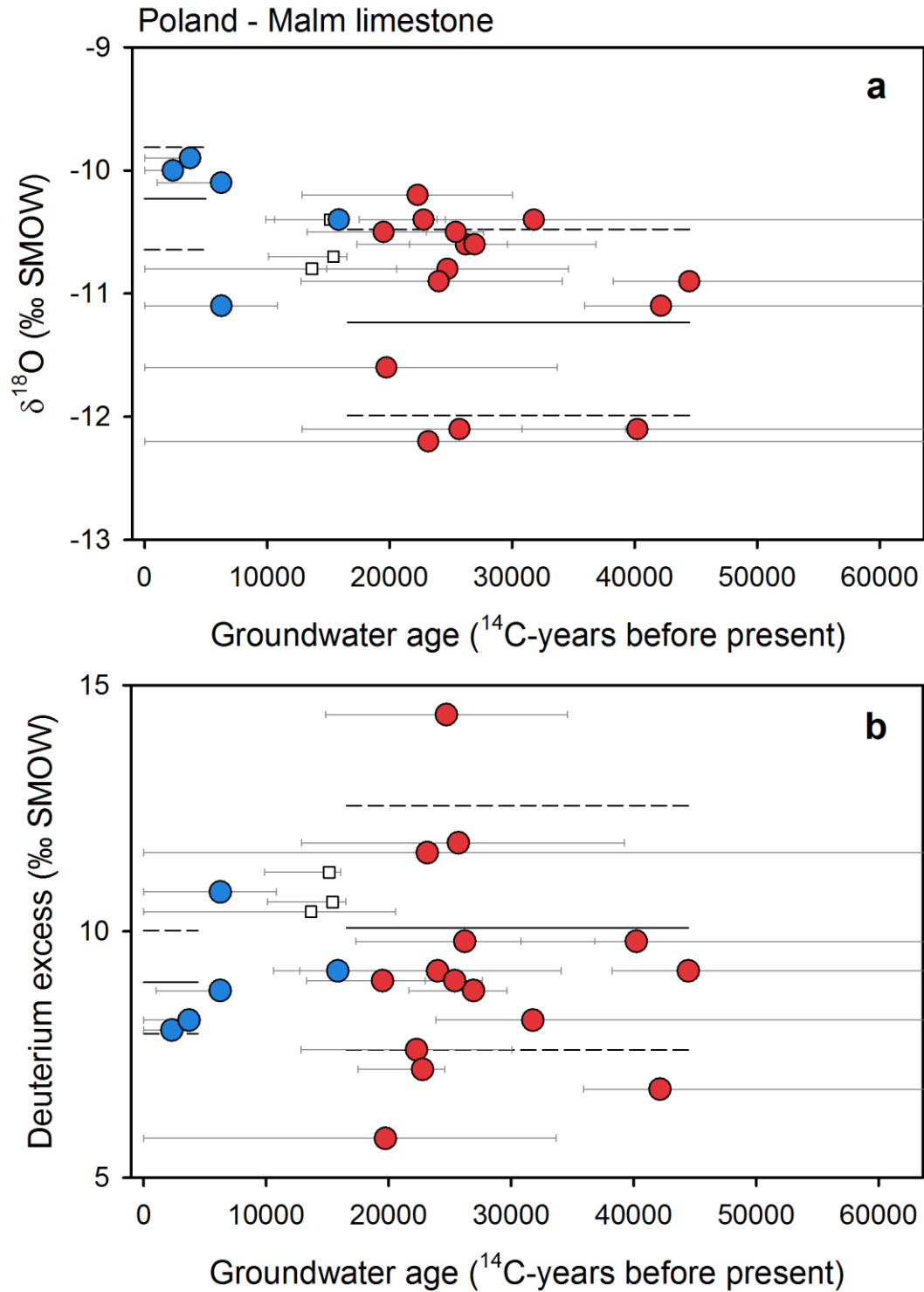
303  
 304 **Figure S36.** Groundwater isotope composition of the Chad aquifer (in Nigeria). Groundwater  
 305  $\delta^{18}\text{O}$  (a) and deuterium excess (b) plotted against corrected  $^{14}\text{C}$  ages for late-Holocene (blue  
 306 circles) and late-glacial (red circles) groundwaters. Lines mark the average (solid line) and one  
 307 standard deviation (dashed lines) for each age group (Maduabuchi et al., 2006).



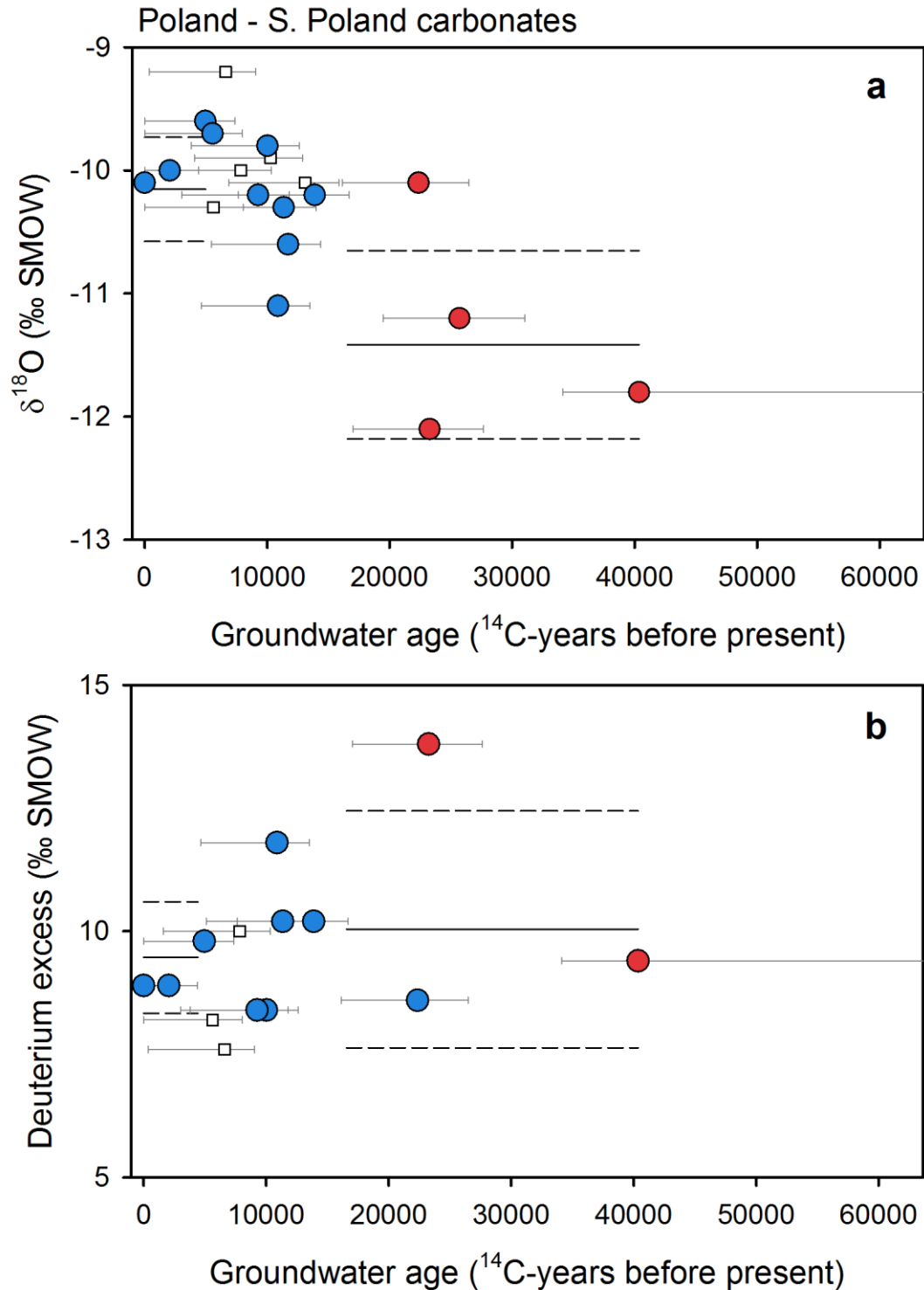
308  
 309 **Figure S37.** Groundwater isotope composition of the Batinah coastal aquifer system.  
 310 Groundwater  $\delta^{18}\text{O}$  (a) and deuterium excess (b) plotted against corrected  $^{14}\text{C}$  ages for late-  
 311 Holocene (blue circles) and late-glacial (red circles) groundwaters. Lines mark the average (solid  
 312 line) and one standard deviation (dashed lines) for each age group (Weyhenmeyer et al., 2000;  
 313 2002).



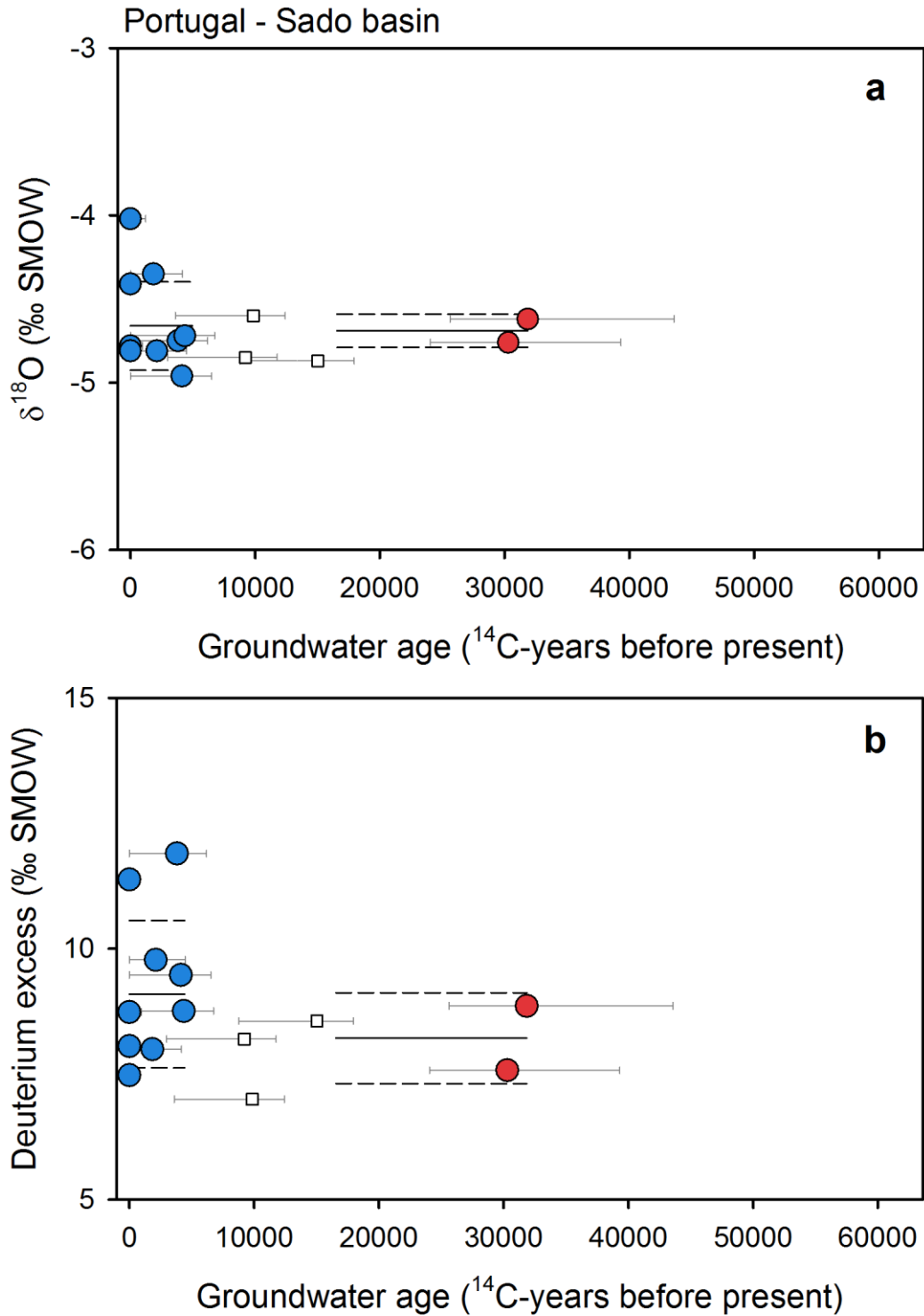
314  
 315 **Figure S38.** Groundwater isotope composition of the Najd aquifer. Groundwater  $\delta^{18}\text{O}$  (a) and  
 316 deuterium excess (b) plotted against corrected  $^{14}\text{C}$  ages for late-Holocene (blue circles) and late-  
 317 glacial (red circles) groundwaters. Lines mark the average (solid line) and one standard deviation  
 318 (dashed lines) for each age group (Clark et al., 1987; Al-Mashaikhi et al., 2012).



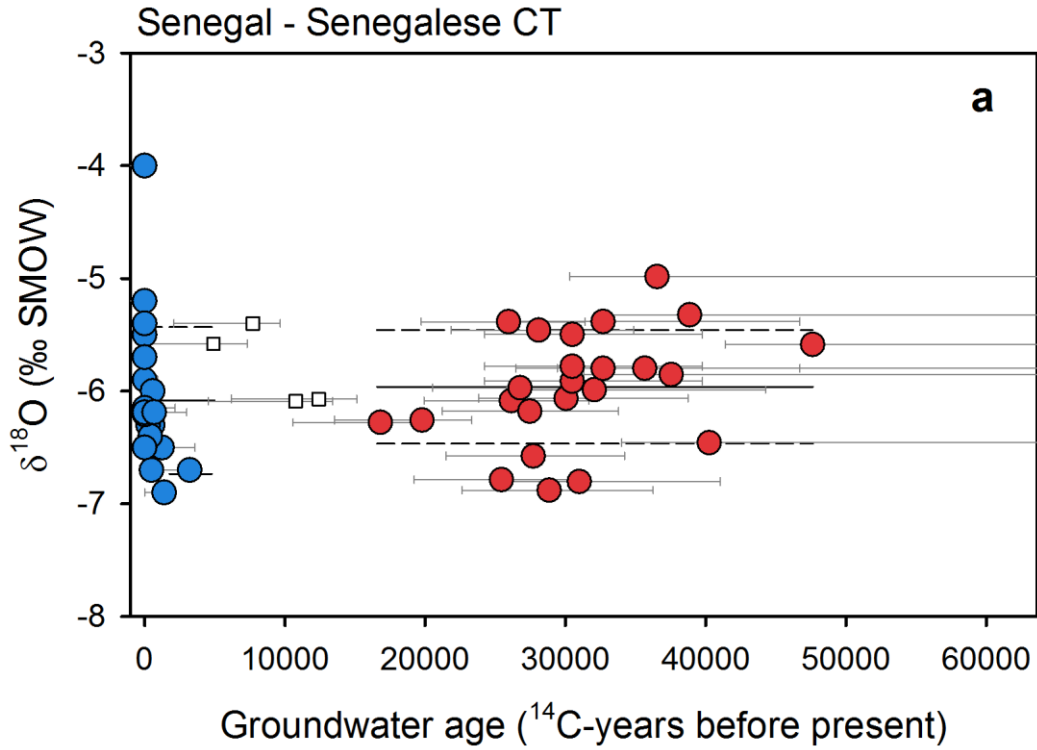
319  
 320 **Figure S39.** Groundwater isotope composition of the Malm limestone aquifer. Groundwater  
 321  $\delta^{18}\text{O}$  (a) and deuterium excess (b) plotted against corrected  $^{14}\text{C}$  ages for late-Holocene (blue  
 322 circles) and late-glacial (red circles) groundwaters. Lines mark the average (solid line) and one  
 323 standard deviation (dashed lines) for each age group (Zuber et al., 2004).



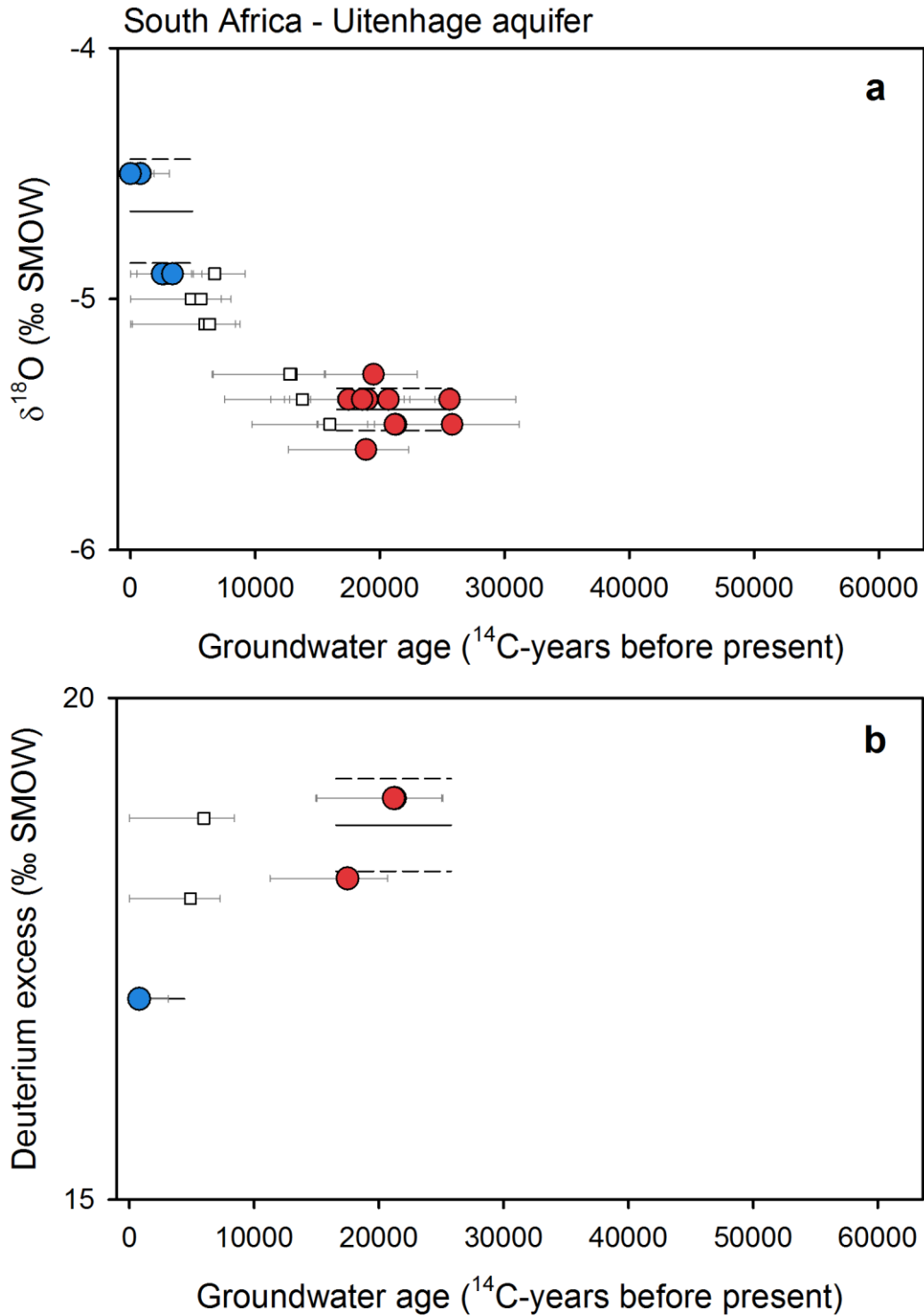
324  
 325 **Figure S40.** Groundwater isotope composition of the carbonate aquifer system of southern  
 326 Poland. Groundwater  $\delta^{18}\text{O}$  (a) and deuterium excess (b) plotted against corrected  $^{14}\text{C}$  ages for  
 327 late-Holocene (blue circles) and late-glacial (red circles) groundwaters. Lines mark the average  
 328 (solid line) and one standard deviation (dashed lines) for each age group (Samborska et al.,  
 329 2013).



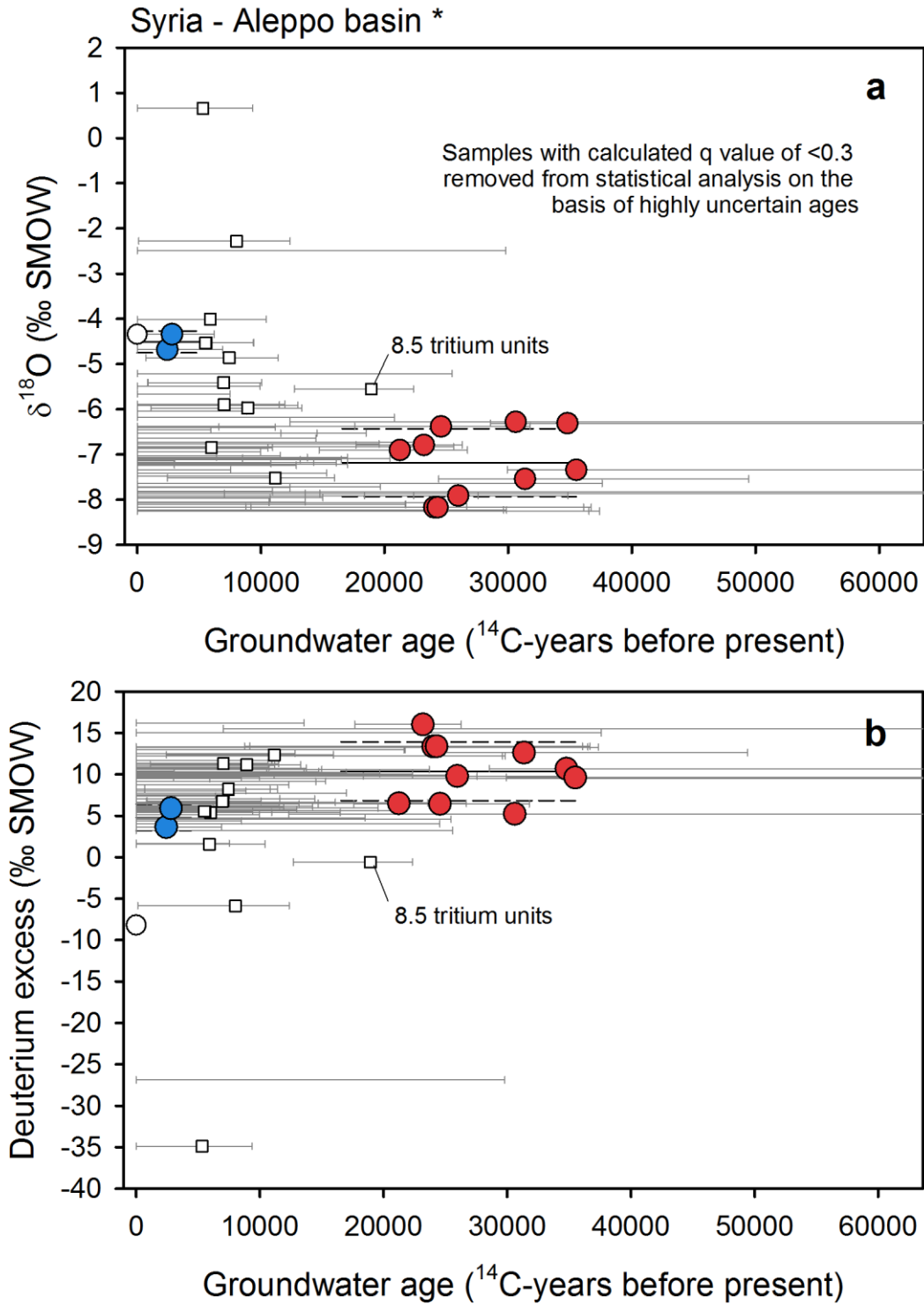
330  
 331 **Figure S41.** Groundwater isotope composition of the Sado basin. Groundwater  $\delta^{18}\text{O}$  (a) and  
 332 deuterium excess (b) plotted against corrected  $^{14}\text{C}$  ages for late-Holocene (blue circles) and late-  
 333 glacial (red circles) groundwaters. Lines mark the average (solid line) and one standard deviation  
 334 (dashed lines) for each age group (Galego Fernandes and Carreira, 2008).



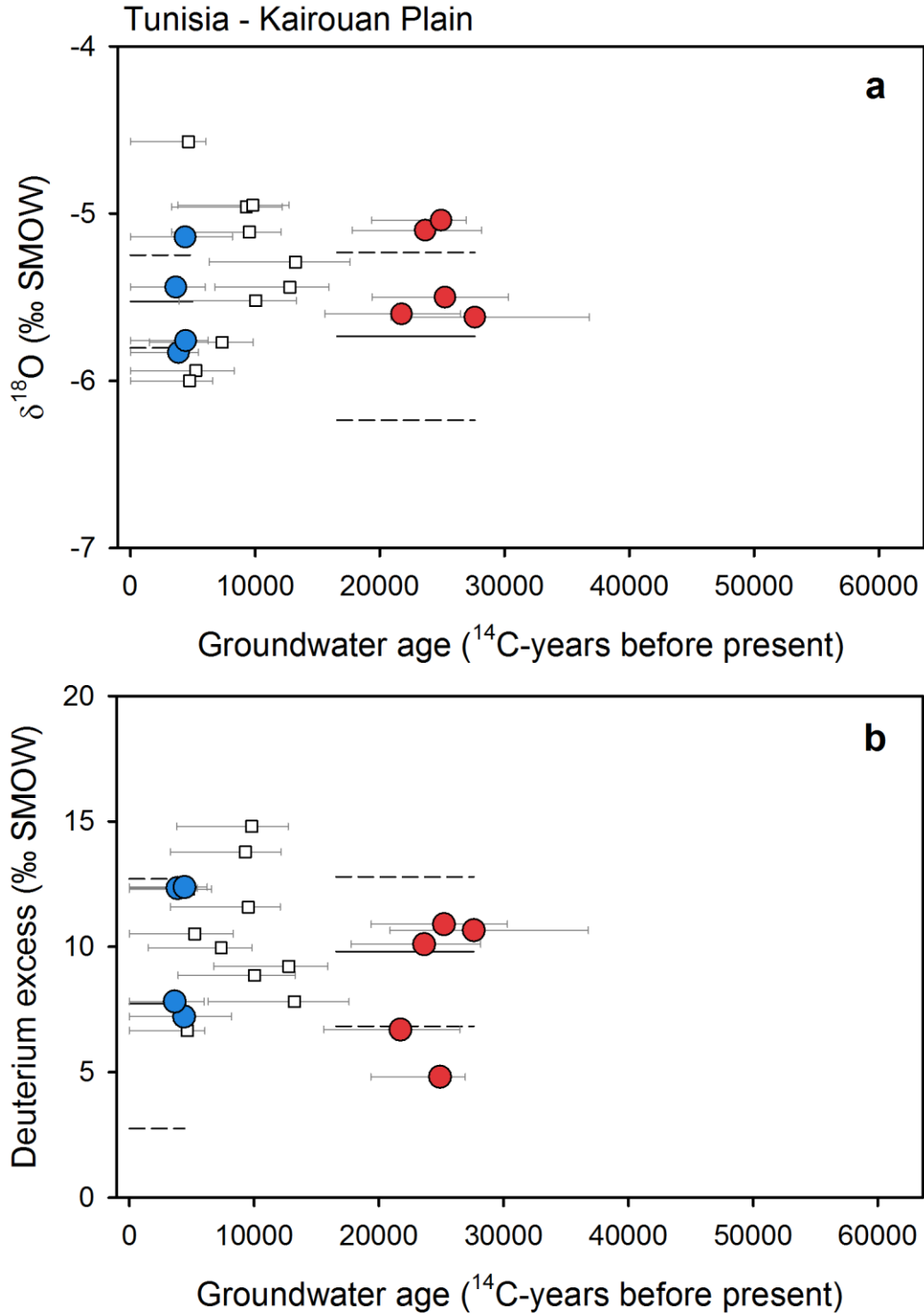
335  
 336 **Figure S42.** Groundwater isotope composition of the Senegalese Continental Terminal aquifer.  
 337 Groundwater  $\delta^{18}\text{O}$  plotted against corrected  $^{14}\text{C}$  ages for late-Holocene (blue circles) and late-  
 338 glacial (red circles) groundwaters. Lines mark the average (solid line) and one standard deviation  
 339 (dashed lines) for each age group (Castany et al., 1974; Edmunds, 2009).



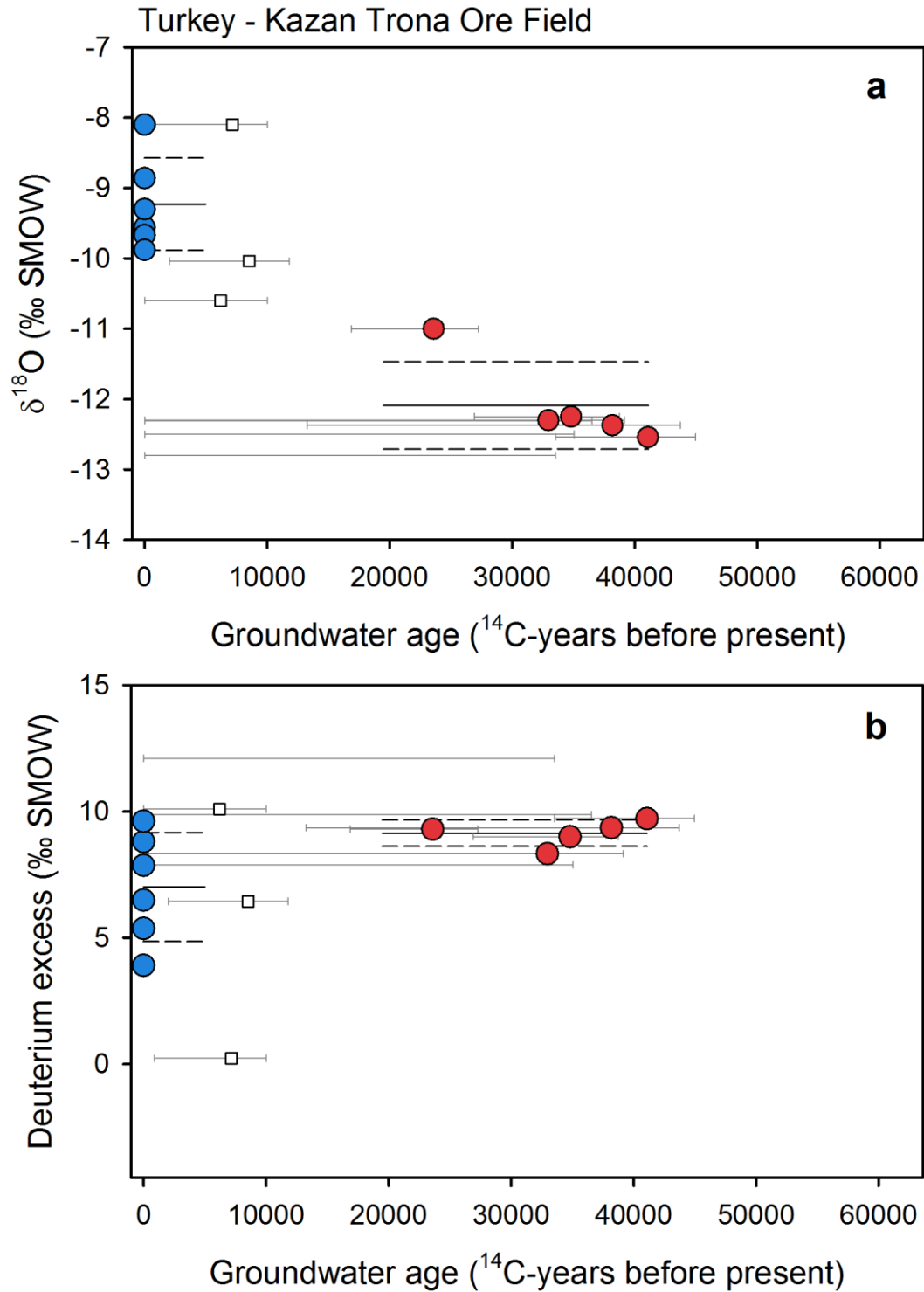
340  
 341 **Figure S43.** Groundwater isotope composition of the Uitenhage aquifer. Groundwater  $\delta^{18}\text{O}$  (a)  
 342 and deuterium excess (b) plotted against corrected  $^{14}\text{C}$  ages for late-Holocene (blue circles) and  
 343 late-glacial (red circles) groundwaters. Lines mark the average (solid line) and one standard  
 344 deviation (dashed lines) for each age group (Heaton et al., 1986).



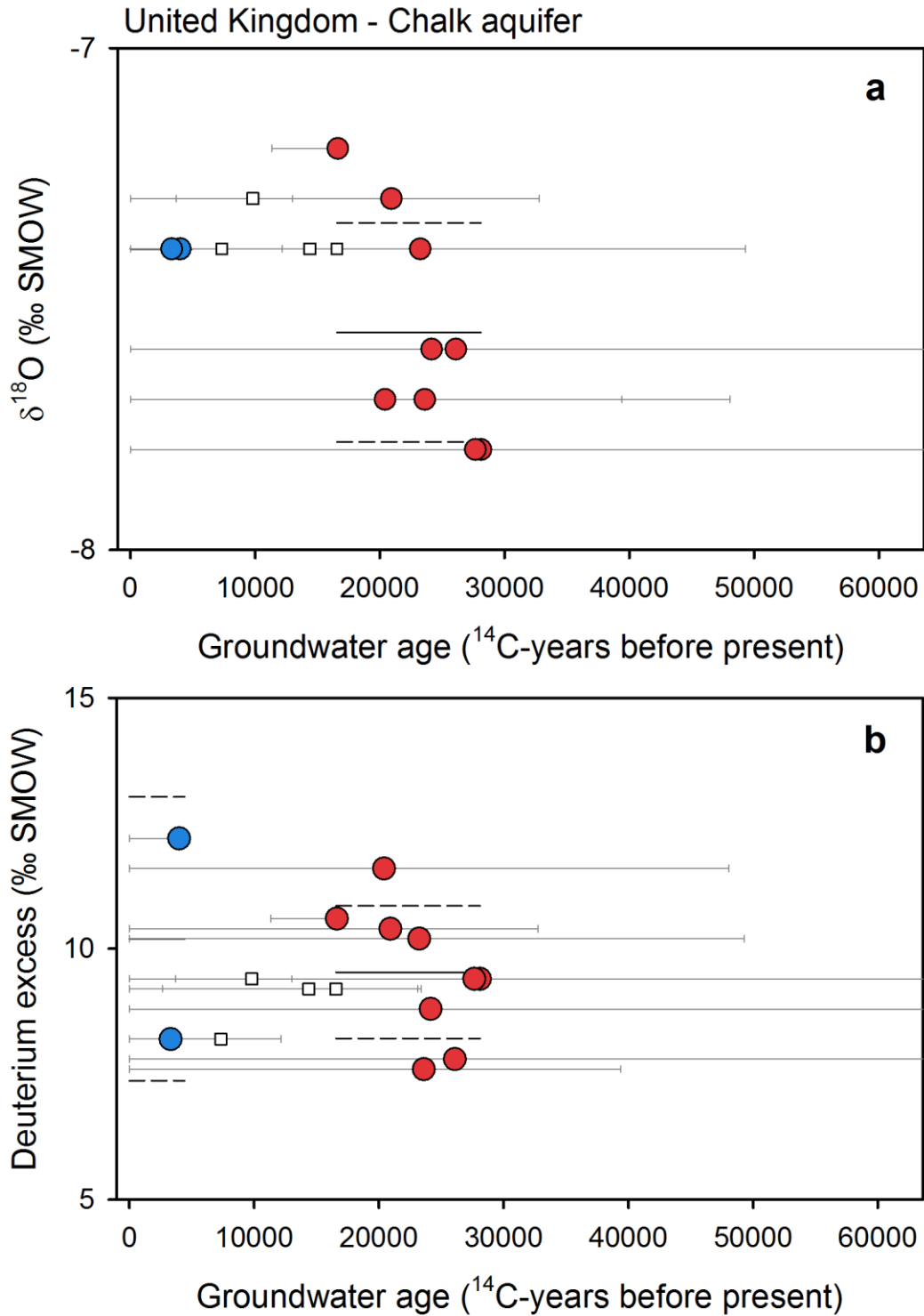
345  
 346 **Figure S44.** Groundwater isotope composition of the Aleppo basin. Groundwater  $\delta^{18}\text{O}$  (a) and  
 347 deuterium excess (b) plotted against corrected  $^{14}\text{C}$  ages for late-Holocene (blue circles) and late-  
 348 glacial (red circles) groundwaters. Lines mark the average (solid line) and one standard deviation  
 349 (dashed lines) for each age group (Al-Charideh, 2012; Stadler et al., 2012).



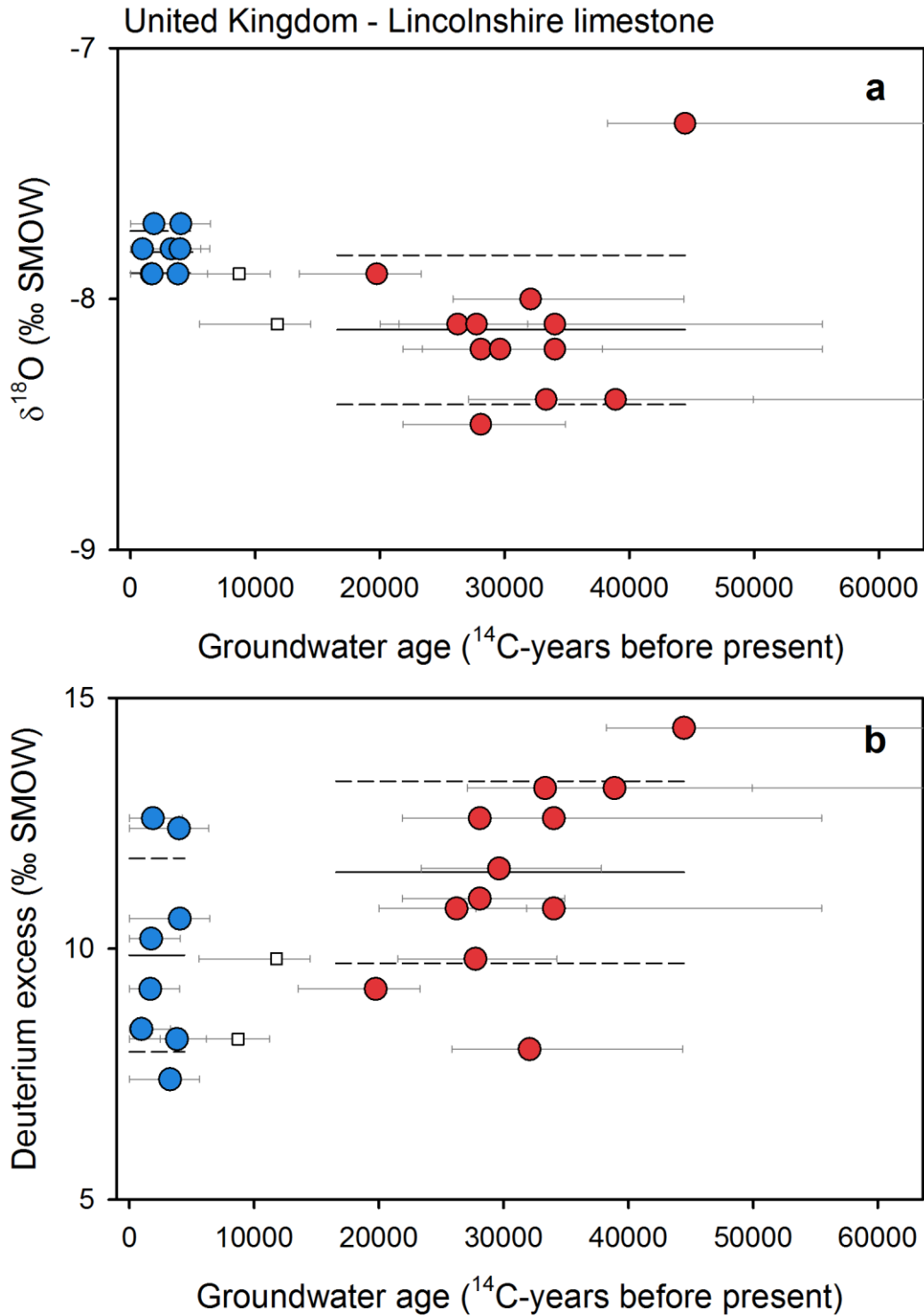
350  
 351 **Figure S45.** Groundwater isotope composition of the Kairouan Plain. Groundwater  $\delta^{18}\text{O}$  (a) and  
 352 deuterium excess (b) plotted against corrected  $^{14}\text{C}$  ages for late-Holocene (blue circles) and late-  
 353 glacial (red circles) groundwaters. Lines mark the average (solid line) and one standard deviation  
 354 (dashed lines) for each age group (Derwich et al., 2012).



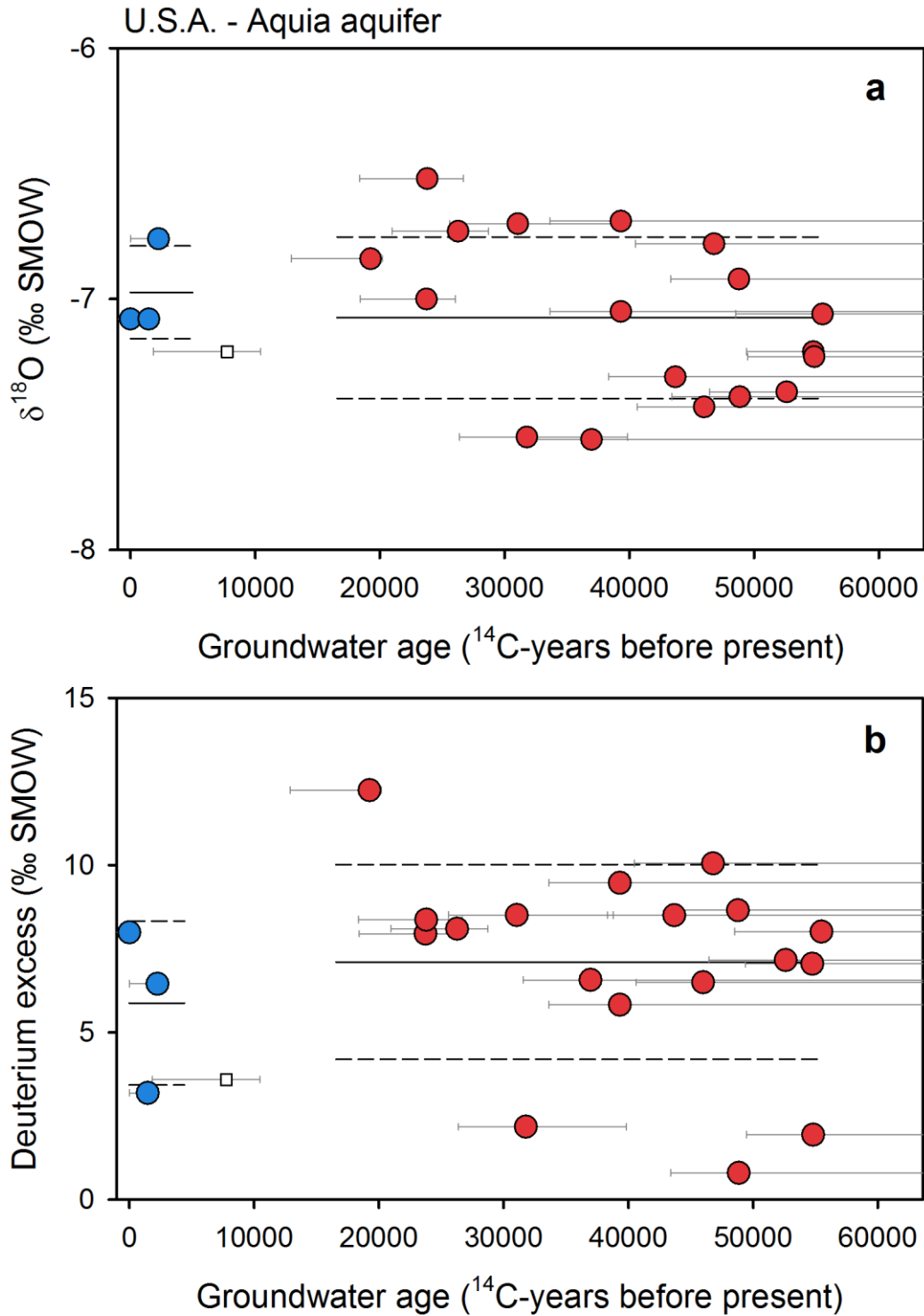
355  
 356 **Figure S46.** Groundwater isotope composition of the Kazan Trona ore field aquifer system.  
 357 Groundwater  $\delta^{18}\text{O}$  (a) and deuterium excess (b) plotted against corrected  $^{14}\text{C}$  ages for late-  
 358 Holocene (blue circles) and late-glacial (red circles) groundwaters. Lines mark the average (solid  
 359 line) and one standard deviation (dashed lines) for each age group (Arslan et al., 2014).



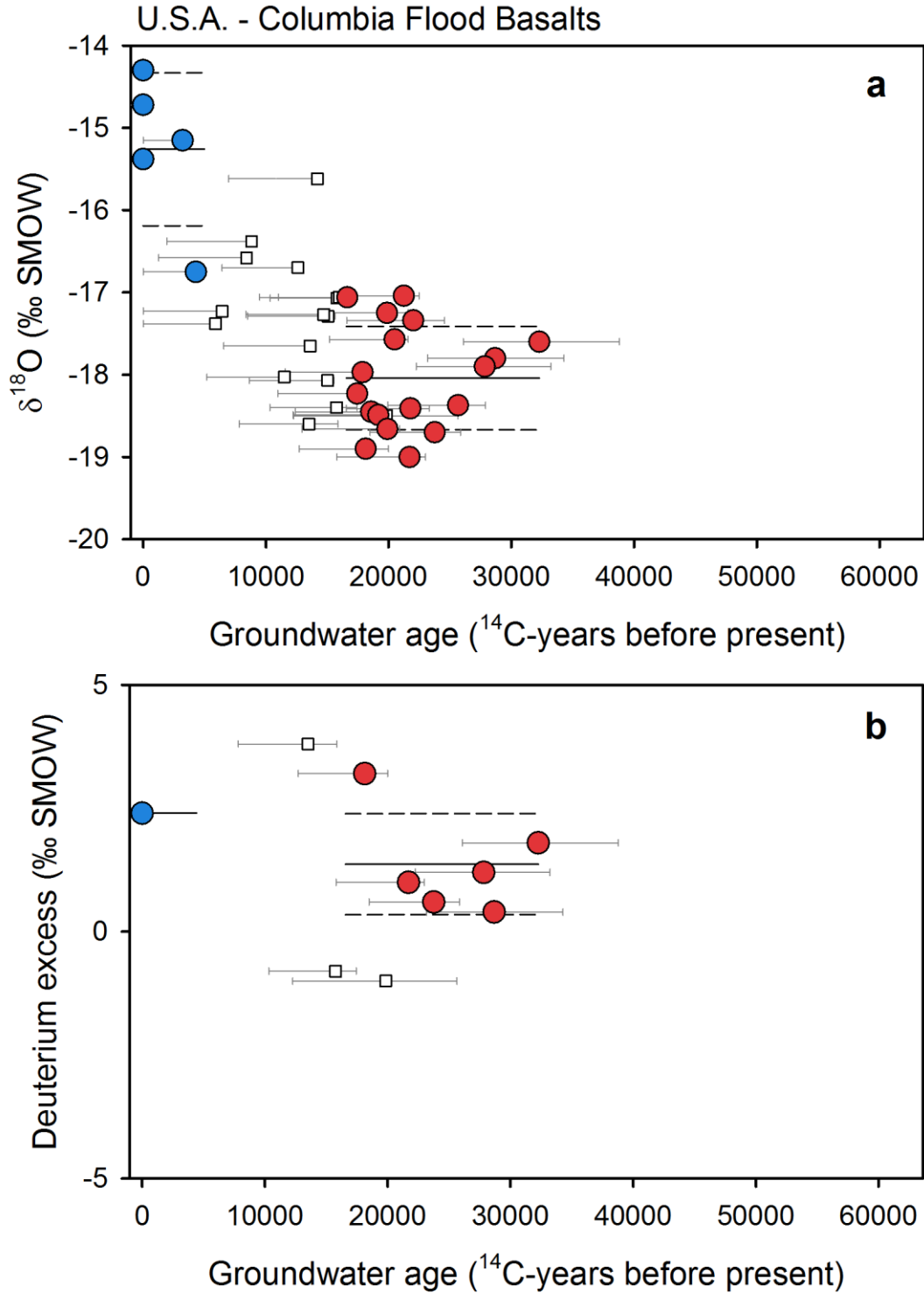
360  
 361 **Figure S47.** Groundwater isotope composition of the Chalk aquifer (in the United Kingdom).  
 362 Groundwater  $\delta^{18}\text{O}$  (a) and deuterium excess (b) plotted against corrected  $^{14}\text{C}$  ages for late-  
 363 Holocene (blue circles) and late-glacial (red circles) groundwaters. Lines mark the average (solid  
 364 line) and 1 s.d. (dashed lines) for each group (Darling and Bath, 1988; Dennis et al., 1997; Elliot  
 365 et al., 1999).



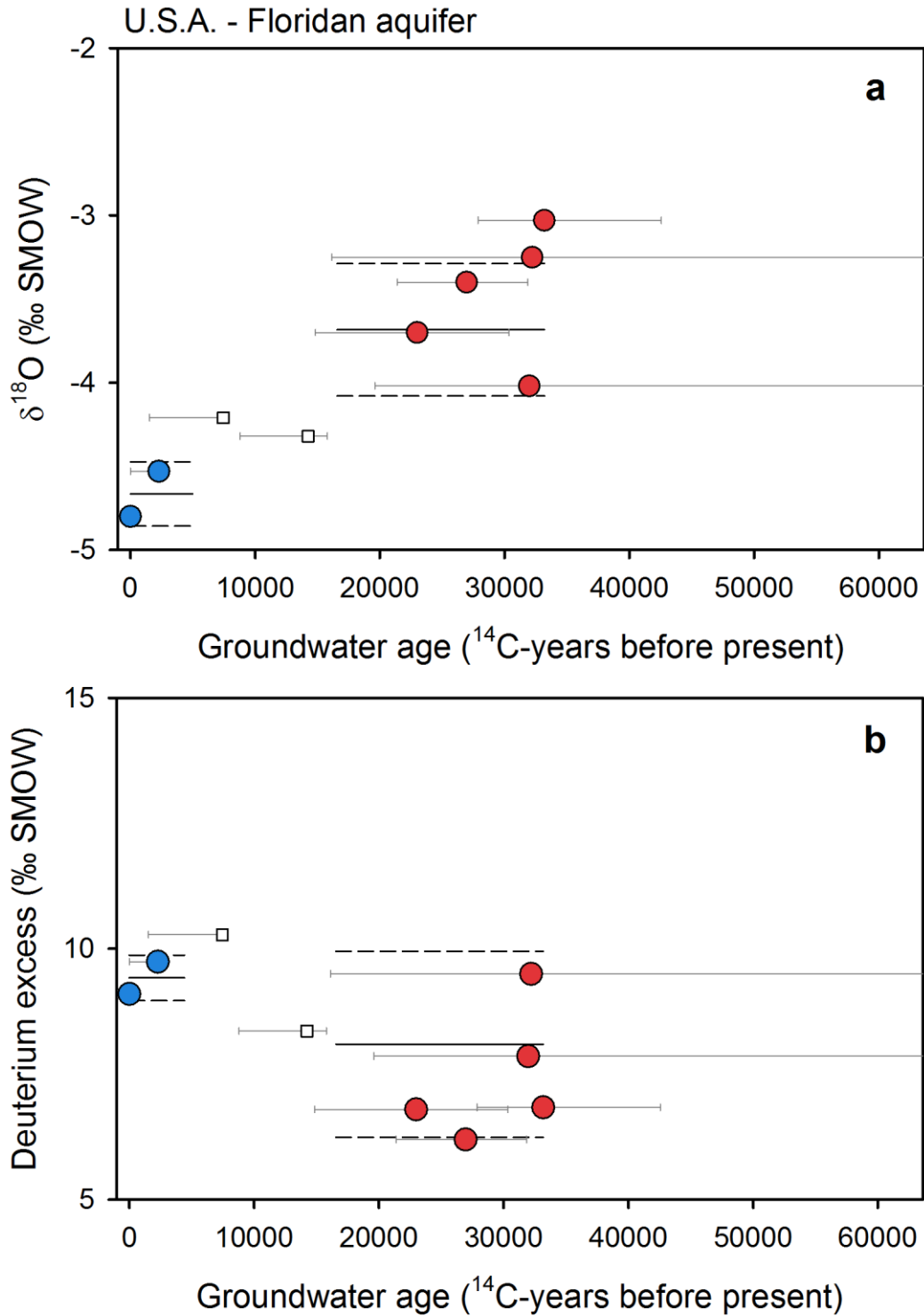
366  
 367 **Figure S48.** Groundwater isotope composition of the Lincolnshire limestone aquifer.  
 368 Groundwater  $\delta^{18}\text{O}$  (a) and deuterium excess (b) plotted against corrected  $^{14}\text{C}$  ages for late-  
 369 Holocene (blue circles) and late-glacial (red circles) groundwaters. Lines mark the average (solid  
 370 line) and one standard deviation (dashed lines) for each age group (Darling et al., 1997).



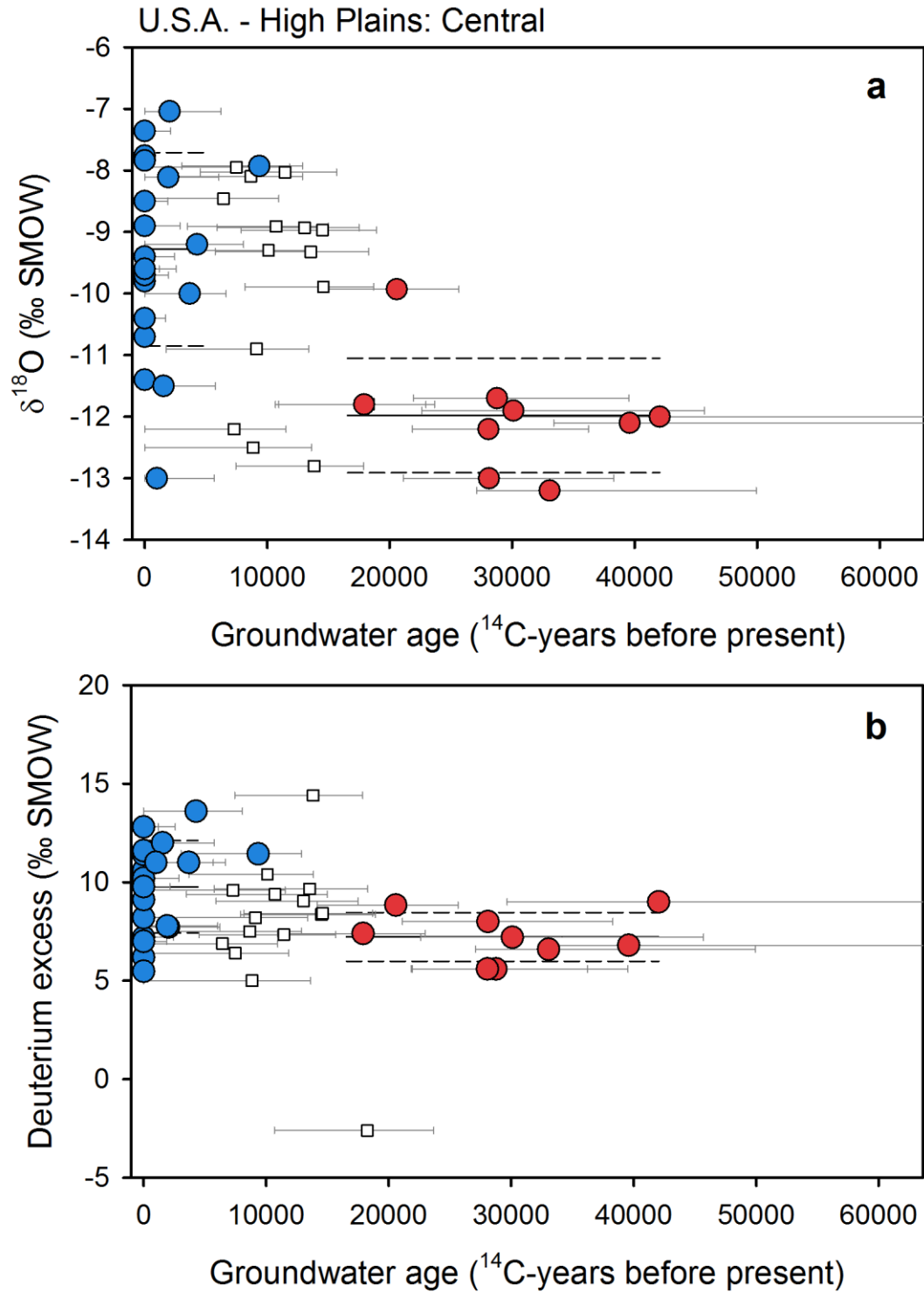
371  
 372 **Figure S49.** Groundwater isotope composition of the Aquia aquifer. Groundwater  $\delta^{18}\text{O}$  (a) and  
 373 deuterium excess (b) plotted against corrected  $^{14}\text{C}$  ages for late-Holocene (blue circles) and late-  
 374 glacial (red circles) groundwaters. Lines mark the average (solid line) and one standard deviation  
 375 (dashed lines) for each age group (Aeschbach-Hertig et al., 2002).



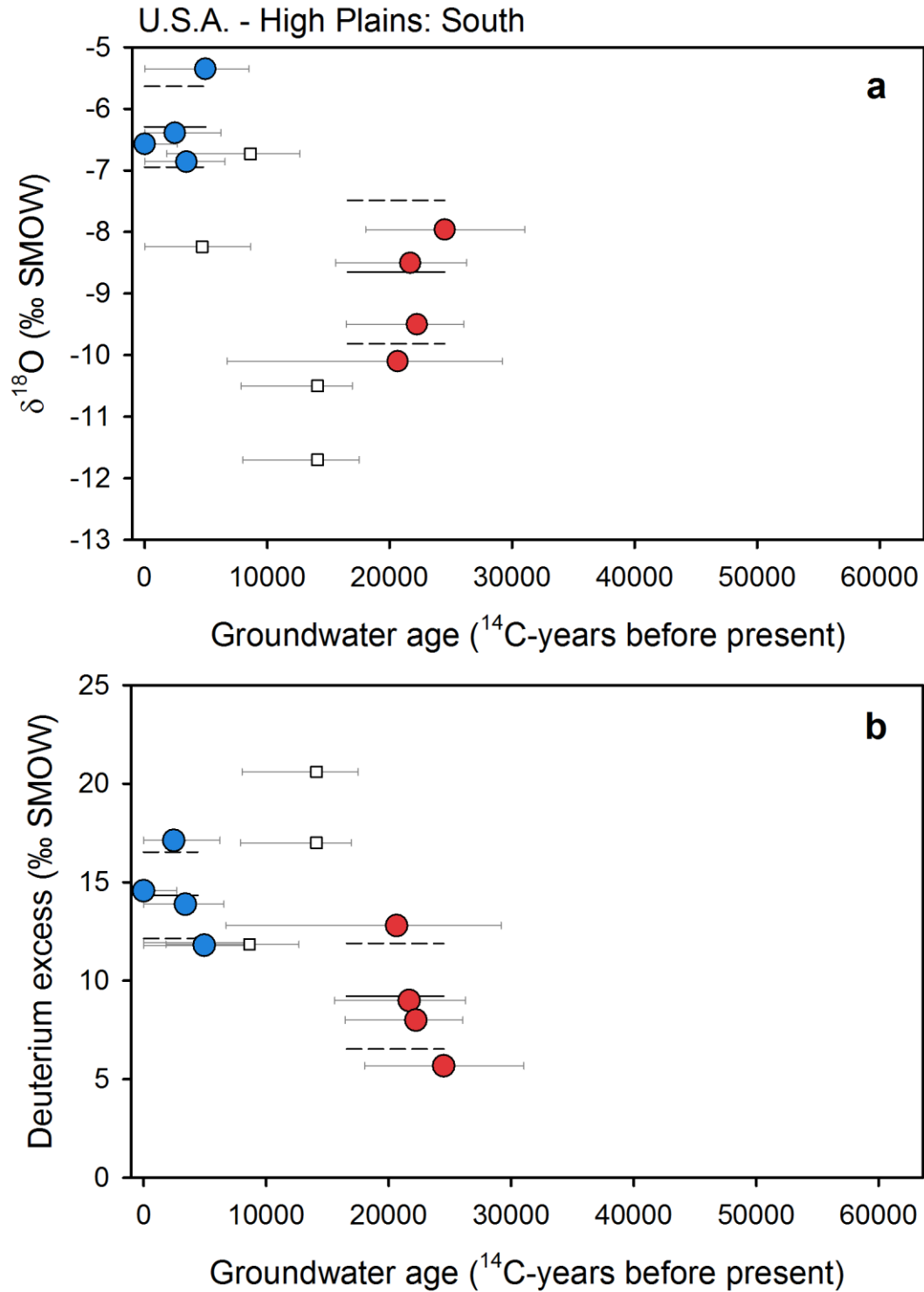
376  
 377 **Figure S50.** Groundwater isotope composition of groundwaters in the Columbia Flood Basalts.  
 378 Groundwater  $\delta^{18}\text{O}$  (a) and deuterium excess (b) plotted against corrected  $^{14}\text{C}$  ages for late-  
 379 Holocene (blue circles) and late-glacial (red circles) groundwaters. Lines mark the average (solid  
 380 line) and one standard deviation (dashed lines) for each age group (Douglas et al., 2007; Brown  
 381 et al., 2010).



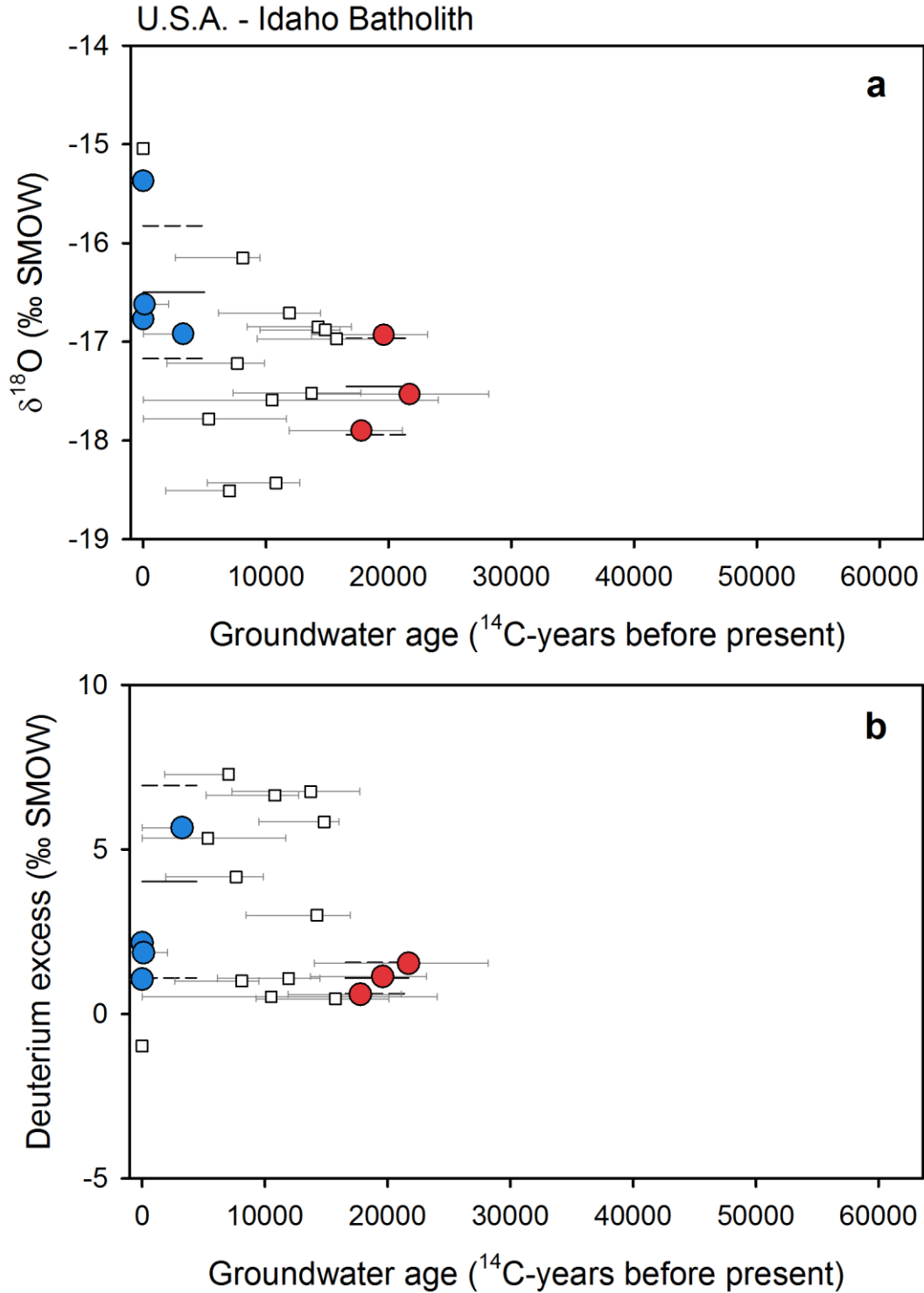
382  
 383 **Figure S51.** Groundwater isotope composition of the Floridan aquifer. Groundwater  $\delta^{18}\text{O}$  (a) and  
 384 deuterium excess (b) plotted against corrected  $^{14}\text{C}$  ages for late-Holocene (blue circles) and late-  
 385 glacial (red circles) groundwaters. Lines mark the average (solid line) and one standard deviation  
 386 (dashed lines) for each age group (Clark et al., 1997).



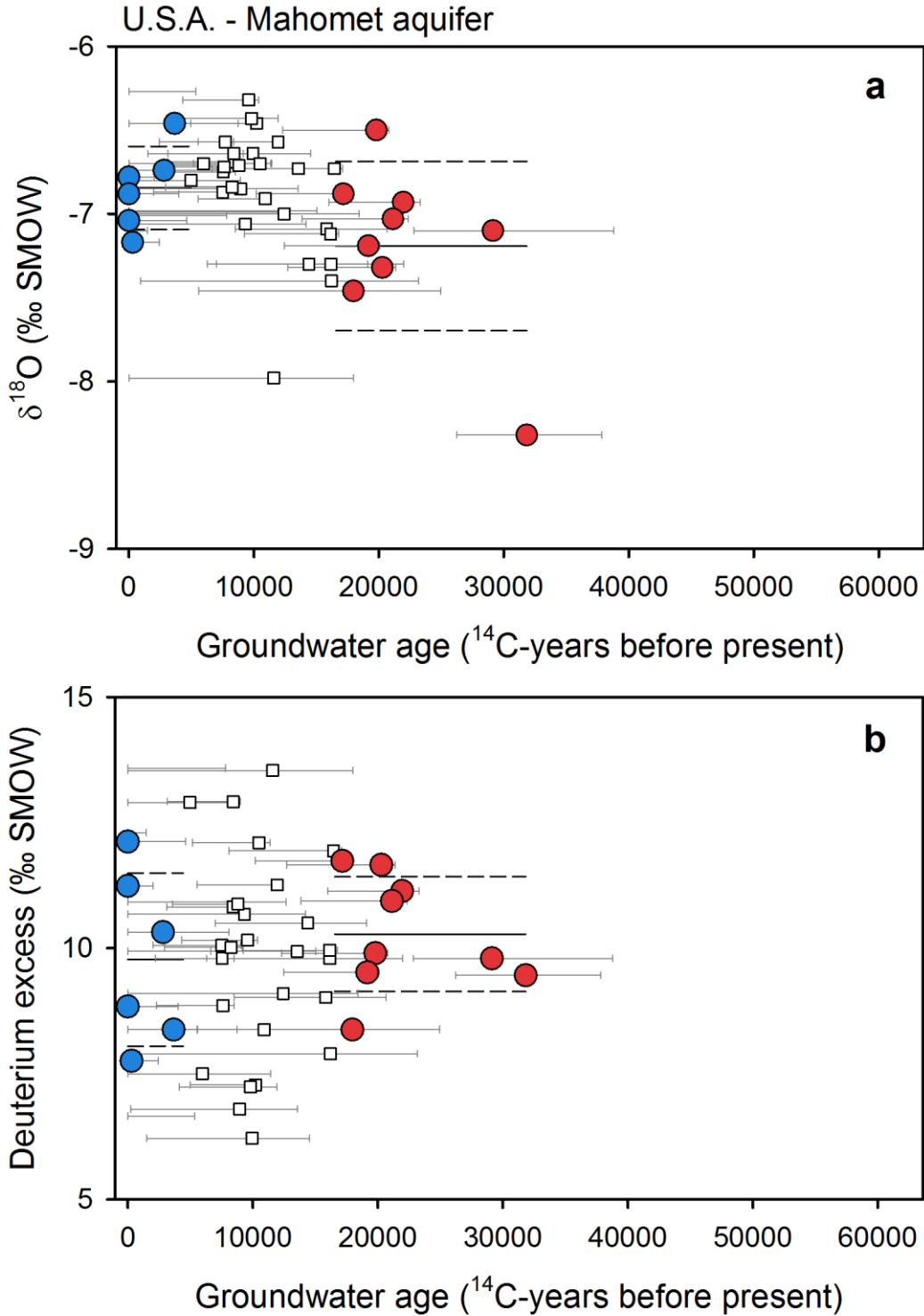
387  
 388 **Figure S52.** Groundwater isotope composition of the central High Plains aquifer. Groundwater  
 389  $\delta^{18}\text{O}$  (a) and deuterium excess (b) plotted against corrected  $^{14}\text{C}$  ages for late-Holocene (blue  
 390 circles) and late-glacial (red circles) groundwaters. Lines mark the average (solid line) and one  
 391 standard deviation (dashed lines) for each age group (Dutton, 1995; Clark et al. 1998).



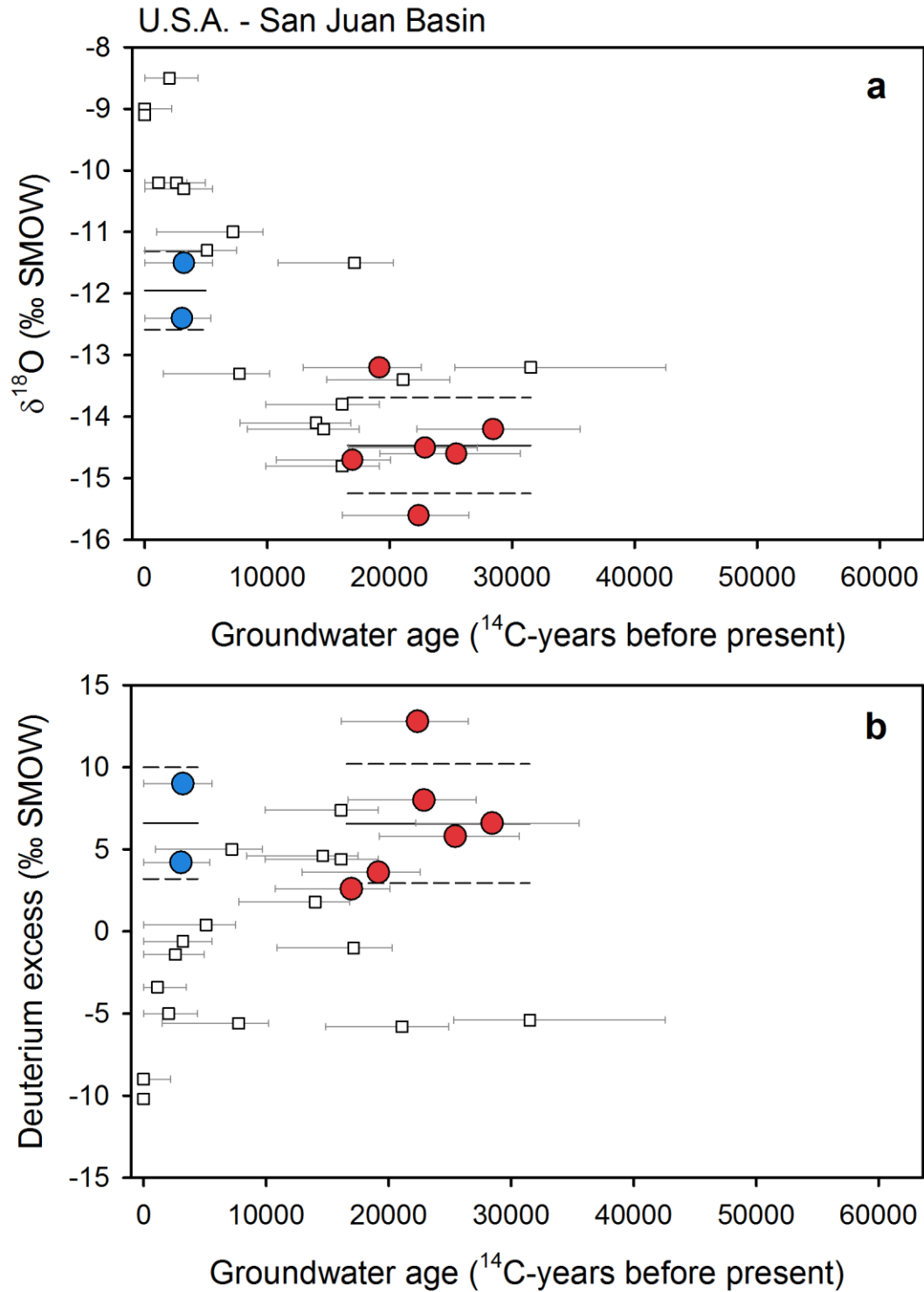
392  
 393 **Figure S53.** Groundwater isotope composition of the southern High Plains aquifer. Groundwater  
 394  $\delta^{18}\text{O}$  (a) and deuterium excess (b) plotted against corrected  $^{14}\text{C}$  ages for late-Holocene (blue  
 395 circles) and late-glacial (red circles) groundwaters. Lines mark the average (solid line) and one  
 396 standard deviation (dashed lines) for each age group (Dutton, 1995; Mehta et al., 2000).



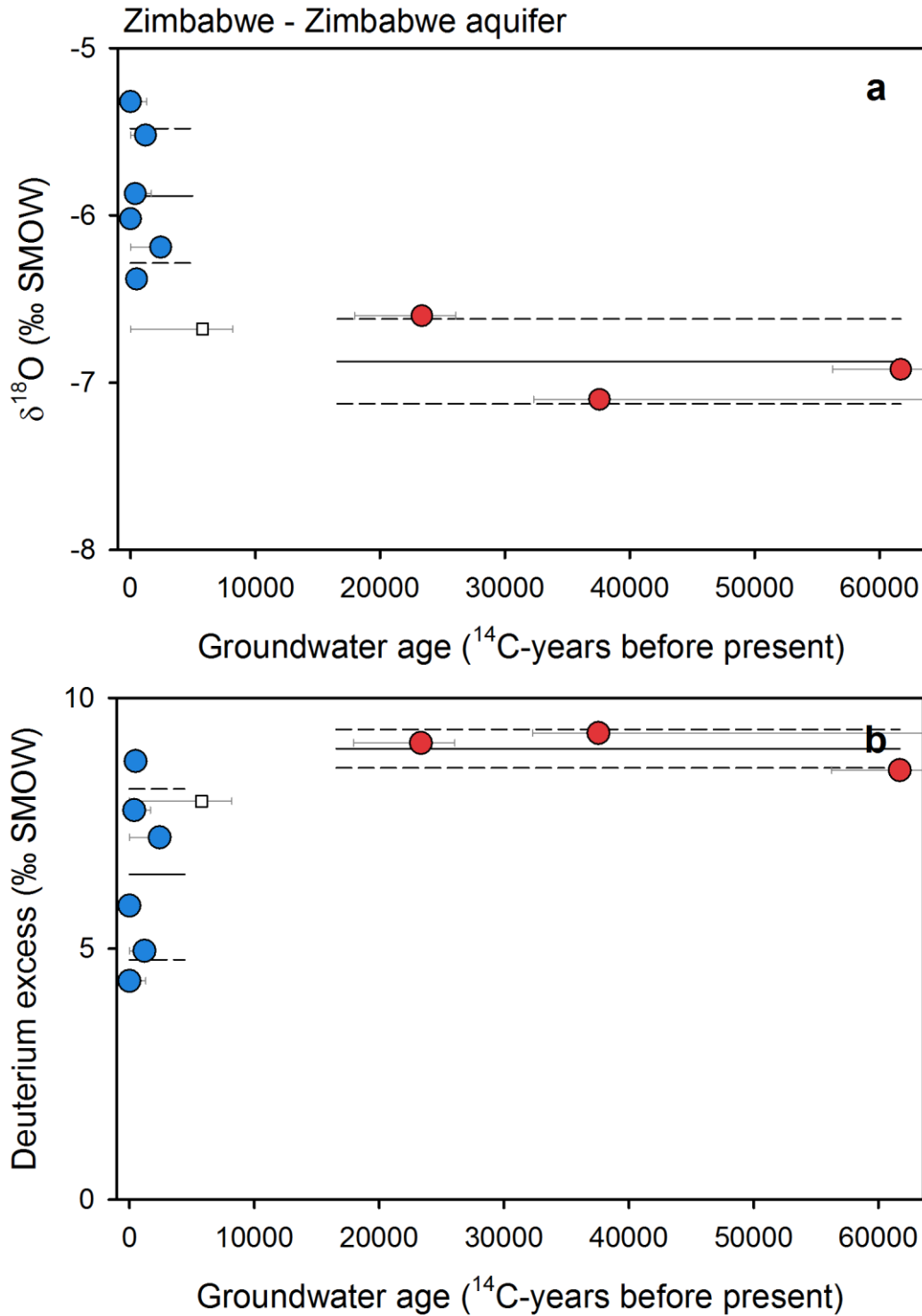
397  
 398 **Figure S54.** Groundwater isotope composition of the Idaho Batholith aquifer. Groundwater  $\delta^{18}\text{O}$   
 399 (a) and deuterium excess (b) plotted against corrected  $^{14}\text{C}$  ages for late-Holocene (blue circles)  
 400 and late-glacial (red circles) groundwaters. Lines mark the average (solid line) and one standard  
 401 deviation (dashed lines) for each age group (Schlegel et al., 2009).



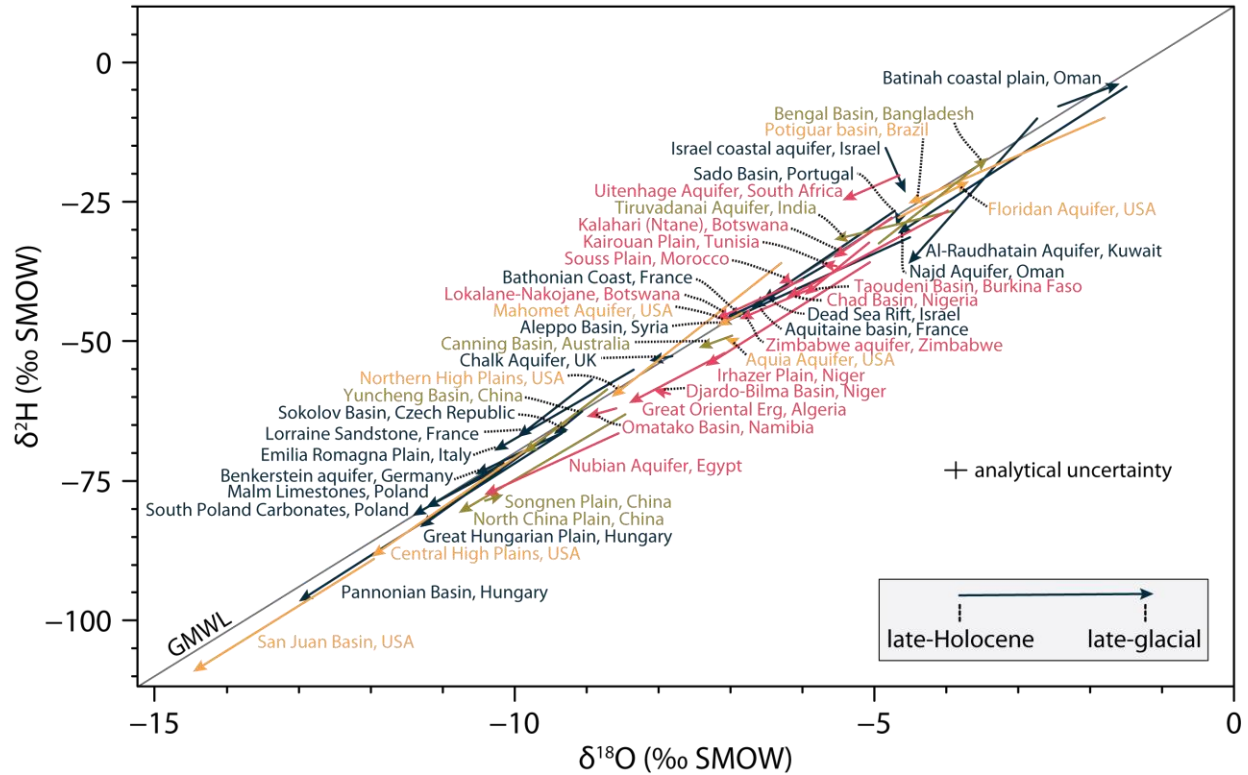
402  
 403 **Figure S55.** Groundwater isotope composition of the Mahomet aquifer. Groundwater  $\delta^{18}\text{O}$  (a)  
 404 and deuterium excess (b) plotted against corrected  $^{14}\text{C}$  ages for late-Holocene (blue circles) and  
 405 late-glacial (red circles) groundwaters. Lines mark the average (solid line) and one standard  
 406 deviation (dashed lines) for each age group (Hackley et al., 2010).



407  
 408 **Figure S56.** Groundwater isotope composition of the San Juan basin. Groundwater  $\delta^{18}\text{O}$  (a) and  
 409 deuterium excess (b) plotted against corrected  $^{14}\text{C}$  ages for late-Holocene (blue circles) and late-  
 410 glacial (red circles) groundwaters. Lines mark the average (solid line) and one standard deviation  
 411 (dashed lines) for each age group (Phillips et al., 1986).



412  
 413 **Figure S57.** Groundwater isotope composition of the Zimbabwe aquifer. Groundwater  $\delta^{18}\text{O}$  (a)  
 414 and deuterium excess (b) plotted against corrected  $^{14}\text{C}$  ages for late-Holocene (blue circles) and  
 415 late-glacial (red circles) groundwaters. Lines mark the average (solid line) and one standard  
 416 deviation (dashed lines) for each age group (Larsen et al., 2002).  
 417



418  
 419 **Figure S58.**  $\delta^{18}\text{O}$  and  $\delta^2\text{H}$  values of late-glacial and late-Holocene groundwaters. Each arrow  
 420 represents one aquifer, the arrow marks the average late-Holocene isotope composition (start of  
 421 the arrow) and the average late-glacial isotope composition (end of the arrow). Each arrow is  
 422 labelled (short dashed black lines). Aquifers are color coded by region: Asia, Australia and  
 423 Oceania (green), Africa (red), North and South America (yellow) and Europe and the Middle  
 424 East (dark blue). The global meteoric water line is shown as a dark black line (Craig, 1961).  
 425 Groundwater data shown here was compiled from publications cited in Table S2.  
 426

427 **References: Supplementary Information text**

- 428 Annan, J. D., and Hargreaves, J. C. (2013), A new global reconstruction of temperature  
429 changes at the Last Glacial Maximum. *Climate of the Past*, **9**, 367–376.
- 430 Bouchaou, L., Michelot, J. L., Vengosh, A., Hsissou, Y., Qurtobi, M., Gaye, C. B., Bullen, T.  
431 D., and Zuppi, G. M. (2008), Application of multiple isotopic and geochemical tracers for  
432 investigation of recharge, salinization, and residence time of water in the Souss–Massa  
433 aquifer, southwest of Morocco, *Journal of Hydrology*, **352**, 267–287.
- 434 Burchuladze, A. A., Chudy, M., Eristavi, I. V., Pagava, S. V., Povinec, P., Sivo, A., and  
435 Togonidze, G. I. (1989), Anthropogenic <sup>14</sup>C variations in atmospheric CO<sub>2</sub> and wines,  
436 *Radiocarbon*, **31**, 771–776.
- 437 Clark, I. D., and Fritz, P. (1997), Environmental isotopes in hydrogeology. CRC press.
- 438 Craig, H. (1961), Isotopic variations in meteoric waters, *Science*, **133**, 1702–1703.
- 439 Ferguson, G. A., Betcher, R. N., and Grasby, S. E. (2007), Hydrogeology of the Winnipeg  
440 formation in Manitoba, Canada, *Hydrogeology Journal*, **15**, 573–587.
- 441 Geyh, M. A., and Söfner, B. (1989), Groundwater analysis of environmental carbon and  
442 other isotopes from the Jakarta Basin Aquifer, Indonesia, *Radiocarbon*, **31**, 919–925.
- 443 Grasby, S. E., and Chen, Z. (2005), Subglacial recharge into the Western Canada  
444 Sedimentary Basin—Impact of Pleistocene glaciation on basin hydrodynamics, *Geological*  
445 *Society of America Bulletin*, **117**, 500–514.
- 446 Karro, E., Marandi, A., and Vaikmäe, R. (2004), The origin of increased salinity in the  
447 Cambrian-Vendian aquifer system on the Kopli Peninsula, northern Estonia, *Hydrogeology*  
448 *Journal*, **12**, 424–435.
- 449 Lisiecki, L. E., and Raymo, M. E. (2005), A Pliocene-Pleistocene stack of 57 globally  
450 distributed benthic  $\delta^{18}\text{O}$  records, *Paleoceanography*, **20**, PA1003.

- 451 Marcott, S. A., Shakun, J. D., Clark, P. U., and Mix, A. C. (2013), A reconstruction of  
452 regional and global temperature for the past 11,300 years, *Science* **339**, 1198–1201.
- 453 McIntosh, J. C., Schlegel, M. E., and Person, M. (2012), Glacial impacts on hydrologic  
454 processes in sedimentary basins: evidence from natural tracer studies, *Geofluids*, **12**, 7–12.
- 455 New, M., Lister, D., Hulme, M., and Makin, I. (2002), A high-resolution data set of surface  
456 climate over global land areas, *Climate Research*, **21**, 1–25.
- 457 O'Neil, J. R., Clayton, R. N., and Mayeda, T. K. (1969), Oxygen isotope fractionation in  
458 divalent metal carbonates, *The Journal of Chemical Physics*, **51**, 5547–5558.
- 459 Reimer, P. J. et al. (2013), IntCal13 and Marine13 radiocarbon age calibration curves 0-  
460 50,000 years cal BP, *Radiocarbon*, **55**, 1869–1887.
- 461 Stotler, R. L., Frapce, S. K., Ruskeeniemi, T., Pitkänen, P., and Blowes, D. W. (2012), The  
462 interglacial–glacial cycle and geochemical evolution of Canadian and Fennoscandian Shield  
463 groundwaters, *Geochimica et Cosmochimica Acta*, **76**, 45–67.
- 464 Veizer, J., et al. (1999).  $^{87}\text{Sr}/^{86}\text{Sr}$ ,  $\delta^{13}\text{C}$  and  $\delta^{18}\text{O}$  evolution of Phanerozoic seawater.  
465 *Chemical Geology*, **161**, 59–88.

466 **References: General circulation models – additional references in Table S1**

- 467 Argus, D. F., and Peltier, W. R. (2010), Constraining models of postglacial rebound using  
468 space geodesy: a detailed assessment of model ICE-5G (VM2) and its relatives, *Geophysical*  
469 *Journal International* **181**, 697–723.
- 470 Braconnot, P. et al. (2012), Evaluation of climate models using palaeoclimatic data. *Nature*  
471 *Climate Change*, **2**, 417–424.
- 472 Collins, W. D. et al. (2006), The formulation and atmospheric simulation of the Community  
473 Atmosphere Model version 3 (CAM3), *Journal Of Climate*, **19**, 2144–2161.
- 474 Hansen, J., et al. (2005), Earth's energy imbalance: Confirmation and implications, *Science*,  
475 **308**, 1431–1435.

- 476 Hourdin, F., et al. (2006), The LMDZ4 general circulation model: Climate performance and  
477 sensitivity to parametrized physics with emphasis on tropical convection, *Climate Dynamics*,  
478 **27**, 787–813.
- 479 Kanamitsu, M., et al. (2002), NCEP dynamical seasonal forecast system 2000, *Bulletin of the*  
480 *American Meteorological Society*, **83**, 1019–1037.
- 481 Koch, D., et al. (2011), Coupled Aerosol-Chemistry–Climate Twentieth-Century Transient  
482 Model Investigation: Trends in Short-Lived Species and Climate Responses, *Journal of*  
483 *Climate*, **24**, 2693–2714.
- 484 LeGrande, A. N., and Schmidt, G. A. (2009), Sources of Holocene variability of oxygen  
485 isotopes in paleoclimate archives, *Climate of the Past*, **5**, 441–455.
- 486 Licciardi, J. M., Clark, P. U., Jenson, J. W., and Macayeal, D. R. (1999), Deglaciation of a  
487 soft-bedded Laurentide Ice Sheet, *Quaternary Science Reviews*, **17**, 427–448.
- 488 Noone, D., and Sturm, C. (2010), Comprehensive dynamical models of global and regional  
489 water isotope distributions. In: *Isoscapes: Understanding Movement, Pattern, and Process on*  
490 *Earth through Isotope Mapping*, Springer, pp. 195–219
- 491 Otto-Bliesner, B. L. et al. (2006), Last Glacial Maximum and Holocene climate in CCSM3,  
492 *Journal of Climate*, **19**, 2526–2544.
- 493 Peltier, W. R. (1994), Ice age paleotopography, *Science*, **265**, 195–201.
- 494 Roeckner, E., Brokopf, R., Esch, M., Giorgetta, M., Hagemann, S., Kornblueh, L., Manzini,  
495 E., Schlese, U., and Schulzweida, U. (2006), Sensitivity of simulated climate to horizontal  
496 and vertical resolution in the ECHAM5 atmosphere model, *Journal Of Climate*, **19**, 3771–  
497 3791.
- 498 Schmidt, G. A., et al. (2014), Configuration and assessment of the GISS ModelE2  
499 contributions to the CMIP5 archive, *Journal of Advances in Modeling Earth Systems*, **6**,  
500 141–184.
- 501 Shindell, D. T., Faluvegi, G., Miller, R. L., Schmidt, G. A., Hansen, J. E., and Sun, S. (2006),  
502 Solar and anthropogenic forcing of tropical hydrology, *Geophysical Research Letters*, **33**,  
503 L24706.
- 504 Sturm, C., Zhang, Q. and Noone, D. (2010), An introduction to stable water isotopes in  
505 climate models: benefits of forward proxy modelling for paleoclimatology, *Climate of the*  
506 *Past*, **6**, 115–129.
- 507 Toscano, M. A., Peltier, W. R., and Drummond, R. (2011), ICE-5G and ICE-6G models of  
508 postglacial relative sea-level history applied to the Holocene coral reef record of northeastern

- 509 St Croix, USVI: investigating the influence of rotational feedback on GIA processes at  
510 tropical latitudes, *Quaternary Science Reviews*, **30**, 3032–3042.
- 511 Ullman, D. J., LeGrande, A. N., Carlson, A. E., Anslow, F. S., and Licciardi, J. M. (2013),  
512 Assessing the impact of Laurentide Ice-Sheet topography on glacial climate, *Climate of the*  
513 *Past*, **10**, 487–507
- 514 Werner M., Langebroek, P. M., Carlsen T., Herold M., and Lohmann G., (2011), Stable  
515 water isotopes in the ECHAM5 general circulation model: Toward high-resolution isotope  
516 modeling on a global scale, *Journal of Geophysical Research*, **116**, D15109.
- 517 Yoshimura, K., Kanamitsu, M., Noone, D., and Oki, T. (2008), Historical isotope simulation  
518 using Reanalysis atmospheric data, *Journal of Geophysical Research*, **113**, D19108.

519 **References: Groundwater data**

- 520 Aeschbach-Hertig, W., Stute, M., Clark, J. F., Reuter, R. F., and Schlosser, P. (2002), A  
521 paleotemperature record derived from dissolved noble gases in groundwater of the Aquia  
522 Aquifer (Maryland, USA). *Geochimica et Cosmochimica Acta*, **66**, 797–817.
- 523 Aggarwal, P. K. et al. (2000), A report on isotope hydrology of groundwater in Bangladesh:  
524 implications for characterization and mitigation of arsenic in groundwater, International  
525 Atomic Energy Agency, Department of Technical Co-operation, Vienna (Austria).
- 526 Al-Charideh, A. (2012), Geochemical and isotopic characterization of groundwater from  
527 shallow and deep limestone aquifers system of Aleppo basin (north Syria), *Environmental*  
528 *Earth Sciences*, **65**, 1157–1168.
- 529 Al-Mashaikhi, K., Oswald, S., Attinger, S., Büchel, G., Knöller, K., and Strauch, G. (2012),  
530 Evaluation of groundwater dynamics and quality in the Najd aquifers located in the Sultanate  
531 of Oman, *Environmental Earth Sciences*, **66**, 1195–1211.
- 532 Al-Ruwaih, F. M., and Shehata, M. (2004), Hydrochemical processes and environmental  
533 isotopic study of groundwater in Kuwait, *Water International*, **29**, 158–166.

534 Andrews, J. N., Fontes, J. C., Aranyossy, J. F., Dodo, A., Edmunds, W. M., Joseph, A., and  
535 Travi, Y. (1994), The evolution of alkaline groundwaters in the continental intercalaire  
536 aquifer of the Irhazer Plain, Niger, *Water Resources Research*, **30**, 45–61.

537 Arslan, S., Yazicigil, H., Stute, M., Schlosser, P. (2014), Environmental isotopes and noble  
538 gases in the deep aquifer system of Kazan Trona Ore Field, central Turkey and links to  
539 paleoclimate, *Quaternary Research*, **79**, 292–303.

540 Barbecot, F., Marlin, C., Gibert, E., and Dever, L. (2000), Hydrochemical and isotopic  
541 characterisation of the Bathonian and Bajocian coastal aquifer of the Caen area (northern  
542 France), *Applied Geochemistry*, **15**, 791–805.

543 Beyerle, U., Rueedi, J., Leuenberger, M., Aeschbach-Hertig, W., Peeters, F., Kipfer, R. and  
544 Dodo, A. (2003), Evidence for periods of wetter and cooler climate in the Sahel between 6  
545 and 40 kyr BP derived from groundwater, *Geophysical Research Letters*, **30**, 1173.

546 Bouchaou, L., Michelot, J. L., Vengosh, A., Hsissou, Y., Qurtobi, M., Gaye, C. B., Bullen, T.  
547 D., and Zuppi, G. M. (2008), Application of multiple isotopic and geochemical tracers for  
548 investigation of recharge, salinization, and residence time of water in the Souss–Massa  
549 aquifer, southwest of Morocco, *Journal of Hydrology*, **352**, 267–287.

550 Brown, K. B., McIntosh, J. C., Baker, V. R., and Gosch, D. (2010), Isotopically-depleted late  
551 Pleistocene groundwater in Columbia River Basalt aquifers: Evidence for recharge of glacial  
552 Lake Missoula floodwaters? *Geophysical Research Letters*, **37**, L21402.

553 Castany, G., Marce, A., Margat, J., Moussu, H., Vuillaume, Y., and Evin, J. (1974), An  
554 environmental isotope study of the groundwater regime in large aquifers, In: *Isotope  
555 Techniques in Groundwater Hydrology 1974*, Vol. I.

556 Celle-Jeanton, H., Huneau, F., Travi, Y., and Edmunds, W. M. (2009), Twenty years of  
557 groundwater evolution in the Triassic sandstone aquifer of Lorraine: impacts on baseline  
558 water quality, *Applied Geochemistry*, **24**, 1198–1213.

559 Chen, Z., Qi, J., Xu, J., Xu, J., Ye, H., and Nan, Y. (2003), Paleoclimatic interpretation of the  
560 past 30 ka from isotopic studies of the deep confined aquifer of the North China plain,  
561 *Applied Geochemistry*, **18**, 997–1009.

562 Chen, Z., Wei, W., Liu, J., Wang, Y., and Chen, J. (2011), Identifying the recharge sources  
563 and age of groundwater in the Songnen Plain (Northeast China) using environmental  
564 isotopes, *Hydrogeology Journal*, **19**, 163–176.

565 Clark, I. D., Fritz, P., Quinn, O. P., Rippon, P. W., Nash, H., and al Said, S. B. B. G. (1987),  
566 Modern and fossil groundwater in an arid environment: a look at the hydrogeology of  
567 southern Oman, In: *Isotope Techniques in Water Resources Development*.

568 Clark, J. F., Davisson, M. L., Hudson, G. B., and Macfarlane, P. A. (1998), Noble gases,  
569 stable isotopes, and radiocarbon as tracers of flow in the Dakota aquifer, Colorado and  
570 Kansas, *Journal of Hydrology*, **211**, 151–167.

571 Clark, J. F., Stute, M., Schlosser, P., Drenkard, S., and Bonani, G. (1997), A tracer study of  
572 the Floridan aquifer in southeastern Georgia: Implications for groundwater flow and  
573 paleoclimate, *Water Resources Research*, **33**, 281–289.

574 Currell, M. J., Cartwright, I., Bradley, D. C., and Han, D. (2010). Recharge history and  
575 controls on groundwater quality in the Yuncheng Basin, north China, *Journal of Hydrology*,  
576 **385**, 216–229.

577 Darling, W. G., and Bath, A. H. (1988), A stable isotope study of recharge processes in the  
578 English Chalk, *Journal of Hydrology*, **101**, 31–46.

579 Darling, W. G., Edmunds, W. M., and Smedley, P. L. (1997), Isotopic evidence for  
580 palaeowaters in the British Isles, *Applied Geochemistry*, **12**, 813–829.

581 Dennis, F., Andrews, J. N., Parker, A., Poole, J. and Wolf, M. (1997), Isotopic and noble gas  
582 study of Chalk groundwater in the London Basin, England, *Applied Geochemistry*, **12**, 763–  
583 773.

584 Derwich, L. J., Zouar, K., and Michelot, J. L. (2012), Recharge and paleorecharge of the  
585 deep groundwater aquifer system in the Zeroud Basin (Kairouan plain, Central Tunisia),  
586 *Quaternary International*, **257**, 56–63.

587 Dodo, A., and Zuppi, G. M. (1997), Groundwater flow study in the Bilma–Djado Basin  
588 (Niger) by means of environmental isotopes, *Comptes Rendus de l'Academie des Sciences.*  
589 *Serie 2, Sciences de la Terre et des Planetes*, **30**, 845–852.

590 Dodo, A., and Zuppi, G. M. (1999), Variabilité climatique durant le Quaternaire dans la  
591 nappe du Tarat (Arlit, Niger), *Comptes Rendus de l'Académie des Sciences–Series IIA–Earth*  
592 *and Planetary Science*, **328**, 371–379.

593 Douglas, A. A., Osiensky, J. L., and Keller, C. K. (2007). Carbon–14 dating of ground water  
594 in the Palouse Basin of the Columbia River basalts, *Journal of Hydrology*, **334**, 502–512.

595 Dutton, A. R. (1995), Groundwater isotopic evidence for paleorecharge in US High Plains  
596 aquifers, *Quaternary Research*, **43**, 221–231.

597 Edmunds, W. M. (2009), Palaeoclimate and groundwater evolution in Africa—implications  
598 for adaptation and management, *Hydrological Sciences Journal*, **54**, 781–792.

599 Edmunds, W. M. et al. (2003), Groundwater evolution in the Continental Intercalaire aquifer  
600 of southern Algeria and Tunisia: trace element and isotopic indicators, *Applied*  
601 *Geochemistry*, **18**, 805–822.

602 Edmunds, W. M. et al. (2004), Groundwater as an archive of climatic and environmental  
603 change: Europe to Africa, in: Past climate variability through Europe and Africa (eds. R.W.  
604 Battarbee, F. Gasse, C.E. Stickley), pp. 279–306, Springer, Netherlands.

605 Elliot, T., Andrews, J. N., and Edmunds, W. M. (1999), Hydrochemical trends,  
606 palaeorecharge and groundwater ages in the fissured Chalk aquifer of the London and  
607 Berkshire Basins, UK, *Applied Geochemistry*, **14**, 333–363.

608 Fadlemawla, A., Hadi, K., Zouari, K., and Kulkarni, K. M. (2008), Hydrogeochemical  
609 investigations of recharge and subsequent salinization processes at Al-Raudhatain depression  
610 in Kuwait, *Hydrological Sciences Journal*, **53**, 204–223.

611 Galego Fernandes, P., and Carreira, P. M. (2008), Isotopic evidence of aquifer recharge  
612 during the last ice age in Portugal, *Journal of Hydrology*, **361**, 291–308.

613 Gat, J. R., and Galai, A. (1982). Groundwaters of the Arava Valley-an isotopic study of their  
614 origin and interrelationships, *Israel Journal of Earth Sciences*, **31**, 25–38.

615 Geyh, M. A., and Söfner, B. (1989), Groundwater analysis of environmental carbon and  
616 other isotopes from the Jakarta Basin Aquifer, Indonesia, *Radiocarbon*, **31**, 919–925.

617 Gouvea da Silva, R. B. (1983), Estudo hidroquímico e isotópico das águas subterrâneas do  
618 aquífero Botucatu no estado de Sao Paulo, Ph. D. thesis, University of Sao Paulo, Sao Paulo,  
619 Brazil.

620 Hackley, K. C., Panno, S. V., Anderson, T. F. (2010), Chemical and isotopic indicators of  
621 groundwater evolution in the basal sands of a buried bedrock valley in the midwestern United  
622 States: Implications for recharge, rock-water interactions, and mixing, *Geological Society of  
623 America Bulletin*, **122**, 1047–1066.

624 Harrington, G., Stelfox, L., Gardner, W. P., Davies, P., Doble, R., and Cook, P. G. (2011),  
625 Surface water–groundwater interactions in the lower Fitzroy River, Western Australia,  
626 CSIRO Publications.

627 Heaton, T. H. E., Talma, A. S., and Vogel, J. C. (1986), Dissolved gas paleotemperatures and  
628 <sup>18</sup>O variations derived from groundwater near Uitenhage, South Africa, *Quaternary  
629 Research*, **25**, 79–88.

630 Hinsby, K., Harrar, W. G., Nyegaard, P., Konradi, P. B., Rasmussen, E. S., Bidstrup, T., Gregersen,  
631 U., Boaretto, E. (2001), The Ribe Formation in western Denmark - Holocene and Pleistocene  
632 groundwaters in a coastal Miocene sand aquifer, Geological Society of London, Special Publications,  
633 **189**, 29–48.

634 Hoque, M. A., and Burgess, W. G. (2012),  $^{14}\text{C}$  dating of deep groundwater in the Bengal  
635 Aquifer System, Bangladesh: Implications for aquifer anisotropy, recharge sources and  
636 sustainability, *Journal of Hydrology*, **444**, 209–220.

637 Huneau, F. et al. (2011), Flow pattern and residence time of groundwater within the south–  
638 eastern Taoudeni sedimentary basin (Burkina Faso, Mali), *Journal of Hydrology*, **409**, 423–  
639 439.

640 Kotler, E., and Burn, C. R. (2000), Cryostratigraphy of the Klondike "muck" deposits, west-  
641 central Yukon Territory, *Canadian Journal of Earth Sciences*, **37**, 849–861.

642 Kreuzer, A. M., von Rohden, C., Friedrich, R., Chen, Z., Shi, J., Hajdas, I., Kipfer, R., and  
643 Aeschbach–Hertig, W. (2009), A record of temperature and monsoon intensity over the past  
644 40 kyr from groundwater in the North China Plain, *Chemical Geology*, **259**, 168–180.

645 Külls, C. (2000), Groundwater of the North–Western Kalahari, Namibia. Ph.D. Thesis,  
646 Julius–Maximilian University of Würzburg.

647 Kulongoski, J. T., Hilton, D. R., and Selaolo, E. T. (2004), Climate variability in the  
648 Botswana Kalahari from the late Pleistocene to the present day, *Geophysical Research*  
649 *Letters*, **31**, L10204.

650 Kumar, S. U., Sharma, S., Navada, S. V., and Deodhar, A. S. (2009), Environmental isotopes  
651 investigation on recharge processes and hydrodynamics of the coastal sedimentary aquifers  
652 of Tiruvadanai, Tamilnadu State, India, *Journal of Hydrology*, **364**, 23–39.

653 Larsen, F., Owen, R., Dahlin, T., Mangeya, P., and Barmen, G. (2002), A preliminary  
654 analysis of the groundwater recharge to the Karoo formations, mid–Zambezi basin,  
655 Zimbabwe, *Physics and Chemistry of the Earth*, **27**, 765–772.

656 Le Gal La Salle, C., Marlin, C., Savoye, S., and Fontes, J. C. (1996), Geochemistry and  $^{14}\text{C}$   
657 dating of groundwaters from Jurassic aquifers of North Aquitaine Basin (France), *Applied*  
658 *Geochemistry*, **11**, 433–445.

659 Le Gal La Salle, C., Marlin, C., Leduc, C., Taupin, J. D., Massault, M., and Favreau, G.  
660 (2001), Renewal rate estimation of groundwater based on radioactive tracers  $^3\text{H}$ ,  $^{14}\text{C}$  in an  
661 unconfined aquifer in a semi-arid area, Iullemeden Basin, Niger, *Journal of Hydrology*, **254**,  
662 145–156.

663 Leaney, F. W., and Allison, G. B. (1986), Carbon-14 and stable isotope data for an area in  
664 the Murray Basin: its use in estimating recharge, *Journal of Hydrology*, **88**, 129–145.

665 Maduabuchi, C., Faye, S., and Maloszewski, P. (2006), Isotope evidence of palaeorecharge  
666 and palaeoclimate in the deep confined aquifers of the Chad Basin, NE Nigeria, *Science of*  
667 *the Total Environment*, **370**, 467–479.

668 Majumder, R. K., Halim, M. A., Saha, B. B., Ikawa, R., Nakamura, T., Kagabu, M., and  
669 Shimada, J. (2011), Groundwater flow system in Bengal Delta, Bangladesh revealed by  
670 environmental isotopes, *Environmental Earth Sciences*, **64**, 1343–1352.

671 Martinelli, G., Chahoud, A., Dadomo, A., Fava, A. (2014), Isotopic features of Emilia-Romagna  
672 region (North Italy) groundwaters: Environmental and climatological implications, *Journal of*  
673 *Hydrology*, **519**, 1928–1938.

674 Mazor, E., Gilad, D., and Fridman, V. (1995). Stagnant aquifer concept Part 2. Small scale  
675 artesian systems-Hazeva, Dead Sea Rift Valley, Israel, *Journal of Hydrology*, **173**, 241–261.

676 Mehta, S., Fryar, A. E., and Banner, J. L. (2000), Controls on the regional-scale salinization of the  
677 Ogallala aquifer, Southern High Plains, Texas, USA, *Applied Geochemistry*, **15**, 849–864.

678 Meyer, H., Derevyagin, A. Y., Siegert, C., and Hubberten, H. W. (2002), Paleoclimate  
679 studies on Bykovsky Peninsula, North Siberia-hydrogen and oxygen isotopes in ground ice.  
680 *Polarforschung*, **70**, 37–51.

681 Noseck, U. et al. (2009), Carbon chemistry and groundwater dynamics at natural analogue  
682 site Ruprechtov, Czech Republic: insights from environmental isotopes, *Applied*  
683 *Geochemistry*, **24**, 1765–1776.

684 Patterson, L. J. et al. (2005), Cosmogenic, radiogenic, and stable isotopic constraints on  
685 groundwater residence time in the Nubian Aquifer, Western Desert of Egypt, *Geochemistry,*  
686 *Geophysics, Geosystems*, **6**, Q01005.

687 Phillips, F. M., Peeters, L. A., Tansey, M. K., and Davis, S. N. (1986), Paleoclimatic  
688 inferences from an isotopic investigation of groundwater in the central San Juan Basin, New  
689 Mexico, *Quaternary Research*, **26**, 179–193.

690 Rahube, T. B. (2003), Recharge and groundwater resources evaluation of the Lokalane–  
691 Ncojane Basin (Botswana) using numerical modelling, MSc Thesis, *International Institute*  
692 *for Geoinformation Science and Earth Observation*, Enschede, Netherlands, 104.

693 Robinson, B. W., and Gunatilaka, A. (1991), Stable isotope studies and the hydrological  
694 regime of sabkhas in southern Kuwait, Arabian Gulf, *Sedimentary Geology*, **73**, 141–159.

695 Salati, E., Menezes Leal, J., and Mendes Campos, M. (1974), Environmental isotopes used in  
696 a hydrogeological study of northeastern Brazil, In: *Isotope Techniques in Groundwater*  
697 *Hydrology 1974*, Vol. I. 379–398.

698 Samborska, K., Rózkowski, A., and Małoszewski, P. (2013), Estimation of groundwater  
699 residence time using environmental radioisotopes ( $^{14}\text{C}$ , T) in carbonate aquifers, southern  
700 Poland, *Isotopes in Environmental and Health Studies*, **49**, 73-97.

701 Schlegel, M. E., Mayo, A. L., Nelson, S., Tingey, D., Henderson, R., and Eggett, D. (2009),  
702 Paleo-climate of the Boise area, Idaho from the last glacial maximum to the present based on  
703 groundwater  $\delta^2\text{H}$  and  $\delta^{18}\text{O}$  compositions, *Quaternary Research*, **71**, 172–180.

704 Shehata, M., and Al-Ruwaih, F. (1999), Major ions geochemistry and environmental isotope  
705 study of the Nubian Aquifer system, Dakhla Oasis, Western Desert, Egypt, *Arabian Journal*  
706 *for Science and Engineering*, **24**, 43–58.

707 Sikdar, P. K., and Sahu, P. (2009), Understanding wetland sub-surface hydrology using  
708 geologic and isotopic signatures, *Hydrology and Earth System Sciences Discussions*, **6**,  
709 3143–3173.

710 Stadler, S., Geyh, M. A., Ploethner, D., and Koeniger, P. (2012), The deep Cretaceous  
711 aquifer in the Aleppo and Steppe basins of Syria: assessment of the meteoric origin and  
712 geographic source of the groundwater, *Hydrogeology Journal*, **20**, 1007–1026.

713 Stute, M., and Deak, J. (1989), Environmental isotope study  $^{14}\text{C}$ ,  $^{13}\text{C}$ ,  $^{18}\text{O}$ , D, noble gases on  
714 deep groundwater circulation systems in Hungary with reference to paleoclimate,  
715 *Radiocarbon*, **31**, 902–918.

716 Stute, M., Clark, J. F., Schlosser, P., Broecker, W. S., and Bonani, G. (1995a), A 30,000 yr  
717 continental paleotemperature record derived from noble gases dissolved in groundwater from  
718 the San Juan Basin, New Mexico, *Quaternary Research*, **43**, 209–220.

719 Sukhija, B. S., Reddy, D. V., and Nagabhushanam, P. (1998), Isotopic fingerprints of  
720 paleoclimates during the last 30,000 years in deep confined groundwaters of Southern India,  
721 *Quaternary Research*, **50**, 252–260.

722 van Geldern, R., Baier, A., Subert, H. L., Kowol, S., Balk, L., Barth, J. A. C. (2014), Pleistocene  
723 paleo-groundwater as a pristine fresh water resource in southern Germany – evidence from stable and  
724 radiogenic isotopes, *Science of the Total Environment*, **496**, 107–115.

725 Varsányi, I., Palcsu, L., and Kovács, L. Ó. (2011), Groundwater flow system as an archive of  
726 palaeotemperature: Noble gas, radiocarbon, stable isotope and geochemical study in the  
727 Pannonian Basin, Hungary, *Applied Geochemistry*, **26**, 91–104.

728 Walraevens, K. (1990), Natural-isotope research on groundwater from the semi-confined  
729 Ledo-Paniselian aquifer in Belgium: application of  $^{14}\text{C}$ -correction methods.  
730 *Natuurwetenschappelijk Tijdschrift*, **72**, 79–89.

731 Walraevens, K., Van Camp, M., Lermytte, J., Van Der Kemp, W. J. M., and Loosli, H. H.  
732 (2001), Pleistocene and Holocene groundwaters in the freshening Ledo-Paniselian aquifer in  
733 Flanders, Belgium, *Geological Society, London, Special Publications*, **189**, 49–70.

734 Weyhenmeyer, C. E., Burns, S. J., Waber, H. N., Aeschbach-Hertig, W., Kipfer, R., Loosli,  
735 H. H., and Matter, A. (2000), Cool glacial temperatures and changes in moisture source  
736 recorded in Oman groundwaters, *Science*, **287**, 842–845.

- 737 Weyhenmeyer, C. E., Burns, S. J., Waber, H. N., Macumber, P. G., and Matter, A. (2002),  
738 Isotope study of moisture sources, recharge areas, and groundwater flow paths within the  
739 eastern Batinah coastal plain, Sultanate of Oman, *Water Resources Research*, **38**, 1184.
- 740 Yechieli, Y., Kafri, U., and Sivan, O. (2009), The inter-relationship between coastal sub-  
741 aquifers and the Mediterranean Sea, deduced from radioactive isotopes analysis,  
742 *Hydrogeology Journal*, **17**, 265–274.
- 743 Zuber, A., Weise, S. M., Motyka, J., Osenbrück, K., and Róžański, K. (2004), Age and flow  
744 pattern of groundwater in a Jurassic limestone aquifer and related Tertiary sands derived  
745 from combined isotope, noble gas and chemical data, *Journal of Hydrology*, **286**, 87–112.
- 746 **References: Speleothem data**
- 747 Asmerom, Y., Polyak, V. J., and Burns, S. J. (2010), Variable winter moisture in the  
748 southwestern United States linked to rapid glacial climate shifts, *Nature Geoscience*, **3**, 114–117.
- 749 Bar-Matthews, M., Ayalon, A., Gilmour, M., Matthews, A., and Hawkesworth, C. (2003), Sea-  
750 land oxygen isotopic relationships from planktonic foraminifera and speleothems in the Eastern  
751 Mediterranean region and their implication for paleorainfall during interglacial intervals,  
752 *Geochimica et Cosmochimica Acta*, **67**, 3181–3199.
- 753 Cai, Y., Tan, L., Cheng, H., An, Z., Edwards, R. L., Kelly, M. J., Kong, X., and Wang, X.  
754 (2010), The variation of summer monsoon precipitation in central China since the last  
755 deglaciation, *Earth and Planetary Science Letters*, **291**, 21–31.
- 756 Cruz, F. W., Burns, S. J., Karmann, I., Sharp, W. D., Vuille, M., Cardoso, A. O., Ferrari, J. A.,  
757 Dias, P. L. S., and Viana, O. (2005), Insolation-driven changes in atmospheric circulation over  
758 the past 116,000 years in subtropical Brazil, *Nature*, **434**, 63–66.
- 759 Dykoski, C. A., Edwards, R. L., Cheng, H., Yuan, D., Cai, Y., Zhang, M., Lin, Y., Qing, J., An,  
760 Z., and Revenaugh, J. (2005), A high-resolution, absolute-dated Holocene and deglacial Asian  
761 monsoon record from Dongge Cave, China, *Earth and Planetary Science Letters*, **233**, 71–86.

762 Fleitmann, D. *et al.* (2009), Timing and climatic impact of Greenland interstadials recorded in  
763 stalagmites from northern Turkey, *Geophysical Research Letters*, **36**, L19707.

764 Frumkin, A., Ford, D. C., and Schwarcz, H. P. (1999), Continental oxygen isotopic record of the  
765 last 170,000 years in Jerusalem, *Quaternary Research*, **51**, 317–327.

766 Holmgren, K., Lee-Thorp, J. A., Cooper, G. R., Lundblad, K., Partridge, T. C., Scott, L.,  
767 Sithaldeen, R., Talma, A. S., and Tyson, P. D. (2003), Persistent millennial-scale climatic  
768 variability over the past 25,000 years in Southern Africa, *Quaternary Science Reviews*, **22**,  
769 2311–2326.

770 Partin, J. W., Cobb, K. M., Adkins, J. F., Clark, B., and D. P. Fernandez (2007), Millennial-scale  
771 trends in west Pacific warm pool hydrology since the Last Glacial Maximum, *Nature*, **449**, 452–  
772 455.

773 Shakun, J. D., Burns, S. J., Fleitmann, D., Kramers, J., Matter, A., and Al-Subary, A. (2007), A  
774 high-resolution, absolute-dated deglacial speleothem record of Indian Ocean climate from  
775 Socotra Island, Yemen, *Earth and Planetary Science Letters*, **259**, 442–456.

776 Wagner, J. D. M., Cole, J. E., Beck, J. W., Patchett, P. J., Henderson, G. M., and Barnett, H. R.  
777 (2010), Moisture variability in the southwestern United States linked to abrupt glacial climate  
778 change, *Nature Geoscience* **3**, 110–113.

779 Wang, X. F. *et al.* (2007), Millennial-scale precipitation changes in southern Brazil over the past  
780 90,000 years, *Geophysical Research Letters*, **34**, L23701.

781 Wang, Y. J., Cheng, H., Edwards, R. L., An, Z. S., Wu, J. Y., Shen, C-C., and Dorale, J. A.  
782 (2001), A high-resolution absolute-dated late pleistocene monsoon record from Hulu Cave,  
783 China, *Science*, **294**, 2345–2348.

784 Williams, P. W., Neil, H. L., and Zhao, J. X. (2010), Age frequency distribution and revised  
785 stable isotope curves for New Zealand speleothems: palaeoclimatic implications, *International*  
786 *Journal of Speleology*, **39**, 99–112.

787 Yang, Y., Yuan, D., Cheng, H., Zhang, M., Qin, J., Lin, Y., XiaoYan, Z. and Edwards, R. L.  
788 (2010), Precise dating of abrupt shifts in the Asian Monsoon during the last deglaciation based  
789 on stalagmite data from Yamen Cave, Guizhou Province, China, *Science China Earth Sciences*,  
790 **53**, 633–641.

791 Yuan, D. et al. (2004), Timing, Duration, and Transitions of the Last Interglacial Asian  
792 Monsoon, *Science*, **23**, 575–578.

793 **References: Ice core data**

794 Blunier, T., and Brook, E. J. (2001), Timing of millennial-scale climate change in Antarctica and  
795 Greenland during the last glacial period, *Science*, **291**, 109–112.

796 Buiron, D. et al. (2011), TALDICE-1 age scale of the Talos Dome deep ice core, East Antarctica,  
797 *Climate of the Past*, **7**, 1–16.

798 EPICA community members (2006), One-to-one coupling of glacial climate variability in  
799 Greenland and Antarctica. *Nature*, **444**, 195–198.

800 Kawamura, K., et al. (2007), Northern Hemisphere forcing of climatic cycles in Antarctica over  
801 the past 360,000 years, *Nature*, **448**, 912–916.

802 Paterson, W. S. B., Koerner, R. M., Fisher, D., Johnsen, S. J., Clausen, H. B., Dansgaard, W.,  
803 Bucher, P., and Oeschger, H. (1977), An oxygen-isotope climatic record from the Devon Island  
804 ice cap, arctic Canada, *Nature*, **266**, 508–511.

805 Pedro, J. B., Van Ommen, T. D., Rasmussen, S. O., Morgan, V. I., Chappellaz, J., Moy, A. D.,  
806 Masson-Delmotte, V. and Delmotte, M. (2011), The last deglaciation: timing the bipolar seesaw,  
807 *Climate of the Past*, **7**, 671–683.

808 Thompson, L. G. et al. (1998), A 25,000-year tropical climate history from Bolivian ice cores.  
809 *Science*, **282**, 1858–1864.

810 Thompson, L. G., Mosley-Thompson, E., Davis, M. E., Lin, P. N., Henderson, K. A., Cole-Dai,  
811 J., Bolzan, J. F., and Liu, K. B. (1995), Late glacial stage and Holocene tropical ice core records  
812 from Huascarán, Peru, *Science*, **269**, 46–50.

813 Thompson, L. O., Yao, T., Davis, M. E., Henderson, K. A., Mosley-Thompson, E., Lin, P. N.,  
814 Beer, J., Synal, H.-A., Cole-Dai, J., and Bolzan, J. F. (1997), Tropical climate instability: The  
815 last glacial cycle from a Qinghai-Tibetan ice core, *Science*, **276**, 1821–1825.

816 Vinther, B. M. et al. (2006), A synchronized dating of three Greenland ice cores throughout the  
817 Holocene, *Journal of Geophysical Research*, **111**, D13102.

818 Vinther, B. M., Clausen, H. B., Fisher, D. A., Koerner, R. M., Johnsen, S. J., Andersen, K. K.,  
819 Dahl-Jensen, D., Rasmussen, S. O., Steffensen, J. P., and Svensson, A. M. (2008), Synchronizing  
820 ice cores from the Renland and Agassiz ice caps to the Greenland Ice Core Chronology, *Journal*  
821 *of Geophysical Research: Atmospheres*, **113**, D08115.